Dynamics and statistics of hydrodynamically interacting particles in laminar flows

Von der Universität Bayreuth
zur Erlangung des Grades eines
Doktors der Naturwissenschaften (Dr. rer. nat.)
genehmigte Abhandlung

von

Jochen Bammert

geboren in Illingen (Saar)

1. Gutachter: Prof. Dr. W. Zimmermann
2. Gutachter: Prof. Dr. C. Misbah

Tag der Einreichung: 20.12.2010
Tag des Kolloquiums: 24.03.2011

Contents

Abstract ii
Kurzdarstellung iv
Extended Abstract 1
Publications 18

Bibliography **85**

Abstract

The subject of this thesis is the investigation of the dynamics and statistics of hydrodynamically interacting particles in low Reynolds number flows, which is discussed in three interrelated themes.

The first theme focuses on polymer fractionation. With our basic model we explore the possibility to sort dumbbells with respect to their size using a two-dimensional periodic potential. It turns out that the purely diffusive behavior of a dumbbell in this structured landscape is dominated by the ratio of two characteristic length scales, namely the wavelength of the potential λ and the size of the dumbbell b [1]. We explain why the diffusion constant in the potential plane shows a pronounced local maximum around $\lambda/b \approx 3/2$. Furthermore, the influence of the spring rigidity and the hydrodynamic interaction on the diffusive motion are examined as well as the dumbbell statistics. If the dumbbell is driven by an external flow through the periodic landscape two different kinds of motion occur: transport along a potential valley and a stair-like motion oblique to the trenches [2]. In the latter case, the dumbbell jumps regularly to a neighboring valley which results in an effective deflection. The onset of the oblique movement as well as the deflection angle β depend on the hydrodynamic interaction, on the ratio λ/b, and on the Brownian motion of the beads. Especially the significant dependence of β on λ/b enables particle sorting. The results are published, cf. *pub1*, *pub2*.

The second theme deals with the Brownian dynamics in shear flows. Here, we investigate the correlations of particle fluctuations in order to characterize the direct interplay between thermal motion, hydrodynamic interactions, and non-uniform flows. With respect to the experimental implementation the particles are caught by harmonic potentials. First, we consider one trapped Brownian bead in linear shear and Poiseuille flows. The correlation functions of the particle's position and velocity fluctuations are calculated analytically [3]. The main result is the occurrence of shear-induced cross-correlations between orthogonal fluctuations in the shear plane which are asymmetric in time. Moreover, the positional probability distribution, $\mathcal{P}(\mathbf{r})$, of a single bead in both types of flow is determined [4]. In Poiseuille flow, where no analytical solutions can be obtained, we use perturbation expansions to derive formulas for $\mathcal{P}(\mathbf{r})$ that are valuable for the analysis of experimental data. In the case of a linear shear flow, a connection between the static correlations and the distribution functions is derived which allows a consistency check between independent measurements. Considering a system with several Brownian particles it is obvious that hydrodynamic interactions influence the correlations. In order to investigate this effect, we calculate the positional correlation functions for a setup of

two trapped Brownian beads which are exposed to a linear shear flow [5]. As expected, the one-particle correlations change compared to the single particle case described above. They depend on the distance between the two beads. In addition, we find inter-particle correlations between orthogonal positional fluctuations of different particles. The structure of these new cross-correlations depends significantly on the relative orientation of the two beads in the shear flow. They can have zero, one, or two local extrema as a function of time. In collaboration with Prof. Wagner from Saarbrücken some of our predictions are already confirmed by experiments, where polystyrene beads are caught by optical traps and simultaneously exposed to linear shear flows in a special microfluidic device [6]. The results are published, cf. *pub3*, *pub4*, *pub5*, *pub6*, and further investigations are in progress.

The third theme concentrates on the rheology of colloidal suspensions. Our deterministic model system consists of Hookean dumbbells suspended in a confined Newtonian fluid under constant shear. We perform a numerical study using fluid particle dynamics simulations, where the effective viscosity of the suspension, η_{eff}, and the dumbbell statistics are determined [7]. The investigations on the tumbling motion of a single dumbbell reveals that η_{eff} is influenced by three different contributions: the volume fraction occupied by the dumbbell, the hydrodynamic interaction between the beads, and elastic correlation effects. For a suspension of independent spheres we observe in our simulations that the viscosity, as a function of the volume fraction Φ, differs from the prediction of Einstein, Batchelor and Green if Φ becomes larger than 8%. Replacing the beads by dumbbells leads to an increase of η_{eff}, which depends significantly on the length of the springs connecting the two beads. The distribution function for the orientation angle of the dumbbells indicates the complex motion of the individual objects in the suspension, which may lead to the so-called elastic turbulence, as experimentally discovered by Groisman and Steinberg.

Kurzdarstellung

Der Schwerpunkt der vorliegenden Dissertation ist die Untersuchung der Dynamik und Statistik von hydrodynamisch wechselwirkenden Teilchen in Strömungen mit kleiner Reynolds Zahl. Diese Arbeit umfasst drei miteinander verknüpfte Projekte.

Das erste Projekt beschäftigt sich mit der Fraktionierung von Polymeren. Im Rahmen eines einfachen Modells wird die Möglichkeit untersucht, wie man Hanteln in einem zweidimensionalen, periodischen Potential ihrer Größe nach sortieren kann. In einem solchen System gibt es zwei charakteristischen Längenskalen: Die Hantellänge b und die Wellenlänge des Potentials λ. Ihr Verhältnis zueinander bestimmt maßgeblich das diffusive Verhalten der Hantel in der Potentialebene [1]. Die Diffusionskonstante als Funktion von λ/b hat im Bereich $\lambda/b \approx 3/2$ ein lokales Maximum. Des Weiteren wird neben der Hantelstatistik auch der Einfluß der Federsteifigkeit und der hydrodynamischen Wechselwirkung auf die Diffusion untersucht. Falls die Hantel mittels einer Strömung durch das Potential gezogen wird, ergeben sich je nach Parameterwahl zwei verschiedene Transportmuster: Die Hantel bewegt sich entweder geradlinig entlang eines Potentialtals oder sie springt regelmäßig von einer Rinne zur nächsten [2]. Im zweiten Fall entsteht eine stufenartige Trajektorie mit einem mittleren Ablenkwinkel β. Sowohl der Übergang zwischen den beiden Bewegungsmustern als auch β hängen von der hydrodynamischen Wechselwirkung, dem Verhältnis λ/b und der Amplitude der thermischen Fluktuationen ab. Besonders die Abhängigkeit des Ablenkwinkels vom relativen Längenverhältnis ermöglicht die Fraktionierung von Hantelsuspensionen. Die gefundenen Resultate sind bereits veröffentlicht (vgl. *pub1*, *pub2*).

Im zweiten Projekt geht es um Brownsche Bewegung von kolloidalen Teilchen in Scherströmungen. Die Korrelationen der Teilchenfluktuationen werden untersucht, um das Wechselspiel zwischen thermischer Bewegung, hydrodynamischer Wechselwirkung und Scherflüssen zu charakterisieren. Im Hinblick auf eine experimentelle Realisierung werden die betrachteten Teilchen in harmonischen Potentialen gefangen. Zuerst wird das Verhalten einer Brownschen Kugel in einem linearen Scherfluss und in einem Poiseuille-Fluss untersucht und deren Geschwindigkeits- und Ortskorrelationen analytisch berechnet [3]. Dabei stellt sich heraus, dass eine Scherströmung Kreuzkorrelationen zwischen zueinander senkrechten Teilchenfluktuationen verursacht, die eine zeitliche Asymmetrie aufweisen. Darüber hinaus wird die Aufenthaltswahrscheinlichkeit $\mathcal{P}(\mathbf{r})$ des Teilchens in den beiden Strömungstypen bestimmt [4]. Da es im Poiseuille-Fluss keine geschlossene Lösung für $\mathcal{P}(\mathbf{r})$ gibt, wird mit Hilfe einer Störungsrechnung eine Näherungslösung hergeleitet, die besonders für experimentelle Ergebnisse

von Nutzen ist. Im Falle der linearen Scherströmung wird ein Zusammenhang zwischen den statischen Korrelationen und der Aufenthaltswahrscheinlichkeit hergestellt, der eine Überprüfung der Konsistenz zwischen voneinander unabhängigen Messungen erlaubt. Natürlich beeinflussen die hydrodynamischen Wechselwirkungen zwischen mehreren Brownschen Teilchen deren Korrelationen. Um diesen Effekt zu untersuchen, wurde für ein System aus zwei gefangenen Kugeln in einer linearen Scherströmung die Korrelationsfunktionen der Teilchenfluktuationen berechnet. Die Einteilchenkorrelationen hängen wie erwartet vom Kugelabstand ab. Des Weiteren sind zueinander senkrechte Fluktuationen von verschiedenen Teilchen miteinander korreliert. Diese Zweiteilchenkorrelationen haben je nach Kugelkonfiguration ein, zwei oder drei lokale Extrema als Funktion der Zeit. Einige unserer vorhergesagten Ergebnisse wurden bereits in der Gruppe von C. Wagner experimentell bestätigt. In einer speziellen Versuchsanordnung, die einen linearen Scherfluss erzeugt, wurden dabei eine oder zwei Polystyrol-Kugeln in optischen Fallen gefangen und deren Fluktuationen gemessen [6]. Unsere Ergebnisse wurden bereits veröffentlicht (vgl. *pub3*, *pub4*, *pub5*, *pub6*) und weitere Untersuchungen werden folgen.

Das dritte Projekt beschäftigt sich mit der Rheologie von kolloidalen Suspensionen. Unser Modellsystem besteht aus Hanteln mit linearen Federn, die in einer Newtonschen Flüssigkeit suspendiert sind. Mit Hilfe der sogenannten Fluid Particle Dynamics Methode wird die effektive Viskosität η_{eff} der Suspension und die Hanteldynamik im linearen Scherfluss numerisch untersucht [7]. Anhand der Bewegung einer einzelnen Hantel wird gezeigt, dass η_{eff} von drei verschiedenen Beiträgen bestimmt wird: vom Volumenanteil Φ der Hanteln, von der hydrodynamischen Wechselwirkung und von elastischen Korrelationseffekten. Im Falle einer Kugelsuspension weichen unsere Simulationsergebnisse für die effektive Viskosität als Funktion von Φ von der Vorhersage von Einstein, Batchelor und Green ab, sobald Φ größer als 8% wird. Werden zwei Kugel zu einer Hantel verbunden, führt das zu einer signifikanten Erhöhung von η_{eff}, die von der Federlänge abhängt. Die Wahrscheinlichkeitsverteilung der Hantelorientierung weist auf die komplexe Dynamik in diesem Vielteilchensystem hin, die möglicherweise elastische Turbulenz zur Folge hat.

Extended Abstract

This thesis focuses on the dynamics of Brownian particles in low Reynolds number flows. Despite the long history of this field of research it recently regained considerable attention, not only from a fundamental point of view but also due to possible applications in industry enabled by a new technique: Microfluidics. The successful combination of the promising miniaturized fluid-devices with Brownian particles or polymers during the nineties of the last century opened the doors to an abundant world of opportunities. But this was only possible by the development of new methods which facilitate direct access and control over these systems.

Two important examples are modern microscopes, which track particle motions with a high spatial and temporal resolution [8], and laser tweezers [9], which allow a precise manipulation of a colloid [10] as well as the detection of its displacement [11, 12]. A laser can generate inhomogeneous potentials for particles with a refractive index different from the solvent. The structure of these potentials ranges from a simple harmonic trap to spatially periodic, random, or correlated landscapes. This technique triggered a variety of interesting scientific areas such as two-point microrheology [13, 14], the propagation of hydrodynamic interactions [15], anomalous vibrational dispersion [16], and many more.

Microfluidic devices consist of a system of small channels, usually $50-300\mu m$ in diameter, in which the liquid is pumped by pressure gradients or electroosmosis [17]. An overview can be found in the book of P. Tabeling [18]. They are used in chemical engineering to control strong endo- or exothermic reactions as well as in medicine for blood analysis. The ultimate goal are so-called 'lab-on-a-chip' devices [19] which combine a variety of different applications on a single microchip. For instance, they permit to detect biological molecules, and transport, mix, and characterize a raw sample within seconds. Especially for colloidal, biological, and polymer research microfluidics are essential for experimental investigations. But they can be found in nature as well: Blood vessels and the capillary network of plants are prominent examples [20].

Similar to macroscopic systems, like fire hoses or oil pipelines, the dynamics of viscous liquids in microfluidic devices are usually described by the Navier-Stokes equations for incompressible Newtonian fluids [21]. This equation of motion can be formulated in terms of the velocity field $\mathbf{v}$, the pressure p, and the external force density $\mathbf{f}$ according to

$$\rho\left(\partial_t + \mathbf{v}\cdot\nabla\right)\mathbf{v} = -\nabla p + \mu\nabla^2\mathbf{v} + \rho\mathbf{g} + \mathbf{f}\,, \tag{1a}$$

$$\nabla\cdot\mathbf{v} = 0\,, \tag{1b}$$

with the viscosity μ, the density ρ, and the gravitation $\mathbf{g}$. Typical material parameters for water at room temperature are $\mu = 10^{-3} Pa\ s$ and $\rho = 10^3 kg/m^3$. Eq. (1a) ensures the conservation of momentum whereas the continuity equation, Eq. (1b), expresses the conservation of mass. The Navier-Stokes equations can be rescaled by the use of one dimensionless quantity describing the flow, the so-called Reynolds number,

$$\mathrm{Re} = \frac{\rho v L}{\mu}\,, \tag{2}$$

where v and L denote the characteristic velocity and length of the investigated situation. Re is a measure for the ratio between inertial and viscous forces. Macroscopic systems are usually governed by high Reynolds number flows with $\mathrm{Re} > 1000$, for example if $v = 1m/s$ and $L = 0.1m$ in water. In this case, inertia is the dominant factor and complex flow dynamics like turbulence occur [22]. On the contrary, in microfluidics v and L are of the order of $\mu m/s$ respectively μm, which leads to $\mathrm{Re} \ll 1$, and Eq. (1a) can be linearized by neglecting the left hand side. This results in the linear Stokes equations for incompressible fluids,

$$0 = -\nabla p + \mu \nabla^2 \mathbf{v} + \rho \mathbf{g} + \mathbf{f}\,, \tag{3a}$$

$$\nabla \cdot \mathbf{v} = 0\,. \tag{3b}$$

The content of this thesis is constricted to low Reynolds numbers, where the flow is laminar and viscous forces dominate inertia effects. This has several consequences that appear unusual compared to everyday experiences. For instance, two fluids injected in a micro-channel hardly mix. Only diffusion at the fluid-fluid boundary layer starts a mixing process, which is very slow and inefficient if $\mathrm{Re} \ll 1$ because an increase of interfaces does not occur contrary to turbulent flows. However, adding a small amount of micron-sized particles can have a significant effect on the flow dynamics and change the mixing properties. Polymers, for example, can cause elastic turbulence at low Reynolds numbers [23, 24] thus supporting the mixing of fluids [25].

This example reveals that there is a subtle interplay between colloids and the surrounding fluid. The nonlinear interactions among the particles and the feedback of their motion on the solvent causes a variety of complex phenomena. Even the dynamics of one polymer in a simple shear flow can only be quantified in a coarse-grained manner [26, 27]. However, in many cases a simple model may be found to explain basic principles.

In general, the suspended particles perform Brownian motion [28] caused by thermal fluctuations of the solvent molecules. Their random collisions with the bigger colloids are the origin of the stochastic microscopic motion. In fluid mechanics, which is based on a continuum description of the solvent through

the Navier-Stokes equations, cf. Eqs. (1), the fluctuations of the velocity field are the source of Brownian dynamics [29]. In quiescent fluids this process is well understood. However, the Brownian motion in shear flows is a current field of research as discussed later in this thesis.

Besides the Brownian dynamics, the interplay between the colloids via the solvent, which is called hydrodynamic interaction, plays an important role in microfluidic systems [30]. This long-range, nonlinear interaction is crucial for various effects like the coil-globule transition of polymers [31], hydrodynamic instabilities [32], collective motion [33, 34], or the synchronization of micro-mixers [35].

From a theoretical point of view, the origin of hydrodynamic interactions is the response of the fluid to a point force. In the low Reynolds number regime, where the Stokes equations are valid, the force $\mathbf{f}(\mathbf{r})$ in Eq. (3a) creates a flow field $\mathbf{u}(\mathbf{r})$ according to the non-local linear relation

$$\mathbf{u}(\mathbf{r}) = \int d^3\mathbf{r}' \Omega(\mathbf{r} - \mathbf{r}')\mathbf{f}(\mathbf{r}') \,. \tag{4}$$

Note that due to the linearity of the Stokes equations the superposition principle is valid. The integral kernel in Eq. (4) can be calculated by Fourier-transformation of Eq. (3a). The result is the so-called Oseen tensor [36],

$$\Omega(\mathbf{r}) = \frac{1}{8\pi\eta r}\left[\mathcal{I} + \frac{\mathbf{r}\mathbf{r}}{r^2}\right] , \tag{5}$$

with the unity matrix $\mathcal{I}$. This Greens function is the basic expression for the hydrodynamic interaction between point-like particles. Especially in connection with microswimmers the solution (5) is called a Stokeslet [37, 38].

The dynamics of colloidal, spherical particles – often denoted as beads – can be described by over-damped Langevin equations of the form

$$\dot{\mathbf{r}}_i = \mathbf{u}(\mathbf{r}_i) + \mathcal{H}_{ij}\left(\mathbf{f}_j^d + \mathbf{f}_j^s\right) , \tag{6}$$

with the particle indices i and j [39, 30]. The positions are labeled with $\mathbf{r}_i$, and $\mathbf{u}(\mathbf{r})$ is the velocity field of the external flow in the microfluidic device. The mobility matrix $\mathcal{H}_{ij}$ accounts for the friction and the hydrodynamic interactions of the beads. In the Oseen approximation – the simplest case – these matrices are given by

$$\mathcal{H}_{ii} = \frac{1}{\zeta}\mathcal{I} \,, \tag{7a}$$

$$\mathcal{H}_{ij} = \frac{3a}{4\zeta r_{ij}}\left[\mathcal{I} + \frac{\mathbf{r}_{ij}\mathbf{r}_{ij}}{r_{ij}^2}\right] , \qquad (i \neq j) \,, \tag{7b}$$

where $\zeta = 6\pi\mu a$ is the Stokes friction coefficient of a point-particle with effective hydrodynamic radius a [40], and $\mathbf{r}_{ij} = \mathbf{r}_i - \mathbf{r}_j$ describes the distance between two beads. In the limit $r_{ij} \to 0$, $\mathcal{H}_{ij}$ becomes singular, cf. Eq. (7b). If two particles come close to each other, this problem can be solved by introducing excluded volume interactions and higher order terms with respect to a/r_{ij} in Eq. (7b). The latter ones can be calculated by combining the method of reflections and Faxén's theorem [30], which leads to the Rotne-Prager matrix [41],

$$\mathcal{H}_{ij} = \frac{3a}{4\zeta r_{ij}} \left[\left(1 + \frac{2a^2}{3r_{ij}^2} \right) \mathcal{I} + \left(1 - \frac{2a^2}{r_{ij}^2} \right) \frac{\mathbf{r}_{ij}\mathbf{r}_{ij}}{r_{ij}^2} \right], \qquad (i \neq j)\,. \tag{8}$$

In a similar way expressions for hydrodynamic interactions with walls can be derived as demonstrated in [42, 43, 44]. It is worth noting that in the Langevin model, cf. Eq. (6), the colloids are considered as point-particles, so they cannot rotate. However, the mobility matrix $\mathcal{H}_{ij}$ can be modified to include effects of external torque applied on the beads [45].

The vector $\mathbf{f}_i^d$ in Eq. (6) denotes the sum over all deterministic forces acting on the particles. For the stochastic force $\mathbf{f}_i^s$ that incorporates the Brownian motion one assumes a Gaussian distribution, which is completely defined via its first and second moment [46, 47],

$$\langle \mathbf{f}_i^s(t) \rangle = 0\,, \tag{9a}$$

$$\langle \mathbf{f}_i^s(t) \mathbf{f}_j^s(t') \rangle = f_{ij}\delta(t - t')\,. \tag{9b}$$

In quiescent fluids the fluctuation dissipation theorem [48, 49] relates the strength of the fluctuations and the mobility matrix,

$$f_{ij} = 2k_B T \mathcal{H}_{ij}^{-1}\,, \tag{10}$$

but in shear flows the situation is different as discussed later.

There are many applications of Langevin equations. For instance, they allow to determine analytical expressions for positional correlation functions of Brownian particles [3] as well as the characterization of anomalous diffusion in inhomogeneous viscosity landscapes [50]. Moreover, Langevin equations are used in Brownian dynamics simulations in order to model polymers by bead-spring chains [51]. This concept has proven to be valuable for explaining effects like the coil-stretch transition [52, 53] and the dynamics of tethered polymers in flows [54, 55, 56, 44].

Understanding the interaction between colloids and their dynamics in the solvent allows applications like particle sorting. A practical example can be found in medicine, where it is sometimes necessary to separate the blood cells from the plasma. This can be achieved via deterministic hydrodynamics [57].

Dholakia and co-workers realized a related setup, where a monodisperse mixture of silica and polymer beads was separated [58]. In a microfluidic device the rigid, equal-sized beads were transported through a three-dimensional optical lattice created by laser tweezers and thereby separated with respect to their refractive index. With the same setup colloidal particles can be sorted according to their size. Contrary to other methods, the experiment of Dholakia is very efficient and flexible.

Due to its relevance for many applications, the transport of spherical colloidal particles in periodic landscapes has been investigated intensively [59, 60, 61]. In this context interesting questions arise: How do deformable or complex objects like vesicles and polymers behave when they are driven by a flow through such periodic potentials? Is it possible to do fractionation with such kind of setups?

In order to answer part of these questions we investigate the dynamics of a Hookean dumbbell in the two-dimensional periodic landscape,

$$V(\mathbf{r}) = V_0 \left[\cos\left(\frac{2\pi}{\lambda} x\right) + \cos\left(\frac{2\pi}{\lambda} y\right) \right] , \tag{11}$$

in terms of a Langevin equation. The dumbbell is a model system for entities like dimers [62], pom-pom polymers [63], two polystyrene beads connected by actin filaments, or other deformable objects. Its deformability can be tuned via the stiffness of the spring connecting the two beads, and the influence of the hydrodynamic interactions between them can be characterized in a systematic manner. In an experiment the inhomogeneous potentials can be created by interference of several split beams of a laser [10, 58].

Before investigating the dynamics of a flow-driven dumbbell we explore in *pub1* its diffusion in the periodic landscape. The important parameters characterizing the system are the length of the dumbbell b, the amplitude V_0 and the wavelength λ of the potential in x and y direction, as well as the strength of the stochastic force given by the thermal energy $k_B T$. The corresponding Langevin equation is solved numerically. From an ensemble average over the resulting particle trajectories the mean squared displacement can be calculated. For small times t we obtain a sub-diffusive behavior, but at larger values of t the mean squared displacement increases linearly,

$$\langle x^2(t) \rangle = 2 D_x t \, , \tag{12}$$

similar to the case of free Brownian particles, where $D = k_B T/\zeta$ according to the Stokes-Einstein relation [28]. In the present situation $D_x = D_y$ is smaller than $k_B T/\zeta$ because of the potential.

As expected, the diffusive motion in the potential plane and the influence of the hydrodynamic interaction is reduced with increasing values of the ratio

V_0/k_BT. Especially for stiff springs the diffusion constant along the spatially modulated directions, D_x, depends significantly on the ratio λ/b. In the parameter range $\lambda/b \approx 3/2$ this interplay causes a maximum of D_x, because in this case the two beads do neither fit into one single nor into two neighboring potential minima. This mismatch reduces the effective barrier height and enhances diffusion. The height of the maximum decreases if the springs become softer because the dumbbell can easier relax down to potential minima. If λ/b gets larger than 3/2, the diffusion constant reaches a minimum value where the whole dumbbell is essentially trapped in one potential minimum. Increasing λ/b further, the influence of the potential starts to vanish until the free diffusion limit is reached.

A possible application using these results is the fractionation of a polydisperse mixture of dumbbells by diffusion. According to the dependency of the diffusion constant on the ratio λ/b, some dumbbells can diffuse much faster than others. Moreover, different values of the potential wavelength in x and y directions cause an anisotropic diffusive behavior. Some dumbbells would prefer to diffuse along the x direction while others move along the y direction. The drawback of this idea is that the diffusive motion is rather slow.

An obvious extension of the work presented in *pub1* is to consider a dumbbell which is driven by a uniform flow, $\mathbf{u} = u(\cos\alpha, \sin\alpha, 0)$, through the periodic landscape (11) as discussed in *pub2*. In the first step the Brownian motion is neglected, and we investigate the purely deterministic transport. The analysis reveals three different regimes of motion. If the flow velocity u is small, the dumbbell is trapped by the potential. The drag forces are not sufficiently strong to push the two beads over the potential barriers. However, if u exceeds a certain threshold u_{c1}, the dumbbell surmounts the barrages and starts to move straight along a wavy potential trench. The value of u_{c1} depends periodically on the ratio b/λ. Increasing u further at a finite angle α the third regime of motion is reached. Beyond a second threshold velocity u_{c2} the dumbbell jumps regularly to a neighboring potential valley resulting in stair-like particle trajectories. Especially near the onset at u_{c2} the effective deflection angle β of the dumbbell is very sensitive to b/λ. In case of strong flows β approaches the flow angle α. In addition, the critical velocity u_{c2} depends in a monotonous way on the ratio between the two characteristic length scales. It is worth noting that β is independent of b/λ if the hydrodynamic interaction between the two beads is omitted. Just below the critical value u_{c2} thermal fluctuations support the passage of the dumbbell between neighboring potential trenches and therefore induce the stair-like motion in this parameter range. This effect of thermal noise is investigated by taking the stochastic forces in the Langevin model into account. As expected, the onset of the oblique dumbbell motion is shifted to

smaller values of the second critical velocity. Moreover, the deflection angle β shows some interesting resonances as a function of b/λ. If the dumbbell size is a multiple of the wavelength, β is reduced.

These results offer several possibilities to sort dumbbells with respect to their size if they are driven by a flow through a two-dimensional periodic potential. Since u_{c1} depends on b some dumbbells remain caught by the potential at low flow velocities while others start to move along a trench. The same idea holds for the transition to the stair-like motion. Some dumbbells are deflected, others not. The dependency of the deflection angle on the dumbbell size enables efficient fractionation, especially in the parameter range $1/2 < b/\lambda < 3/2$.

In *pub2* the dumbbell is driven by a uniform flow with constant velocity which can be realized in a microfluidic device only by electro-osmosis [17]. But in general, non-uniform flow profiles are present in experimental setups. Two famous examples are the linear shear flow – also called plane Couette flow – and the Poiseuille flow which has a parabolic velocity profile. In such shear flows little is known about the dynamics of Brownian particles and their hydrodynamic interactions, although the interplay between these three ingredients causes a variety of effects. In the literature prominent examples can be found like Taylor dispersion [64], fluid mixing [65], dynamics of individual polymers [66, 26, 67], and elastic turbulence [23]. The obvious attempt to gain more insight into the fundamental principles causing these complex dynamics in shear flows is to consider one free Brownian particle or dilute suspensions. There are already a number of articles investigating this kind of systems using Langevin models [68, 69, 70], mesoscopic non-equilibrium thermodynamics [71, 72], or Fokker-Planck equations [73, 74, 75, 76]. These works usually focus on statistical properties like probability distributions and second moments.

However, even in the simplest case of one Brownian particle in a plane Couette flow there is a fundamental question: What are the exact statistical properties of the stochastic force $\mathbf{f}^s$ in the Langevin equation, cf. Eq. (6)? This is a current field of research because it is known that the fluctuation dissipation theorem in shear flows differs from the one in potential flows [77, 78]. In quiescent fluids the fluctuations of orthogonal fluid-velocity fluctuations are uncorrelated in the bulk [79]. But this is not true anymore in Couette flows [80, 81]. Here, the shear-induced cross-correlations between perpendicular fluid-fluctuations in the shear plane affect the Brownian motion of suspended particles. In the Langevin description this fact should be included in the stochastic force $\mathbf{f}^s$. Several attempts were made to determine the exact amplitudes in Eq. (9b) or corrections to Eq. (10). For example, D. Bedeaux and co-workers started their analysis from the hydrodynamic fluctuation theory [29, 82] and verified that shear-induced cross-correlations in the fluid influence the Brownian motion of

colloidal particles. But their results cannot be directly applied to Langevin equations. However, L. Holzer has recently shown that the corrections to the fluctuation-dissipation theorem for a single-particle,

$$f_{\alpha\beta} = 2k_B T\zeta\delta_{\alpha\beta}, \quad (\alpha, \beta = x, y, z)\,, \tag{13}$$

caused by a linear shear flow are small [83]. These theoretical findings justify the use of Eq. (10), which holds approximately in shear flows as well. In the following we focus on the direct interplay between Brownian motion and shear flow while keeping Eq. (10).

A basic feature of Brownian motion in non-uniform flows can be explained by considering the motion of a single bead. Assuming a linear shear flow in x direction with xy shear plane, it is clear that random jumps of the particle in y direction lead to a change in the particle velocity in x direction and an additional displacement along the streamlines. This simple picture motivates the existence of cross-correlations between orthogonal particle fluctuations in the shear plane which are not present in quiescent fluids. They are a direct consequence of the shear flow and not caused by a coupling between perpendicular directions of the stochastic forces in the Langevin model. Formula (10) remains untouched. These shear-induced correlations for Brownian motion are expected to be strongly asymmetric in time [70, 83]. However, a direct experimental observation of this prediction was missing until 2009 as described in [6], *pub3*.

The dynamics of free Brownian particles in shear flows can be investigated indirectly in light scattering experiments [84, 85, 86]. The basic principle is as follows: Light emerges from a laser and strikes a sample cell. A detector measures the electric field amplitude of the scattered beam. The autocorrelation function of the electric field, $G(\mathbf{q}, t)$, where $\mathbf{q}$ is the scattering wave vector, contains the information of the particle diffusion. For instance, in quiescent fluids the relation $G(\mathbf{q}, t) \sim e^{-Dq^2 t}$ holds, but in shear flows the connection is more complicated. One problem in light scattering experiments is that the colloids can enter and leave the laser spot which may lead to significant fluctuations of the particle number.

Stochastic motions of free particles moving along streamlines and trapped particles exposed to the same type of flow are equal in nature, as explained further below. However, from the experimental point of view the second case is more suitable for a precise statistical analysis because the objects do not diffuse out of the focus of the laser beam. Moreover, wall effects can easily be excluded if the Brownian beads are caught distant from the confinement. So, in order to investigate Brownian dynamics in shear flows directly, we consider individual

particles which are caught by harmonic potentials of the form

$$V(\mathbf{r}) = \frac{k}{2}\mathbf{r}^2 \,. \tag{14}$$

We present in *pub4* a basic investigation of the motion of a single bead in such a situation, where in the beginning a quite general analysis is carried out. For the Langevin equation, which includes inertia, we use Eqs. (9) for the stochastic forces without further specifications, and the external flow in x direction is given by

$$\mathbf{u}(\mathbf{r}) = (a + by + cy^2)\hat{\mathbf{x}} \,. \tag{15}$$

From the solution of the equation of motion several statistical properties of the particle are determined, partly using computer algebra [87]. The shift of the mean position in flow direction, $\langle x \rangle$, includes a contribution proportional to cf_{yy} which is caused by Faxén's law. Furthermore, the second moments, like $\langle xy \rangle$ and $\langle v_x^2 \rangle$, are calculated under the assumption of a Gaussian distribution of the thermal noise. They can be measured by experiments and depend on the amplitudes $f_{\alpha\beta}$. This creates the opportunity to determine the strength of the stochastic forces experimentally. For example, the measurement of a finite particle-velocity correlation $\langle v_x v_y \rangle \sim f_{xy}$ would confirm the existence of cross-correlations between orthogonal fluid-velocity fluctuations, which is fundamental for the fluctuation-dissipation theorem in shear flows. However, f_{xy} is expected to be small which means that its detection is an intricate issue. The detailed analysis of $\langle v_x v_y \rangle$ in the appendix of our work *pub4* shows that in the limit of a vanishing potential the free-particle results presented in Ref. [70] are obtained. This substantiates the above statement about the similarity of Brownian motion for free and trapped particles in shear flows. Another interesting result is the shear-induced increase of the mean kinetic energy of the bead. A similar observation was made for sheared fluids without colloids [88, 89].

In the second part of *pub4* the discussion is restricted by two assumptions: Inertia effects are neglected, and we use the equilibrium fluctuation-dissipation relation (13). Despite these approximations, the situation in common experiments is well described because the omitted effects can only be detected with a very high temporal and spatial resolution, cf. [6, 90].

In case of a linear shear flow, with $a = c = 0$ in Eq. (15), the time dependent positional correlation functions are discussed in detail. An important parameter in this case is the Weissenberg number $\mathrm{Wi} = b\tau$, which is the product of the shear rate b and the typical relaxation time $\tau = \zeta/k$ of the particle in the harmonic potential. The shear-induced correlations are proportional to Wi and asymmetric in time, which is a characteristic signature in shear flows.

$\langle x(0)y(t)\rangle$ decays exponentially while $\langle y(0)x(t)\rangle$ has a pronounced maximum. Furthermore, the static correlations determine via the covariance matrix the positional probability distribution $\mathcal{P}(\mathbf{r})$ of the trapped bead. The contour lines of $\mathcal{P}(\mathbf{r})$ have an elliptical shape, and the inclination angle of the major axis as well as the ratio between the two principal axes are functions of the Weissenberg number only. The correlation and distribution functions can be measured independently in an experiment which allows a cross-check for the consistency of the results.

A similar discussion is made in *pub4* for a trapped particle in a Poiseuille flow. However, compared to the case of linear shear flow there is a delicate difference. Due to the y^2 dependence of $\mathbf{u}$ in Eq. (15) the particle positions are no longer a linear function of the Gaussian distributed noise $\mathbf{f}^s$ in the Langevin equation. Consequently, the probability distribution of $\mathbf{r}$ is not only determined by the covariance matrix, but higher order moments, like $\langle x^3\rangle$, become important too. Brownian dynamics simulations of the corresponding Langevin equation confirm this fact. In order to obtain an analytical expression for $\mathcal{P}(\mathbf{r})$ in Poiseuille flow, one has to use a Fokker-Planck approach. For the diffusion of free Brownian particles this has already been done by T. van de Ven [74]. He derived analytical expressions for the positional probability distributions which decay in time. Recent works also consider inertia effects [91] and the relation between the Gaussian nature of noise and time reversibility [92]. Compared to these investigations, the probability distribution of a trapped Brownian particle is stationary and can be measured in an experiment by microscopy. In *pub6* we address this question in detail.

In general, the evolution of $\mathcal{P}(\mathbf{r},t)$ is driven by the probability current $\mathbf{j}(\mathbf{r},t)$ according to the Smoluchowski equation

$$\partial_t \mathcal{P} = -\nabla \mathbf{j}\,, \tag{16a}$$

$$\mathbf{j} = -D\nabla\mathcal{P} + \left(\mathbf{u} - \frac{1}{\zeta}\nabla V\right)\mathcal{P}\,, \tag{16b}$$

with the diffusion constant $D = k_B T/\zeta$. In quiescent fluids, where $\mathbf{u} = 0$, Eqs. (16) lead to a Boltzmann distribution, $\mathcal{P}(\mathbf{r}) \sim \exp(-V/k_B T)$. For a linear shear flow, with $a = c = 0$ in Eq. (15), the expected Gaussian distribution is recovered. In our work we discuss briefly the connection between the elliptical shape of the contour lines of $\mathcal{P}(\mathbf{r})$ and the second moments. For a Poiseuille flow there is no exact analytical solution of the Smoluchowski equation. However, $\mathcal{P}(\mathbf{r})$ can be calculated by a perturbation expansion for the parameter c using an ansatz of the form

$$\mathcal{P}(x,y) \sim e^{cf(x,y)+c^2 g(x,y)}\,, \tag{17}$$

with the polynomials $f(x, y)$ and $g(x, y)$ which solves the Smoluchowski equation up to the second order in c. After comparing these results with numerical solutions we find a very good agreement for a large range of the perturbation parameter c. This makes the provided analytical approximations useful for fitting experimental data. In addition, the shape of the probability distribution of one trapped Brownian particle in Poiseuille flow shows similarities with the contour of vesicles in the same type of flow as reported in [20, 93, 94, 95].

So far, the discussion was restricted to the Brownian motion of one particle in shear flows, which means that effects of hydrodynamic interactions were not taken into account. The influence of this nonlinear interaction on the statistical properties of trapped beads has been investigated by J. Meiners and S. Quake in an interesting experiment [90]: Two Brownian particles were caught in two optical traps, separated by a distance d in a quiescent fluid, and the correlations of their positional fluctuations were measured. Due to the hydrodynamic interaction between the beads the one-particle correlations, like $\langle x_1(0)x_1(t)\rangle$, depend on the parameter d. In addition, the fluctuations of two distinct beads along parallel directions are correlated too. This results in inter-particle anti-correlations like $\langle x_1(0)x_2(t)\rangle \leq 0$. The investigations of Meiners and Quake give insight into the coupling between thermal motion and hydrodynamic interactions in fluids at rest. However, the understanding of this interplay in shear flows is still far from being complete, although it is the origin of interesting phenomena in the field of polymer dynamics.

That is why we focus on the question, which kind of cross-correlations can be expected between hydrodynamically interacting particles in shear flows. In *pub5* we consider two Brownian beads, trapped in harmonic potentials at a distance d and simultaneously exposed to a linear shear flow. Three characteristic setups are investigated: The connection vector between the traps can be parallel, perpendicular, or oblique to the flow direction which affects the results substantially. From the solution of the corresponding Langevin equations we calculate the positional correlation functions, which depend on d, on the Weissenberg number, and on the particle configuration. Although the stochastic forces in our model are assumed to be uncorrelated along orthogonal directions, we observe a coupling between perpendicular particle displacements caused by the shear flow, which is similar to the findings presented in [3], *pub4*. The resulting shear-induced cross-correlations are linear in Wi and occur between orthogonal fluctuations of different particles as well. These inter-particle correlations have zero, one, or two extrema as a function of time, depending on the particle configuration. Besides generating new cross-correlations, the shear flow causes a contribution proportional to Wi^2 in the correlation functions of particle fluctuations along parallel directions. In addition, a significant impact of the parameter

d on the positional probability distribution of each particle in the shear flow is observed. The shape of the elliptical distribution is tilted and stretched if the two particles approach each other in the parallel configuration. The same observation is made if the shear rate is increased. So, the shear-flow effects are enhanced by the presence of a second particle. In the oblique configuration the opposite behavior is observed.

These results provide insight into the Brownian motion in shear flows that might be useful for the analysis of the stochastic dynamics of a bead-spring model for polymers too, where the Brownian particles are connected along a chain and fluctuate around some mean distance to their next neighbors. The fluctuations along and perpendicular to the connection vector between two neighboring beads may exhibit similar correlations as for the three investigated model configurations. In this spirit, a profound analysis of the stochastic motion of a bead-spring model in a linear shear flow is an interesting task and may contribute further to the understanding of polymer dynamics.

The theoretical investigations in *pub4*, *pub5*, and *pub6* go along with experiments in the group of C. Wagner. The major aim of this collaboration was the direct detection of the predicted shear-induced cross-correlations of orthogonal particle fluctuations in linear shear flows. This was achieved recently, and the results are published in *pub3*. According to our knowledge, this was the first direct observation of this effect. In the experimental setup, one or two uncharged polystyrene beads with a diameter of $3\mu m$ were caught by optical tweezers. A special microfluidic device was designed in order to generate a perfect linear shear flow with zero velocity at the center, where the particles were trapped. This has the advantage that the Stokes friction force on the beads is kept small, even at high shear rates. A microscope with a resolution of $15kHz$ and $\pm 4nm$ recorded the particle positions [8]. From the experimental data the different correlation functions and the particle distributions were determined. In the single-particle case, a good agreement with the theoretical predictions was found for the correlations as well as for $\mathcal{P}(\mathbf{r})$. The characteristic time-asymmetry in $\langle x(t)y(t')\rangle$ could be confirmed and a consistency check between the positional distribution and the second moments was made. For the two particle system the shear-induced inter-particle correlations were measured for the parallel configuration, where a good agreement with our calculations was observed too.

Further challenges in this project are measurements on the two-bead system in the perpendicular or oblique setup in order to confirm the characteristic dependency of $\langle x_1(0)y_2(t)\rangle$ on the configuration. In addition, experiments on the probability distribution of trapped particles in Poiseuille flow should be made and compared with the predictions in *pub6*. Current projects investigate wall

effects on hydrodynamically interacting beads (S. Schreiber) [44], the Brownian dynamics in a double-well potential, and the motion of a periodically driven particle in shear flows (D. Kienle) as well as the anomalous diffusion in confining potentials (J. Greber).

In *pub5* we have shown that the interplay between hydrodynamic interactions and shear flows influences the dynamics and statistics of individual colloids. Above all, the behavior of the whole suspension is strongly affected as well, because the suspended particles have a significant influence on the bulk properties, even if their volume fraction is small. For example, adding only a few *ppm* of the polymer polyethylene oxide into water reduces the effective viscosity substantially, so it is easier to pump the liquid through a fire hose. This effect, called turbulent drag reduction [96, 97], is utilized for the transport of oil in pipelines as well. In general, polymer suspensions are complex fluids. In experiments, this class of liquids shows a variety of astonishing phenomena such as shear thinning [98], where the effective viscosity of the suspension decreases with increasing magnitude of the applied stress. An overview of the structure and rheology of complex fluids can be found in the book of R. Larson [99].

Despite the huge amount of experimental investigations, there is a lack of theoretical models explaining the observed effects. One approach to address this complex problem is the kinetic theory [21], where the investigations start from the general Navier-Stokes equations

$$\rho \left(\partial_t + \mathbf{v} \cdot \nabla\right) \mathbf{v} = -\nabla \cdot \sigma + \rho \mathbf{g} + \mathbf{f} \,, \tag{18}$$

for incompressible fluids. The effect of suspended particles is included in the total stress tensor σ, which consists of two parts,

$$\sigma = p\mathcal{I} + \varsigma \,, \tag{19}$$

where p is the pressure, $\mathcal{I}$ is the unity matrix, and ς is given by a constitutive equation. For Newtonian fluids, one has

$$\varsigma = -\mu \left(\nabla \mathbf{v} + (\nabla \mathbf{v})^T\right) \,, \tag{20}$$

which leads to Eq. (1a). In order to describe complex fluids, more elaborate formulas for ς are used which usually include the distribution function of the underlying bead-spring models, cf. convected Jeffreys model in [21]. One example for a constitutive equation is given by the Oldroyd-B model, which is motivated by the influence of the motion of a Hookean dumbbell on the stress tensor. In this case, the expression for the matrix ς includes a contribution

$$\lambda = \langle \mathbf{RF} \rangle \,, \tag{21}$$

where $\mathbf{R}$ is the connection vector between the two beads and $\mathbf{F}$ is the spring force. For the evaluation of the ensemble average in Eq. (21) the distribution function for the dumbbell configuration is required. If such a suspension is exposed to the linear shear flow

$$\mathbf{v}(\mathbf{r}) = \dot{\gamma} x \hat{\mathbf{z}} \,, \tag{22}$$

in z direction with a shear rate $\dot{\gamma}$, one can determine the effective viscosity, η_{eff}, via the xz component of the stress tensor σ according to

$$\eta_{eff} = \frac{\sigma_{xz}}{\dot{\gamma}} \,. \tag{23}$$

The Oldroyd-B model is one of few examples, where the resulting equations can be solved analytically, but it does not reproduce shear thinning. Further details can be found in the book of R. Bird [21].

Another way to investigate the behavior of polymer solutions is to perform computer simulations. Depending on the numerical method, the polymers are often represented by bead-spring models. For the simulation of their dynamics, one can choose between different methods. Famous examples are Brownian dynamics [51], multiparticle-collision dynamics [100], and lattice Boltzmann methods [101].

It is needless to say that every numerical scheme has its benefits and drawbacks. Depending on the problem under consideration one has to make an appropriate choice. In order to perform simulations on the rheology of polymer solutions, there is a method which is superior to the examples described above. It is called fluid particle dynamics (FPD) and was introduced by H. Tanaka and T. Araki [102]. The advantages of FPD become obvious when the method is explained.

The basic idea of this scheme is to identify the body of a colloidal particle at the position $\mathbf{r}_i$ as a region of high viscosity in an incompressible Newtonian fluid. This leads to a spatially dependent viscosity field, $\eta(\mathbf{r})$,

$$\eta(\mathbf{r}) = \eta_s + (\eta_p - \eta_s) \sum_{i=1}^{N} \varphi_i(\mathbf{r}) \,, \tag{24}$$

where η_s is the solvent viscosity and $\eta_p = 100\eta_s$ is the viscosity inside a bead. The spheres at $\mathbf{r}_i$ are described by the density field,

$$\varphi_i(\mathbf{r}) = \frac{1}{2} \left[1 + \tanh \left(\frac{\nu - |\mathbf{r} - \mathbf{r}_i|}{\xi} \right) \right] \,. \tag{25}$$

The parameter ν describes the width of the η_p plateau, and ξ is the thickness of the depletion layer. The viscosity field enters the unsteady Stokes equations

$$\rho\partial_t\mathbf{v} = -\nabla p + \nabla\cdot\left[\eta(\mathbf{r})\left(\nabla\mathbf{v} + (\nabla\mathbf{v})^T\right)\right] + \mathbf{f} + \rho\mathbf{g}\,, \tag{26a}$$

$$\nabla\cdot\mathbf{v} = 0\,, \tag{26b}$$

which are solved numerically in order to obtain the velocity and pressure field of the fluid. The averaged velocity field around a particle is used to update the particle position which leads to a new viscosity field, and the procedure starts again. For further details and tests of the method we refer to [102, 103]. Note that thermal fluctuations can be included by adding a stochastic tensor on the right hand side of Eq. (26a), as described in [104].

The advantage of FPD is the clever implementation of the moving boundary conditions on the particle surfaces. Compared to other schemes like Brownian dynamics [105] and multiparticle-collision dynamics [106], the beads have a finite size and rotate in shear flows. Moreover, the complete hydrodynamic interactions between the particles are included in the velocity and pressure field of the solvent. Even at high volume fractions or large particle numbers no approximations must be made. Since the velocity field in the whole solvent is computed, one can calculate the stress tensor, σ, which allows rheological investigations. The possible applications of FPD are wide-ranging. It has been successfully applied to explore the dynamics of colloids in complex fluids [107], the polymer coil-globule transition [31], the effect of confinement on the rheology of a suspension of spheres [108], and the effective viscosity of microswimmer suspensions [109].

In *pub7*, we use the FPD method in order to investigate the connection between the motion of suspended objects and the rheology of the whole suspension. Therefore, we perform a numerical study on the following deterministic model system: One or several Hookean dumbbells are immersed in a Newtonian fluid in a rectangular flow channel. The equilibrium length of the spring between two beads is denoted with R_0. We create a linear shear flow in z direction with xz shear plane, as given by Eq. (22). During the simulation we measure the trajectories of all suspended objects as well as the effective viscosity, η_{eff}, via the stress tensor σ, cf. Eq. (23). We show that the effective viscosity is a function of the dumbbell length R_0.

The analysis of the motion of a single dumbbell reveals interesting effects. In the considered parameter range, the dumbbell is tumbling continuously, while the relative spring deformation, $\epsilon = (R(t)-R_0)/R_0$, changes periodically in time. The angle θ of the connection vector $\mathbf{R}$ between the two beads with respect to the flow direction characterizes the rotational dynamics, which are reflected in the course of $\eta_{eff}(t)$. Our detailed examination in *pub7* shows that the effective

viscosity consists of three different contributions. The volume fraction of the suspended object causes a constant offset, whereas the hydrodynamic interaction leads to an increase of $\eta_{eff}(t)$ when θ equals $\pi/2$. The third contribution is caused by elastic correlation effects, which are described by the force-orientation tensor $\lambda = \langle \mathbf{RF} \rangle$, as given by Eq. (21).

Increasing the number of dumbbells in the flow channel, and therefore the volume fraction Φ, leads to complex dynamics caused by the nonlinear hydrodynamic interactions. The resulting particle trajectories indicate a chaotic behavior. In this situation, we measure the averaged effective viscosity $\bar{\eta}_{eff} = \langle \eta_{eff}(t) \rangle$ as well as the dumbbell statistics. It turns out that the distribution function of the orientation angle, $\mathcal{P}(\theta)$, has two peaks at $\theta_1 \approx 0.1\pi$ and $\theta_2 \approx 0.9\pi$. The maximum at θ_1 is enhanced because the shear flow breaks the symmetry with respect to $\theta = \pi/2$. The distribution function of the relative spring deformation, $\mathcal{P}(\epsilon)$, shows a symmetric peak around $\epsilon = 0$, which broadens with increasing Weissenberg number.

Our numerical results for the effective viscosity of the dumbbell suspension can be compared with analytical predictions. In general, $\bar{\eta}_{eff}$ can be given in terms of a virial expansion for the volume fraction Φ,

$$\bar{\eta}_{eff}(\Phi) = \eta_s \left(1 + w_1 \Phi + w_2 \Phi^2 + \mathcal{O}(\Phi^3)\right) . \tag{27}$$

For a suspension of spheres in the dilute regime, where hydrodynamic interactions between the beads are negligible, A. Einstein calculated $w_1 = 2.5$ [110, 111], while G. Batchelor and J. Green determined the second order coefficient $w_2 = 5.2$ [112]. By the use of FPD it was shown that both coefficients, w_1 and w_2, change if the suspension of spheres is strongly confined [109]. Note that the shape of the suspended objects influences the viscosity as well [113].

First, we perform simulations on a suspension of beads in order to obtain a reference curve for the effective viscosity as a function of the volume fraction. Our numerical results are in good agreement with the Einstein-Batchelor-Green prediction as long as Φ is smaller than 8%. Above this value, the increase of $\bar{\eta}_{eff}$ is enhanced and higher order terms in the expansion (27) have to be included. For a suspension of dumbbells, the effective viscosity is increased compared to the case of spheres. A significant dependence of $\bar{\eta}_{eff}$ on the spring length R_0 is observed. For example, a duplication of R_0 at $\Phi = 10\%$ leads to an increase of the effective viscosity by 25%.

Our results, as presented in *pub7*, lead to the following outlook: According to Ref. [103] we expect to observe shear thinning for the investigated model system at large values of the Weissenberg number, but we did not yet investigate this parameter regime. Moreover, the complex nature of the individual particle trajectories at high volume fractions gives rise to another interesting question:

A. Groisman and V. Steinberg have shown in an experiment that polymers induce a chaotic motion in a microfluidic flow [23]. They observed a turbulent fluid motion, although the Reynolds number in the polymer solution was small. The effect is called elastic turbulence, as already mentioned before. However, the origin of this behavior is not completely understood due to the complexity of the experimental system. The suspended polymers have many degrees of freedom and are subjected to Brownian motion. Compared to that, we investigate a deterministic minimal model with simple deformable objects. However, the finding of complex, irregular motion in our simulations may contribute to the understanding of the elastic turbulence.

Publications

List of included publications as referred to in this thesis:

pub1 *Dumbbell diffusion in a spatially periodic potential*
J. Bammert, S. Schreiber, and W. Zimmermann,
Phys. Rev. E **77**, 042102 (2008)

pub2 *Dumbbell transport and deflection in a spatially periodic potential*
J. Bammert and W. Zimmermann,
Eur. Phys. J. E **28**, 331 (2009)

pub3 *Direct Measurement of Shear-Induced Cross-Correlations of Brownian Motion*
A. Ziehl, J. Bammert, L. Holzer, C. Wagner, and W. Zimmermann,
Phys. Rev. Lett. **103**, 230602 (2009)

pub4 *Dynamics of a trapped Brownian particle in shear flows*
L. Holzer, J. Bammert, R. Rzehak, and W. Zimmermann,
Phys. Rev. E **81**, 041124 (2010)

pub5 *Dynamics of two trapped Brownian particles: Shear-induced cross-correlations*
J. Bammert, L. Holzer, and W. Zimmermann,
Eur. Phys. J. E **33**, 313 (2010)

pub6 *The probability distribution of a trapped Brownian particle in plane shear flows*
J. Bammert and W. Zimmermann,
Phys. Rev. E **82**, 052102 (2010)

pub7 *Dynamics and rheology of dumbbell suspensions: a numerical study*
J. Bammert, P. Peyla, and W. Zimmermann,
preprint

Other publications not related to this thesis:

Wall attraction and repulsion of hydrodynamically interacting particles
S. Schreiber, J. Bammert, P. Peyla, and W. Zimmermann,
preprint

Publication 1

Dumbbell diffusion in a spatially periodic potential
J. Bammert, S. Schreiber, and W. Zimmermann,
Physical Review E **77**, 042102 (2008)

Copyright by The American Physical Society 2008
DOI: 10.1103/PhysRevE.77.042102

Dumbbell diffusion in a spatially periodic potential

Jochen Bammert, Steffen Schreiber, and Walter Zimmermann
Theoretische Physik I, Universität Bayreuth, D-95440 Bayreuth, Germany
(Received 2 October 2007; published 21 April 2008)

We present a numerical investigation of the Brownian motion and diffusion of a dumbbell in a two-dimensional periodic potential. Its dynamics is described by a Langevin model including the hydrodynamic interaction. With increasing values of the amplitude of the potential we find along the modulated spatial directions a reduction of the diffusion constant and of the impact of the hydrodynamic interaction. For modulation amplitudes of the potential in the range of the thermal energy the dumbbell diffusion exhibits a pronounced local maximum at a wavelength of about 3/2 of the dumbbell extension. This is especially emphasized for stiff springs connecting the two beads.

DOI: 10.1103/PhysRevE.77.042102 PACS number(s): 05.40.−a, 87.15.Vv, 82.35.Lr

Investigations of the diffusion of different colloidal particles in a homogeneous solvent have a long history [1,2], while studies of the diffusion of small spheres, dimers, and polymers in different potentials attracted considerable interest only for a short time [3–9]. Laser-tweezer arrays are a new powerful tool for generating the desired spatially periodic, correlated, or unstructured potentials in order to study the effects of inhomogeneous potential landscapes on the motion of colloidal particles [3–5,10]. Furthermore, recent studies of dumbbells and polymers in random potentials have created exciting results in statistical physics [11,12].

Several of these investigations are motivated by possible applications like particle sorting in inhomogeneous potentials. For example, cross-streamline migration of colloidal particles has been found in a flow through an optically induced periodic potential. Since this migration depends on the extent of the colloidal particles, the laser-tweezer array has been successfully used for sorting particles with respect to their size [4,10].

We investigate Brownian motion and the diffusion of dumbbells through a two-dimensional periodic potential, which is described by a Langevin model. In doing so we include the effects of the hydrodynamic interaction between the two beads of the dumbbell and focus on the interplay between the dumbbell extension b and the wavelength λ of the spatially periodic potential. In the context of this work the dumbbell may be considered as a simple model for anisotropic colloids [13] pom-pom polymers [14] or two spheres which are connected either by a rather flexible λ-DNA molecule or by a semi-flexible actin filament.

Our numerical studies reveal a significant dependence of the dumbbell diffusion on the ratio λ/b. With the potential amplitude V_0 of the order of the thermal excitation energy k_BT we find a remarkable maximum of the dumbbell diffusion constant in the range of $\lambda \approx 3b/2$. The height of this diffusion maximum increases with the stiffness of the spring connecting the two beads of the dumbbell. Another remarkable effect is the reduction of the influence of the hydrodynamic interaction with increasing potential amplitude.

We describe the Brownian motion of a dumbbell in a two-dimensional periodic potential by the Langevin equation (without inertia)

$$\dot{\mathbf{r}}_i = \mathbf{H}_{ij}(\mathbf{F}_j^{\Phi} + \mathbf{F}_j^{V}) + \mathbf{F}_i^{S} \quad (i,j=1,2) \tag{1}$$

for the bead positions $\mathbf{r}_i=(x_i,y_i,z_i)$. The linear spring force $\boldsymbol{F}_i^{\Phi}$ between them is determined by the harmonic potential

$$\Phi(\mathbf{r}_1,\mathbf{r}_2) = \frac{k}{2}(b-|\mathbf{r}_1-\mathbf{r}_2|)^2, \tag{2}$$

with the equilibrium length b of the spring and the corresponding spring constant k. The spatially periodic force $\mathbf{F}_i^V=-\boldsymbol{\nabla} V(\mathbf{r}_i)$ is derived from the two-dimensional potential in the xy plane,

$$V(\mathbf{r}_i) = 2V_0 \cos\left(\frac{x_i+y_i}{\lambda}\pi\right)\cos\left(\frac{x_i-y_i}{\lambda}\pi\right), \tag{3}$$

which can be realized in experiments by a laser-tweezer array. Its amplitude V_0 may be changed by varying the intensity of the laser light. The same wavelength λ is chosen in the x and y directions.

In the absence of hydrodynamic interactions (HI) between the beads the mobility matrix $\mathbf{H}$ is a diagonal matrix ($\mathbf{H}_{ii}=\frac{1}{\zeta}\mathbf{I}$, $\mathbf{H}_{ij}=0$ for $i\neq j$) being inversely proportional to the Stokes friction coefficient $\zeta=6\pi\eta a$ which depends on the solvent viscosity η as well as on the effective hydrodynamic bead radius a. The HI between the two beads is taken into account by the Rotne-Prager tensor [15] where the mobility matrix for $i\neq j$ has the following structure:

$$\mathbf{H}_{ij} = \frac{1}{8\pi\eta r_{ij}}\left[\left(1+\frac{2}{3}\frac{a^2}{r_{ij}^2}\right)\mathbf{I} + \left(1-2\frac{a^2}{r_{ij}^2}\right)\hat{\mathbf{r}}_{ij}\hat{\mathbf{r}}_{ij}^T\right]. \tag{4}$$

Note that $\mathbf{r}_{ij}=\mathbf{r}_i-\mathbf{r}_j$ is the distance vector between the beads and r_{ij} is its norm.

The stochastic forces $\mathbf{F}_i^S$ caused by the thermal heat bath are related to the dissipative drag by the fluctuation dissipation theorem which ensures the correct equilibrium properties. They can be combined to a single supervector $\mathbf{F}^S=(\mathbf{F}_1^S,\mathbf{F}_2^S)$, which reads

$$\mathbf{F}^S = \sqrt{2k_BT\mathbf{H}}\boldsymbol{\xi}. \tag{5}$$

T is the temperature, k_B the Boltzmann constant, and $\boldsymbol{\xi}(t)$ is the uncorrelated Gaussian white-noise vector with zero mean and unit variance:

 ©2008 The American Physical Society

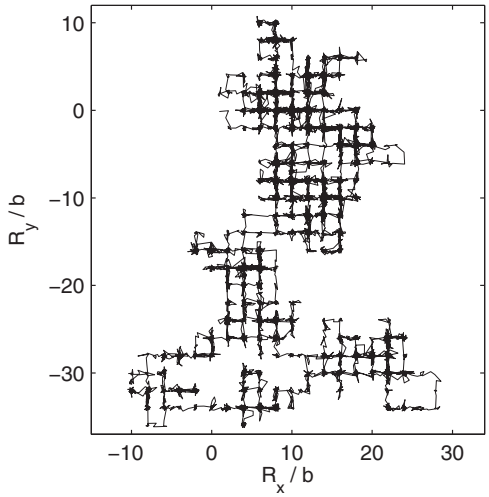

FIG. 1. The trajectory of the c.m. of the dumbbell in the xy plane follows predominantly along the saddles between the minima of the potential. Parameters: $k=10$, $V_0/k_BT=2$, and $\lambda=2b$.

$$\langle \boldsymbol{\xi}(t) \rangle = 0, \tag{6}$$

$$\langle \boldsymbol{\xi}(t) \boldsymbol{\xi}^T(t') \rangle = \delta(t-t')\mathbf{I}. \tag{7}$$

The fixed parameters in our simulations are $b=1$ for the typical length scale and $k_BT=1$ which determines the energy scale. If not stated otherwise, we use $\frac{a}{b}=\frac{1}{5}$, $\eta=1$. k determines the binding energy of the spring in units of the thermal energy $\frac{kb^2}{k_BT}$. Most of our results were observed after averaging over more than 10^4 ensembles.

A typical trajectory of the center of mass (c.m.) of the dumbbell, $\mathbf{R}=(\mathbf{r}_1+\mathbf{r}_2)/2$, in the xy plane is shown in Fig. 1 for $k=10$, $\lambda=2b$, and $V_0=2k_BT$. It passes the saddles between the maxima of the potential, and accordingly the trajectory adapts to the quadratic structure of the potential landscape. If one of the two parameters k or λ/b is reduced, larger excursions of the c.m. away from the potential minima occur and more diagonal jumps between the valleys are found.

The mean-square displacement $\langle R_l^2(t) \rangle = 2D_l t$ $(l=x,y,z)$ increases linearly in time along each spatial direction as shown for one parameter set in Fig. 2. This behavior is typical for normal diffusion. Parallel to the z direction one has an undisturbed diffusion and therefore the mean-square displacement and thus D_z are much larger than in the modulated x and y directions. Along these two directions the saddles and the local maxima between neighboring potential valleys act as barriers for the dumbbell motion and therefore D_x (equal to D_y) is smaller than D_z. Moreover, for a dumbbell in a solvent the HI between the two beads comes into play, which in general enhances the diffusion as can be seen by the shift between the solid and dashed lines in Fig. 2.

The decay of the dumbbell diffusion as a function of the ratio between the modulation amplitude of the potential and the thermal energy V_0/k_BT is shown in Fig. 3 for one parameter set with HI (solid line) and without HI (dashed line) between the beads. The decay of D_x is similar to the results described in Refs. [6,7] on the diffusion of point like particles. The difference between the two cases with and without HI is shrinking with an increasing modulation amplitude of the potential, because the higher diffusivity caused by HI becomes less important with increasing potential barriers. Accordingly, the ratio D_x/D_z between the diffusion along one modulated direction and the unmodulated direction is smaller with HI than for the case without HI, as shown in Fig. 3.

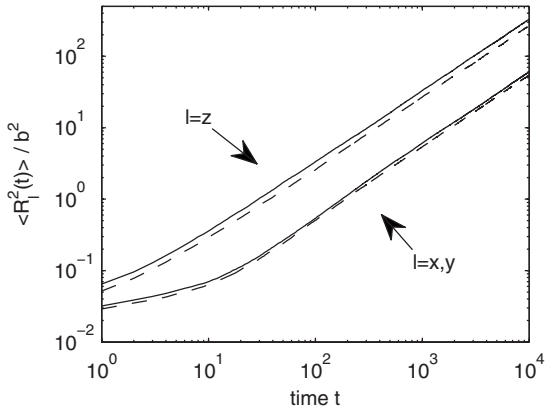

FIG. 2. The mean-square displacement of the c.m. of the dumbbell is shown along the x and y directions (lower lines) and along the z direction (upper lines) with HI between the beads (solid lines) and without (dashed lines). The parameters are the same as in Fig. 1.

In contrast to the diffusion of point particles the diffusion of a dumbbell along one modulated direction also depends on the interplay between the two length scales: namely, the bead distance b and the wavelength λ of the periodic potential modulation. A typical functional dependence of the dumbbell diffusion on the ratio λ/b is shown in Fig. 4, where the diffusion is remarkably enhanced for λ close to $\lambda_1=3b/2$. Further beyond this value the dumbbell diffusion decreases with increasing values of the wavelength up to a minimum $D_x(\lambda_2)$, which is at about $\lambda_2 \approx 6b$ for the given parameters (not shown in Fig. 4). The decay of D_x in the range $\lambda_1 < \lambda < \lambda_2$ can be explained in the following way. For increasing values $\lambda \gtrsim \lambda_1$ the beads become essentially caged within one single potential valley and an escape from such a

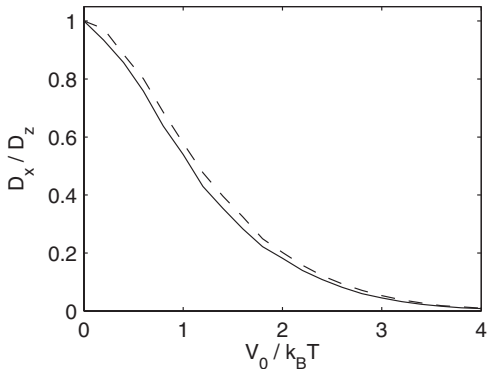

FIG. 3. The diffusion D_x $(=D_y)$ in the x direction is normalized by the free diffusion D_z in the z direction and plotted as a function of V_0/k_BT for the case with HI (solid line) and without HI (dashed line). The following parameters have been used: $k=10$ and $\lambda=2b$.

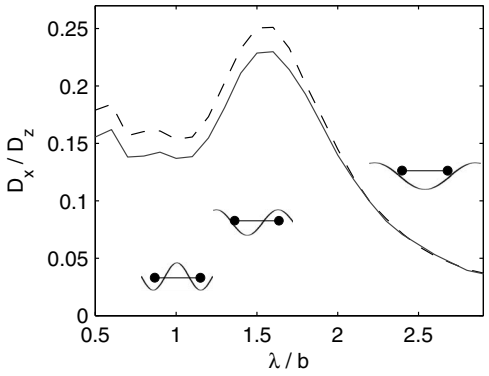

FIG. 4. The normalized diffusion constant D_x/D_z $(=D_y/D_z)$ of the dumbbell is shown as a function of the ratio between the equilibrium bead distance b and the wavelength λ for the case with HI (solid line) and without HI (dashed line). The insets illustrate possible locations of the dumbbell with respect to the periodic potential for different values of λ/b. The parameters are $V_0/k_BT=2$ and $k=10$.

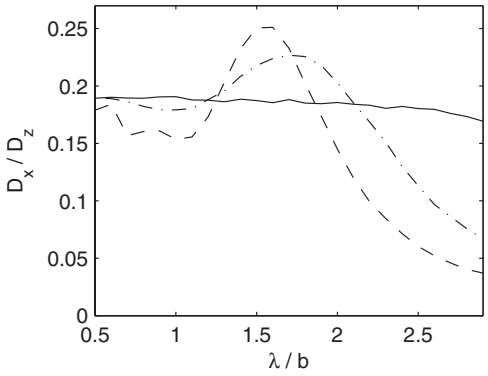

FIG. 5. The ratio between the diffusion constants D_x/D_z of the dumbbell is shown for three different values of the spring constant (solid line, $k=0.1$; dash-dotted line, $k=1$; dashed line, $k=10$) as a function of the ratio λ/b. The potential amplitude is $V_0=2k_BT$.

trap gets more and more unlikely (see right inset in Fig. 4). If the wavelength λ is increased further beyond λ_2, the mean-square displacement and the dumbbell diffusion increase again and finally approach the value of the unmodulated case, because for large wavelengths the dumbbell does not feel the potential anymore.

If on the other hand the modulation wavelength is reduced below λ_2, the distance from the potential minimum to a saddle is shortened. In such a case it becomes more likely that the dumbbell is kicked over a saddle to a neighboring potential valley. So the diffusion D_x increases with decreasing values in the range $\lambda_1<\lambda<\lambda_2$.

Near the maximum of the diffusion constant at $\lambda\approx\lambda_1$ an additional effect comes into play which supports a dumbbell movement from one potential valley to another and accordingly enhances the dumbbell diffusion. In this range the two beads hardly fit into one single potential valley as indicated by the middle inset in Fig. 4. Moreover, for a rather stiff spring both beads cannot reach the minima of two neighboring potential valleys simultaneously. So the required excitation energy is smaller than V_0 and for this reason the diffusive motion is enhanced.

In the range $\lambda\leq b$ the dumbbell easily finds an orientation in the potential plane where the two beads are located in two distinct minima; cf. the left inset of Fig. 4. Only one bead needs to be kicked to another valley in order to make progress for the c.m. of the dumbbell. Therefore, irrespective whether the two beads belong to nearest neighbor valleys or not, the required excitation energy for a shift of the c.m. depends only weakly on λ. This is the origin of the small variations of D_x in the range $\lambda<b$.

The explanation given for the local maximum of the diffusion constant in the range of λ_1 in Fig. 4 is supported by the influence of the spring constant k on the height of $D_x(\lambda_1)$ and on the mean distance $\langle r_{12}\rangle$. The local maximum of D_x is especially pronounced in the case of a rather stiff dumbbell (see Fig. 5) where the distribution of the bead distance $\rho(r_{12})$ is not changed by the periodic potential (see Fig. 6). On the other hand, for smaller values of k the maximum of $\rho(r_{12})$ is more and more shifted from b to λ. In this case the beads relax down to the potential valleys, so a higher excitation energy is required for a shift of the c.m., which results in a smaller diffusion constant as indicated by the solid line in Fig. 5.

The distance between the potential valleys depends on the direction in the xy plane, and therefore the orientational distribution of the dumbbell axis $\rho(\Phi)$ in Fig. 7 provides a complementary piece of information to $\rho(r_{12})$. The two beads of the dumbbell may relax more easily to the potential minima in the case of a soft spring (cf. solid lines in Fig. 7) compared to a stiff spring (cf. dashed lines). So the orientational distribution of the dumbbell axis in the xy plane shows, besides the maxima along the x and y directions, a local maximum for a diagonal orientation of the dumbbell axis. This is displayed in Fig. 7(a). If the wavelength is reduced to $\lambda=b$, one finds, in addition to the maximum in the diagonal direction (11), local maxima along the (21) and (12) directions, as indicated by Fig. 7(b).

The Brownian motion of a dumbbell in a two-dimensional periodic potential has been investigated in terms of a

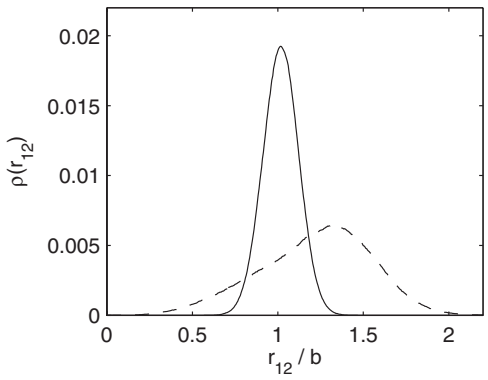

FIG. 6. The distribution $\rho(r_{12})$ of the bead distances is shown for two different values of the spring constant, $k=10$ (solid line) and $k=1$ (dashed line), and for the parameters $V_0/k_BT=2$ and $\lambda/b=3/2$.

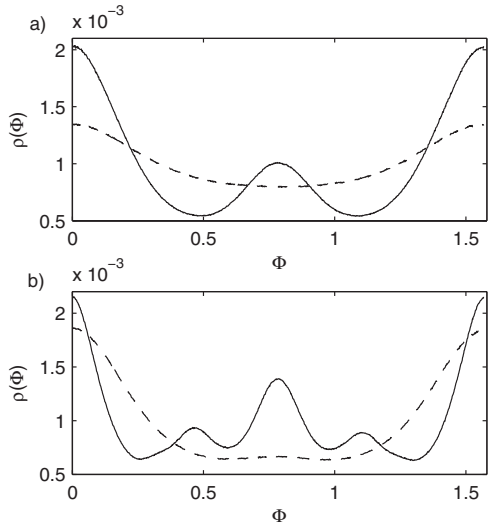

FIG. 7. The orientational distribution $\rho(\Phi)$ of the dumbbell axis in the xy plane is shown for two different values of the spring constant (solid line, $k=1$; dashed line, $k=10$) and for $V_0/k_BT=2$. The angle Φ is measured with respect to the x axis, and the ratio between the wavelength λ and the bead distance b is (a) $\lambda/b=2$ and (b) $\lambda/b=1$.

Langevin model. For an increasing barrier height between the potential minima, we find a decreasing diffusion constant for the center of mass along the modulated spatial directions as well as a reduction of the influence of the hydrodynamic interaction. For stiff springs the diffusion additionally depends on the ratio between the wavelength λ of the potential modulation and the equilibrium dumbbell extension b. In the range $\lambda \approx 3b/2$ this interplay is especially pronounced, because the two beads do not fit into one single or two neighboring potential minima anymore and this mismatch causes a reduced effective barrier height and thus an enhanced diffusion constant. If the spring constant is small, the beads can relax down to the potential minima over a wide range of λ, which results in a diffusion constant that is rather independent from λ in this domain. So the height of the maximum of the diffusion constant at $\lambda \approx 3b/2$ increases with the spring stiffness. For modulation wavelengths further beyond $3b/2$ the diffusion constant decays monotonically until some minimum is reached. In this range the dumbbell is essentially caged in one single potential valley and it is rather unlikely that it escapes. Beyond this minimum as λ goes to infinity the diffusion constant grows until the free diffusion limit is reached.

According to the dependence of the dumbbell diffusion on the ratio λ/b different values of the modulation wavelength λ in x and y directions cause an anisotropic diffusion behavior. In addition, the results presented may be useful for sorting polydisperse particle mixtures with respect to the particles' elasticity and size.

We would like to thank L. Holzer for instructive discussions. This work has been supported by the German Science Foundation through the priority program on micro- and nanofluidics No. SPP 1164.

[1] M. Doi and S. F. Edwards, *The Theory of Polymer Dynamics* (Clarendon Press, Oxford, 1986).
[2] A. Einstein, Ann. Phys. **17**, 549 (1905).
[3] P. T. Korda, M. B. Taylor, and D. G. Grier, Phys. Rev. Lett. **89**, 128301 (2002).
[4] M. P. MacDonald, G. C. Spalding, and K. Dholakia, Nature (London) **426**, 421 (2003).
[5] K. Ladavac, K. Kasza, and D. G. Grier, Phys. Rev. E **70**, 010901(R) (2004).
[6] A. H. Romero, A. M. Lacasta, and J. M. Sancho, Phys. Rev. E **69**, 051105 (2004).
[7] A. M. Lacasta, J. M. Sancho, A. H. Romero, and K. Lindenberg, Phys. Rev. Lett. **94**, 160601 (2005).
[8] C. Fusco and A. Fasolino, ChemPhysChem **6**, 1749 (2005).
[9] R. Tsekov and E. Ruckenstein, Surf. Sci. **344**, 175 (1995).
[10] Y. Roichman, V. Wong, and D. G. Grier, Phys. Rev. E **75**, 011407 (2007).
[11] V. G. Rostiashvili and T. A. Vilgis, J. Chem. Phys. **120**, 7194 (2004).
[12] M. Schulz, S. Stepanov, and S. Trimper, Europhys. Lett. **54**, 424 (2001).
[13] P. M. Johnson, C. M. van Kats, and A. van Blaaderen, Langmuir **21**, 11510 (2005).
[14] T. C. B. McLeish and R. G. Larson, J. Rheol. **42**, 81 (1998).
[15] J. Rotne and S. Prager, J. Chem. Phys. **50**, 4831 (1969).

Publication 2

Dumbbell transport and deflection in a spatially periodic potential
J. Bammert and W. Zimmermann,
European Physical Journal E **28**, 331 (2009)

Copyright by EDP Sciences, Società Italiana di Fisica, Springer-Verlag 2009
DOI: 10.1140/epje/i2008-10421-5

Eur. Phys. J. E **28**, 331–335 (2009)
DOI 10.1140/epje/i2008-10421-5

THE EUROPEAN PHYSICAL JOURNAL E

Regular Article

Dumbbell transport and deflection in a spatially periodic potential

J. Bammert[a] and W. Zimmermann[b]

Theoretische Physik I, Universität Bayreuth, D-95440 Bayreuth, Germany

Received 3 September 2008 and Received in final form 9 January 2009
Published online: 6 February 2009 – © EDP Sciences / Società Italiana di Fisica / Springer-Verlag 2009

Abstract. We present theoretical results on the deterministic and stochastic motion of a dumbbell carried by a uniform flow through a three-dimensional spatially periodic potential. Depending on parameters like the flow velocity, there are two different kinds of movement: transport along a potential valley and a stair-like motion oblique to the potential trenches. The crossover between these two regimes, as well as the deflection angle, depend on the size of the dumbbell. Moreover, thermal fluctuations cause a resonance-like variation in the deflection angle as a function of the dumbbell extension.

PACS. 47.61.-k Micro- and nano- scale flow phenomena – 05.40.-a Fluctuation phenomena, random processes, noise, and Brownian motion – 05.60.Cd Classical transport

1 Introduction

The exploration of particle motion in microfluidic devices and energy landscapes has attracted considerable attention recently, in particular due to its great potential for applications in chemistry and biotechnology [1–7]. With the successful generation of optically induced potentials by holographic laser tweezers [1,8], a powerful tool has been introduced for investigations of the classical transport of colloidal particles through those two- or three-dimensional landscapes. Since the interaction between the colloids and the potential depends on the size and shape of the particles, such potentials may also be used in microfluidic devices for a spatial decomposition of different particle species. For instance, spherical particles, carried by a flow with low Reynolds number, can be deflected into a direction oblique to the flow lines, while transversing a spatially periodic energy landscape [3,9]. Since the deflection angle is a function of the size and refraction index of the particles, this behavior may be used for particle sorting. For extended and deformable objects like vesicles, instead of spherical particles, a similar cross-streamline deflection has been found in Poiseuille flow even in the absence of a potential [6].

In this context, interesting questions arise: How are deformable objects, like dumbbells that are carried by a flow, deflected by a spatially periodic potential? What effects are related to the interplay between the wavelength of the potential and the size of the dumbbell [10]? What is the role of the hydrodynamic interaction between the two connected spherical particles?

Our numerical investigation of the flow-driven dumbbell motion in spatially periodic potentials can serve as a simple model for other non-spherical objects, such as dimers [11], pom-pom polymers [12], or two small beads connected by polymers. We find in this system two flow velocity thresholds separating three different regimes of motion: a locked stage, transport along a potential trench and a stair-like motion. In addition we detect a remarkable dependence of the dumbbell deflection angle on the ratio λ/b, where λ is the wavelength of the periodic potential and b is the length of the dumbbell. Furthermore, in the presence of stochastic thermal forces, interesting deflection resonances have been found as a function of λ/b.

2 Model

We investigate the dynamics of a dumbbell that consists of two beads connected by a linear spring, and driven by the uniform flow $\mathbf{u} = u(\cos\alpha, \sin\alpha, 0)$ through a three-dimensional spatially periodic potential. The over-damped motion of the dumbbell is described by the Langevin equation,

$$\dot{\mathbf{r}}_i = \mathbf{u} + \mathsf{H}_{ij}\left(\mathbf{F}_j^{\Phi} + \mathbf{F}_j^{V}\right) + \mathbf{F}_i^{S}, \qquad (i,j=1,2) \qquad (1)$$

for the two bead positions $\mathbf{r}_{1,2}$. The spring force, $\mathbf{F}_i^{\Phi} = -\nabla\Phi(\mathbf{r}_1 - \mathbf{r}_2)$, between the beads is derived from the harmonic potential

$$\Phi(\mathbf{r}_1 - \mathbf{r}_2) = \frac{k}{2}\left(b - |\mathbf{r}_1 - \mathbf{r}_2|\right)^2, \qquad (2)$$

[a] e-mail: jochen.bammert@uni-bayreuth.de
[b] e-mail: walter.zimmermann@uni-bayreuth.de

with the spring constant k and the equilibrium bead distance b. The force $\mathbf{F}_i^V = -\nabla V(\mathbf{r}_i)$ is caused by the periodic potential

$$V(\mathbf{r}_i) = -V_0 \left[\cos(qx_i) + \cos(qy_i) + \cos(qz_i)\right], \quad (3)$$

with wavelength $\lambda = 2\pi/q$ in all three spatial directions, and amplitude V_0. The third contribution on the right-hand side of equation (3) is included in order to keep the dumbbell axis in the xy-plane. In experiments such potentials can be realized by laser tweezers [3,9], where V_0 may be changed by varying the intensity of the laser beam.

Equation (1) is a nonlinear function of the bead distance due to the mobility matrix H_{ij}, which describes the hydrodynamic interactions (HI) between the two beads. Within the Rotne-Prager approximation [13] it has, for $i \neq j$, the form

$$\mathsf{H}_{ij} = \frac{3a}{4\zeta r_{ij}} \left[\left(1 + \frac{2}{3}\frac{a^2}{r_{ij}^2}\right) \mathsf{I} + \left(1 - 2\frac{a^2}{r_{ij}^2}\right) \hat{\mathbf{r}}_{ij}\hat{\mathbf{r}}_{ij}^T \right], \quad (4)$$

with $\mathbf{r}_{ij} = \mathbf{r}_i - \mathbf{r}_j$ and $r_{ij} = |\mathbf{r}_{ij}|$. The diagonal component of the mobility tensor, $\mathsf{H}_{ii} = \frac{1}{\zeta}\mathsf{I}$, with unity matrix I, is inversely proportional to the Stokes friction coefficient, $\zeta = 6\pi\eta a$, of a sphere with effective hydrodynamic radius a within a solvent of viscosity η.

The uncorrelated stochastic force $\mathbf{F}_i^S$ in equation (1) has a vanishing mean value. The amplitude of $\mathbf{F}_i^S$ is determined by the fluctuation dissipation theorem [14] and includes the thermal energy k_BT:

$$\langle \mathbf{F}_i^S(t) \rangle = 0, \quad (5)$$

$$\langle \mathbf{F}_i^S(t)\mathbf{F}_j^S(t') \rangle = 2k_BT\mathsf{H}_{ij}\delta(t-t'). \quad (6)$$

Equation (1) has been solved numerically by an Euler method, as approximate analytical solutions can only be obtained in some special cases. In our simulations we have fixed the values of $\lambda = 1$ and $V_0 = 1$, while all other lengths and energies are given in terms of them. Furthermore, we choose a radius of $a = 0.2$ for the beads, a spring constant of $k = 10$ and a Stokes friction coefficient of $\zeta = 10$. Angles are given in radians with respect to the x-axis. The time scale is set by the relaxation time of the spring $\tau = \zeta/k$, therefore the velocities are given in units of λ/τ. Since the flow direction $\mathbf{u}$ is restricted to the xy-plane, the periodic variation of the potential in the z-direction keeps the dumbbell axis in a single minimum with respect to z, *i.e.* $z = 0$. At the initial state of the calculations, we align the dumbbell parallel to the flow lines.

A typical situation investigated in this work is sketched in Figure 1. The dotted lines in the figure indicate the valleys of the periodic potential that are parallel to the x-axis (trenches parallel to the y-axis are not shown). The streamlines of the flow field $\mathbf{u}$ cross these valleys with an angle $\alpha < \pi/4$. This flow imposes a drag force $\mathbf{F}^\zeta$ on the beads of the dumbbell, which is proportional to u, and which depends on the bead distance r_{12}. If $\mathbf{F}^\zeta$ is large enough, the dumbbell moves with the mean velocity $\mathbf{v}$. Its deflection angle is denoted by β.

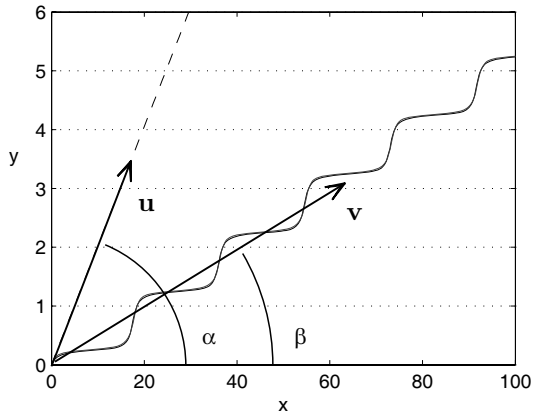

Fig. 1. Characteristic trajectory of the center of mass of a dumbbell (solid line) in the xy-plane, which is driven by the flow $\mathbf{u}$ through a three-dimensional periodic potential V. The mean velocity of the dumbbell is denoted by $\mathbf{v}$ and the horizontal dotted lines indicate the valleys of V parallel to the x-axis.

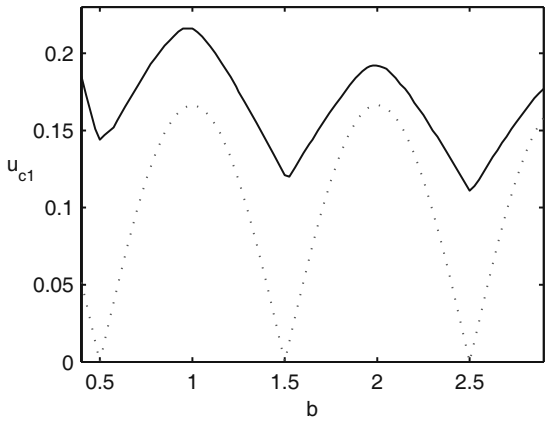

Fig. 2. The threshold velocity u_{c1} for driving the dumbbell along the x-direction is shown as a function of the equilibrium bead distance b (solid line). The dotted line indicates the analytical result calculated from equation (7).

3 Results

We first consider the dumbbell motion in the limit of vanishing thermal noise. For small flow strengths u the dumbbell is captured by the potential. If the flow velocity $\mathbf{u} = u(1,0,0)$ exceeds a certain threshold value u_{c1}, the dumbbell surmounts the saddles of the potential at a height V_0 and moves along a wavy potential trench with a periodically changing velocity parallel to the x-axis. The threshold velocity u_{c1} is a function of the bead distance b as shown in Figure 2 for one parameter set.

The dumbbell aligned with its axis parallel to the x-direction and with a fixed bead distance b experiences a potential force related to equation (3),

$$F^V(x, x+b) = -\frac{\partial}{\partial x}\left(V(x) + V(x+b)\right). \quad (7)$$

This force vanishes at bead distances $b = (2n+1)\lambda/2$, and accordingly the required flow velocity for driving the

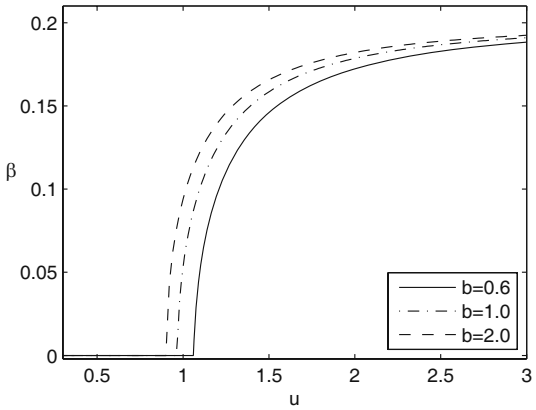

Fig. 3. The deflection angle β of the dumbbell is shown as a function of the flow velocity u at $\alpha = 0.2$ for different values of the bead distance b. In the regime of $\beta = 0$ the dumbbell moves along a potential trench.

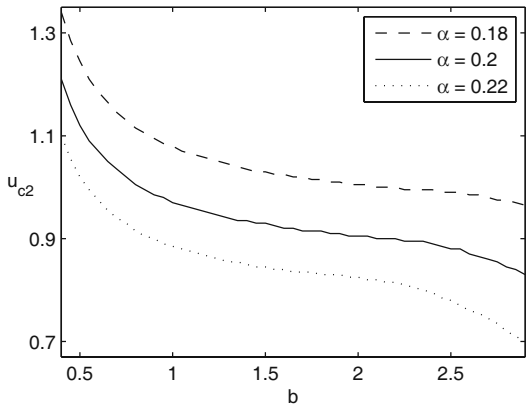

Fig. 4. The critical velocity u_{c2} for the onset of the stair-like motion is shown as function of b for three different inclination angles α and $u = 1$.

dumbbell continously through the potential also vanishes. However, at finite values of the spring constant k, corresponding to flexible objects like polymers etc., the dumbbell is stretched and compressed during its motion through the spatially modulated potential. With this degree of freedom the threshold flow velocity, u_{c1}, still has pronounced minima at the distances $b = (2n + 1)\lambda/2$ but it does not vanish as in the case of a fixed bead distance, especially if the HI is taken into account. This can be seen in Figure 2, where the dotted line indicates the threshold velocity of a rigid dumbbell. Moreover the HI reduces the drag force on the two beads. Since this reduction is proportional to $1/r_{12}$, the maxima of the curve $u_{c1}(b)$ decrease with increasing values of b.

If the flow velocity, $\mathbf{u} = u(\cos\alpha, \sin\alpha, 0)$, is increased further, one reaches, for finite angles α and beyond a second threshold velocity $u_{c2} > u_{c1}$, another regime of dumbbell motion. If the y-component of the drag force $\mathbf{F}^{\zeta}$ is large enough, the beads frequently jump to a neighboring trench of the potential parallel to the x-axis. Consequently the dumbbell performs a stair-like motion in the xy-plane as indicated by the solid line in Figure 1. The mean direction $\mathbf{v}$ of this motion has a finite deflection angle β, which depends on u as shown in Figure 3. In the limit of large values of u, β approaches the inclination angle α of the flow $\mathbf{u}$ as expected.

Since the drag force imposed by the flow on the dumbbell depends on the distance between the two beads, $\mathbf{r}_{12}$, the deflection angle is sensitive to the equilibrium length of the spring as indicated for three different values of b in Figure 3. Consequently the critical value u_{c2}, which marks the transition to finite values of β, is also sensitive to the bead separation. This monotone b-dependence of u_{c2} is shown for three different angles α in Figure 4.

During its stair-like motion in the xy-plane the dumbbell changes its orientation, which is described by the angle δ between $\mathbf{r}_{12}$ and the x-axis, while passing the saddles of the potential as indicated by the lower panel in Figure 5. The amplitude of δ depends on the dumbbell length b. With increasing values of u and α, those re-

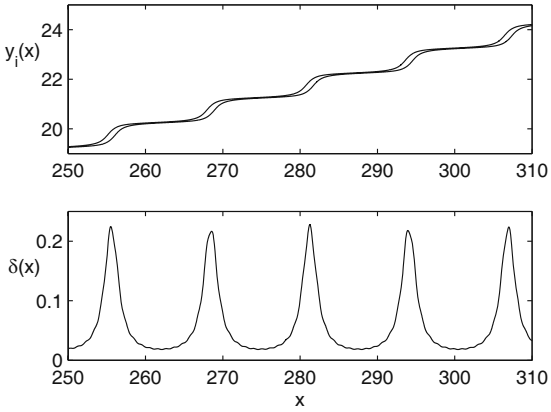

Fig. 5. The trajectories of the two beads in the xy-plane are shown in the upper panel for the parameters $\alpha = 0.2, u = 1, b = 1.5$. The lower panel shows the corresponding evolution of the orientation angle δ of the dumbbell.

orientation steps occur more often, accordingly the typical frequency of $\delta(t)$ increases as well as the angle β.

Alternatively one may vary the inclination angle α instead of the flow velocity u. If u is fixed at values larger than u_{c1}, the drag force $\mathbf{F}^{\zeta}$ is too weak at a small angle α to move the dumbbell across the potential barriers in the y-direction. But above a critical value α_c, which again depends on the length b of the dumbbell, one finds the transition from the motion along a potential valley to stair-like trajectories. The relation between β and the inclination angle α is shown in Figure 6. Note that, if the HI is neglected, all curves $\beta(\alpha)$ for dumbbells of different sizes coincide with the one of a single bead [15], which means that without HI the deflection angle has no b-dependence.

Just below the critical values α_c and u_{c2} thermal fluctuations support the passage of the beads between neighboring potential trenches and therefore may induce a stair-like motion in this parameter range. We investigated this influence of the thermal noise by taking into account the additive stochastic force $\mathbf{F}_i^S$ in the equation of motion (1).

The deflection angle β as a function of α is shown for different values of the noise amplitude in Figure 7. These

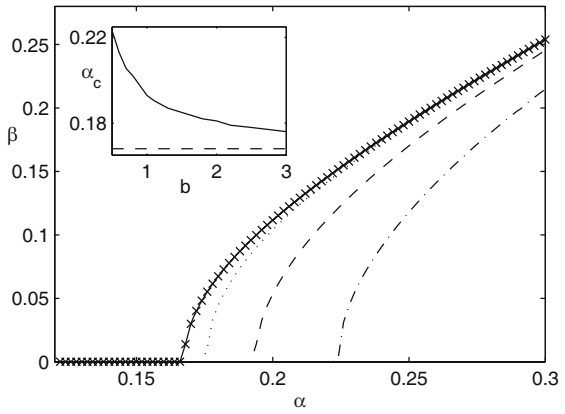

Fig. 6. The deflection angle β is shown as a function of the flow inclination angle α for different values of the dumbbell extension (dotted: $b = 3$, dashed: $b = 1$, dash-dotted: $b = 0.5$) and $u = 1$. The solid line is obtained for a dumbbell in the free-draining limit (without HI) and does not change with b. It coincides with the curve $\beta(\alpha)$ of a single bead (crosses). The inset shows the critical angle α_c versus b for a dumbbell with HI (solid) and without HI (dashed).

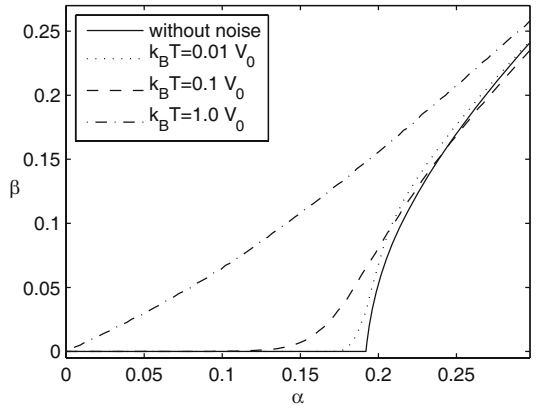

Fig. 7. The deflection angle β, averaged over 500 independent runs, of a dumbbell with $b = 1$ as a function of the flow angle α at $u = 1$ for different noise amplitudes.

numerical results, which are obtained by averaging over 500 independent runs, show that the dumbbell motion is most sensitive to thermal fluctuations close to the critical angle α_c or close to the critical velocity u_{c2}. The onset of the stair-like motion is shifted to smaller values of u or α as explained above, and in the limit of small noise amplitudes the deterministic result is approached. In the case of a noise amplitude in the order of V_0, the angles α and β become similar, indicating that the thermal motion is strong enough to kick the beads across the saddles of the potential. In this case all dumbbells are equally deflected and particle sorting is no longer possible.

Another interesting dependence of the deflection angle on the noise strength is shown in Figure 8, where β exhibits an interesting resonance-like behavior as a function of the bead distance b. The deflection angle is clearly reduced in the regime, where the dumbbell length is a multiple of the wavelength and a higher excitation energy

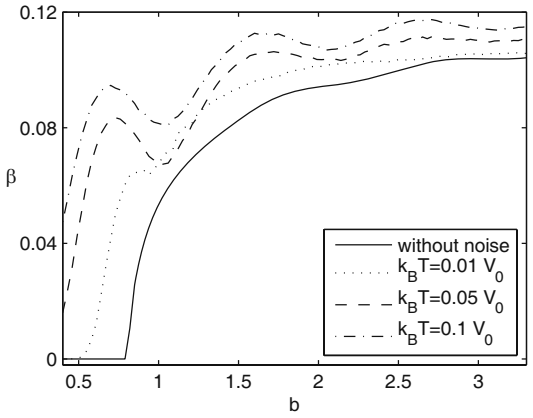

Fig. 8. The deflection angle β, averaged over 500 independent runs, shown as function of the dumbbell size b. It exhibits an interesting resonance-like behavior, especially for the noise amplitude $k_BT/V_0 = 0.1$. Parameters: $u = 1$, $\alpha = 0.2$.

of the dumbbell is required. According to the behavior shown in Figure 8, dumbbell sorting with respect to the size is most efficient within the range $0.5 < b/\lambda < 1.5$ in the limit of $k_BT \ll V_0$.

4 Conclusions and discussion

We investigated the flow-induced transport of mesoscopic and deformable dumbbells through a spatially periodic potential and found three different regimes of motion. The transitions between these regimes depend sensitively on the flow velocity, on the size of the dumbbell, and therefore on the hydrodynamic interactions between the two beads. Below a first critical velocity the dumbbell is locked by the potential while above this threshold the two beads start to move along a potential valley. The critical flow strength depends on the length of the dumbbell in a periodic way. If the flow velocity increases further at a finite inclination angle and crosses a second threshold, then a transition to a stair-like motion occurs. The preferred mean direction of this motion is neither along the flow nor along a symmetry direction of the potential, and the resulting deflection angle depends on the length of the dumbbell. This allows for the use of periodic potentials, with their symmetry axis oblique to the flow direction, to deflect particles with respect to their size. The strongest sensitivity of the deflection angle on the dumbbell length, which may be employed for particle sorting purposes, occurs in the crossover regime to the stair-like motion. This crossover is sensitive to thermal noise because thermal fluctuations make the transition less sharp. Moreover they induce a resonance-like structure in the deflection angle caused by the interplay between the wavelength of the potential and the size of the dumbbell. These effects, which weaken the efficency of particle sorting, may be suppressed by increasing the potential amplitude and the flow velocity simultaneously. Note that the results in the regime of the transition to the stair-like motion can be obtained qualitatively too, if an experimentally easier accessible potential

is chosen by neglecting the first contribution on the right-hand side of equation (3).

We would like to thank L. Holzer and S. Schreiber for instructive discussions. This work has been supported by the German Science Foundation through the priority program on micro- and nanofluidics SPP 1164.

References

1. P.T. Korda, M.B. Taylor, D.G. Grier, Phys. Rev. Lett. **89**, 128301 (2002).
2. M. De Lucia, A. Mazzino, A. Vulpiani, Europhys. Lett. **60**, 181 (2002).
3. M.P. MacDonald, G.C. Spalding, K. Dholakia, Nature **426**, 421 (2003).
4. J.A. Davis *et al.*, Proc. Natl. Acad. Sci. U.S.A. **103**, 14779 (2006).
5. R.L. Smith, G.C. Spalding, K. Dholakia, M.P. MacDonald, J. Opt. A: Pure Appl. Opt. **9**, S134 (2007).
6. B. Kaoui *et al.*, Phys. Rev. E **77**, 021903 (2008).
7. S. Kapishnikov, V. Kantsler, V. Steinberg, J. Stat. Mech. P01012 (2006).
8. M.P. MacDonald *et al.*, Science **296**, 1101 (2002).
9. K. Ladavac, K. Kasza, D.G. Grier, Phys. Rev. E **70**, 010901(R) (2004).
10. J. Bammert, S. Schreiber, W. Zimmermann, Phys. Rev. E **77**, 042102 (2008).
11. P.M. Johnson, C.M. van Kats, A. van Blaaderen, Langmuir **21**, 11510 (2005).
12. T.C.B. McLeish, R.G. Larson, J. Rheol. **42**, 81 (1998).
13. J. Rotne, S. Prager, J. Chem. Phys. **50**, 4831 (1969).
14. J.K.G. Dhont, *An Introduction to Dynamics of Colloids* (Elsevier, Amsterdam, 1996).
15. M. Pelton, K. Ladavac, D.G. Grier, Phys. Rev. E **70**, 031108 (2004).

Publication 3

Direct Measurement of Shear-Induced Cross-Correlations of Brownian Motion
A. Ziehl, J. Bammert, L. Holzer, C. Wagner, and W. Zimmermann,
Physical Review Letters **103**, 230602 (2009)

Copyright by The American Physical Society 2009
DOI: 10.1103/PhysRevLett.103.230602

Direct Measurement of Shear-Induced Cross-Correlations of Brownian Motion

A. Ziehl,[1] J. Bammert,[2] L. Holzer,[2] C. Wagner,[1] and W. Zimmermann[2]
[1]*Technische Physik, Universität des Saarlandes, 66041 Saarbrücken, Germany*
[2]*Theoretische Physik I, Universität Bayreuth, 95440 Bayreuth, Germany*
(Received 26 July 2009; published 3 December 2009)

Shear-induced cross-correlations of particle fluctuations perpendicular and along streamlines are investigated experimentally and theoretically. Direct measurements of the Brownian motion of micron-sized beads, held by optical tweezers in a shear-flow cell, show a strong time asymmetry in the cross-correlation, which is caused by the non-normal amplification of fluctuations. Complementary measurements on the single particle probability distribution substantiate this behavior and both results are consistent with a Langevin model. In addition, a shear-induced anticorrelation between orthogonal random displacements of two trapped and hydrodynamically interacting particles is detected, having one or two extrema in time, depending on the positions of the particles.

DOI: 10.1103/PhysRevLett.103.230602 PACS numbers: 05.40.Jc, 47.15.G−, 82.70.−y, 87.80.Cc

The Brownian motion of particles in fluids and their hydrodynamic interactions are of central importance in chemical and biological physics as well as in material science and engineering [1–4]. However, our understanding of the dynamics of particles in flows is still far from complete. Direct observations of particles at the mesoscale substantially contribute to our understanding of their dynamics. At this scale optical tweezers are a powerful experimental technique [5] with a number of innovative applications. They include the detection of anticorrelations between hydrodynamically interacting Brownian particles [6], propagation of hydrodynamic interactions [7], short-time inertial response of viscoelastic fluids [8], two-point microrheology [9], anomalous vibrational dispersion [10], and particle sorting techniques [11].

Neutral colloidal particles moving relatively to each other interact via the fluid and these hydrodynamic interactions decay with the particle distance [2]. In shear flow little is known about the dynamics of Brownian particle motion and the hydrodynamic interaction effects in spite of their fundamental relevance and importance in applications in microfluidics, Taylor dispersion [12], and in fluid mixing [4,13]. In time dependent fields and in shear flow surprising deterministic particle dynamics may be induced by hydrodynamic interactions [14]. For polymers it is the interplay of shear flow and fluctuations which leads already at low Reynolds numbers, to rich dynamics [15], the so-called molecular individualism [16], causing elastic turbulence even in diluted polymer solutions [17] and spectacular mixing behavior [13].

It is the contribution $(\mathbf{u}\cdot\nabla)\mathbf{u}$ to the Navier-Stokes equation which causes interesting transient phenomena in shear flows near the onset of turbulence [18], as well as amplifications of fluctuations and their cross-correlations along and perpendicular to straight streamlines [19,20]. A cross-correlation is also expected between orthogonal particle-fluctuations in the shear plane, because random jumps of a particle between neighboring streamlines of different velocity lead to a change of the particle's velocity and displacement along the streamlines, similar as via fluctuations. In some parameter ranges, inertia effects may become important [21–23]. Cross-correlations between perpendicular fluid-velocity fluctuations and perpendicular fluctuations of particles are expected to be strongly asymmetric in time [19,23,24]. In dynamic light-scattering experiments certain aspects of these shear-induced cross-correlations were observed indirectly [25], but a direct measurement and characterization of related particle fluctuations is missing.

Here we investigate in a linear shear flow the fluctuations of a single particle in a potential minimum and of two hydrodynamically interacting particles trapped by two neighboring potentials. We use a special shear-flow cell, where one or two micron-sized beads are held at its center by optical tweezers. The time asymmetry of shear-induced cross-correlations were determined directly by measuring the particle's positional fluctuations. In addition the probability distribution of a single particle in a trap was measured, which can be also calculated in terms of a Langevin model, similar to the correlations. Both the probability distribution and the correlation can be fitted by using the same value of the shear rate, which altogether gives a consistent picture of not yet directly observed shear-induced cross-correlations of particle fluctuations.

By a dual beam optical tweezer setup, composed of two solid state lasers and an oil immersion objective with a numerical aperture of 1.4, two harmonic potentials are generated in an inverted microscope (Nikon TE 2000-S) to capture uncharged polystyrene beads (Duke Scientific Corporation, R0300) with a diameter of 3 μm in a flow of distilled water. The beads were observed with a high speed camera (IDT, X-Stream, XS-5) of 15 kHz and their positions were determined with a correlation tracking algorithm with a spatial resolution of ± 4 nm [26]. To avoid any interference of the two potentials at small distances and to maximize the hydrodynamic interaction effect between the

 © 2009 The American Physical Society

two particles, they where held at a distance of $d = 4\ \mu$m. In a microfluidic device with two counter flows, as shown in Fig. 1, a linear shear gradient with a vanishing mean velocity was generated at the center of the cell, as experimentally verified by micro-PIV (see inset in Fig. 1). The design of the flow chamber was optimized by numerical simulations of the incompressible Navier-Stokes equation (Multiphysics 3.4, Comsol AB, Stockholm, Sweden). The small width in x direction of the center piece of the chamber was chosen in order to minimize flow in y direction. The curved form of the boundaries was found to suppress vortices. The channel was manufactured by standard soft lithographic techniques and the flow was driven by gravitational potential difference. The distance of the beads from the wall was always larger than 10 μm in the z direction and 25 μm in the xy plane. Hence boundary effects on the bead fluctuations could be excluded within our experimental resolution, as verified by measurements without flow, which were in very good agreement with previous results (see, e.g., Ref. [6]). However, with flow the experimental noise becomes larger, especially at longer correlation times. The value of the shear rate $\dot{\gamma}$ has been extracted from the fits of the correlation data and by particle tracking methods. The highest shear rate that did not lead to an escape of the particles from the traps was $\dot{\gamma} \simeq 50\ \mathrm{s}^{-1}$ [27].

One or two Brownian particles with coordinates $\mathbf{r}_i = (x_i, y_i, z_i)$ $(i = 1, 2)$ are held in a linear shear flow $\mathbf{u}(y_i) = \dot{\gamma} y_i \hat{\mathbf{e}}_x$ by forces $\mathbf{f}_i^V = k(\mathbf{p}_i - \mathbf{r}_i)$ close to the minima $\mathbf{p}_i$ of two harmonic potentials $V_i = \frac{k}{2}(\mathbf{p}_i - \mathbf{r}_i)^2$ (spring constant k). The overdamped particle motion is described by a Langevin equation [2]:

$$\dot{\mathbf{r}}_i = \mathbf{u}(\mathbf{r}_i) + \mathsf{H}_{ij}(\mathbf{f}_j^V + \mathbf{f}_j^S). \tag{1}$$

The mobility matrix H_{ij} accounts for the Stokes friction and the hydrodynamic interactions between them. Here we use the Oseen approximation

$$\mathsf{H}_{11} = \mathsf{H}_{22} = \frac{1}{\zeta}\mathsf{E}, \tag{2}$$

$$\mathsf{H}_{12} = \mathsf{H}_{21} = \frac{1}{\zeta}\frac{3a}{4r_{12}}\left[\mathsf{E} + \frac{\mathbf{r}_{12}\mathbf{r}_{12}^T}{r_{12}^2}\right], \tag{3}$$

with the Stokes friction coefficient $\zeta = 6\pi\eta a$ of a point particle of effective hydrodynamic radius a in a fluid of viscosity η and the unity matrix E. $\mathbf{r}_{12} = \mathbf{r}_1 - \mathbf{r}_2$ is the bead distance and r_{12} is its norm, $\tau = \zeta/k$ the particle relaxation time in the potential and $W = \dot{\gamma}\tau$ the Weissenberg number. The Brownian particle motion is driven by the stochastic forces $\mathbf{f}_i^S(t)$ in Eq. (1), for which we assume vanishing mean values and correlation times:

$$\langle \mathbf{f}_i^S(t) \rangle = 0, \tag{4}$$

$$\langle \mathbf{f}_i^S(t)\mathbf{f}_j^S(t') \rangle = 2k_BT\mathsf{H}_{ij}^{-1}\delta(t - t'). \tag{5}$$

At first we investigate the Brownian motion of a single trapped particle in shear flow. Its autocorrelation along the flow direction, $\langle x(0)x(0) \rangle = \frac{k_BT}{k}(1 + W^2/2)$, depends on W, but along the perpendicular direction, $\langle y(t)y(0) \rangle = \frac{k_BT}{k}\exp(-\frac{t}{\tau})$, it does not depend on W [24]. In a quiescent fluid cross-correlations between particle displacements in *orthogonal directions* vanish: $\langle x(t)y(t') \rangle = 0$. But shear flow causes in the shear plane finite cross-correlations [21,23,28], which are asymmetric with respect to $t \longrightarrow -t$ [24]:

$$\langle x(t)y(0) \rangle = \frac{k_BT}{k}\frac{W}{2}e^{-t/\tau}\left(1 + 2\frac{t}{\tau}\right), \tag{6}$$

$$\langle x(0)y(t) \rangle = \frac{k_BT}{k}\frac{W}{2}e^{-t/\tau}. \tag{7}$$

The algebraic prefactor in Eq. (6) illustrates that a fluctuation $y(0) \neq 0$ of a particle is carried away by the flow in the x direction before the initial displacement $y(0)$ relaxes. This leads, during an initial period shorter than the relaxation time τ, to a growth of $\langle x(t)y(0) \rangle$, while the expression in Eq. (7) decays monotonically. As shown in Fig. 2, the predicted elementary signatures for the shear-induced cross-correlations, cf. Eq. (6), are in agreement with our experimental data (triangles). Here $\langle x(t)y(0) \rangle$ takes its maximum roughly at $t \approx 0.009s$, corresponding via Eq. (6) to a particle's relaxation time $\tau \approx 0.018s$. Also the initial decay of $\langle x(0)y(t) \rangle$ (squares in Fig. 2) agrees with our model; cf. Eq. (7). The additionally observed minimum is possibly caused by a slight inclination of the laser beam or it is a reminiscent of a long wavelength oscillation due to the limited number of samples taken [27]. For fluid velocity fluctuations in orthogonal directions in the shear plane a similar signature as in Eq. (6) has been found [19]. According to Eq. (6) and (7) one obtains the normalized ratios of the static cross-correlations: $\langle x(0)y(0) \rangle / \langle y(0)y(0) \rangle = W/2$ and $\langle x(0)y(0) \rangle / \langle x(0)x(0) \rangle = \frac{W/2}{1+W^2/2}$ [24]. From the fits, as indicated by the red and blue line

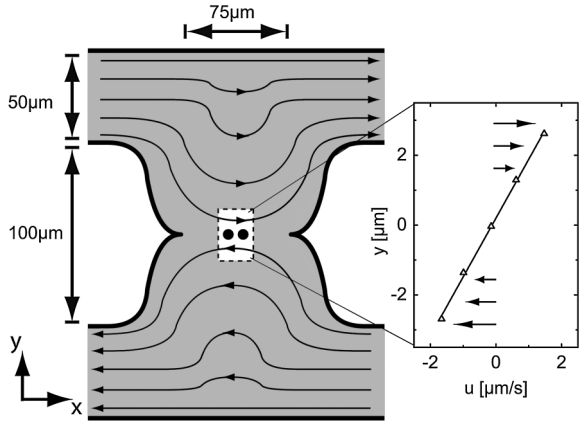

FIG. 1. A cell cross section (lithographic mask) is shown with 150 μm depth in the z direction having opposite flow directions in its upper and lower channel and a linear shear profile at its center: see inset with PIV data (Δ) and linear fit. One or two particles at a distance $d = 4\ \mu$m were held by optical tweezers in the center of the linear velocity profile $\mathbf{u}(y)$.

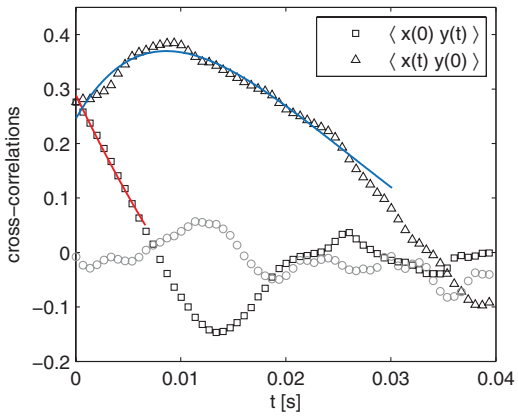

FIG. 2 (color). Shear-induced cross-correlations between orthogonal random displacements: $\langle x(t)y(0)\rangle$ (triangles) and $\langle x(0)y(t)\rangle$ (squares). Lines are fits according to Eq. (6) and (7) and open circles represent $\langle x(0)y(t)\rangle$ in the absence of flow.

in Fig. 2, we obtain $\langle x(0)y(0)\rangle/\langle x(0)x(0)\rangle \approx 0.26$, which corresponds to a Weissenberg number $W \approx 0.62$.

The probability distribution of a Brownian particle in a harmonic potential and exposed to a linear shear flow has an elliptical cross section as shown by the particle's position in Fig. 3 but it has circular symmetry in the absence of flow. The angle ϕ enclosed by the major axis of the particle's probability distribution and the x axis, as well as the ratio R between the lengths of the two principal axes, in the shear plane, depend on the Weissenberg number W as follows [24]:

$$\tan\phi = \tfrac{1}{2}[\sqrt{4+W^2} - W], \tag{8}$$

$$R = \left(\frac{\sqrt{4+W^2} - W}{\sqrt{4+W^2} + W}\right)^{1/2}. \tag{9}$$

Using $W \approx 0.62$ as determined above, one obtains via Eq. (8) the angle $\phi \approx 37°$ and via Eq. (9) the ratio $R \approx 0.72$. Within errors this is consistent with the angle $\phi \approx 38°$ and the ratio $R \approx 0.75$ obtained from the measured particle's distribution shown in Fig. 3.

For two particles, each trapped in a potential minimum in shear flow, we investigated the correlations between their random displacements for two different configurations: With the connection vector $\mathbf{p}_{12} = \mathbf{p}_1 - \mathbf{p}_2$ parallel to the flow direction as in Fig. 1 or perpendicular to it.

For Brownian displacements of the two distinct particles along the same direction the quantities $\langle x_i(t), x_j(0)\rangle$ and $\langle y_i(t), y_j(0)\rangle$ describe anticorrelations for $i \neq j$ (see, e.g., Ref. [6]). The shear-induced corrections for both are of the order of W^2 as described in more detail in Ref. [24]. For random displacements of distinct particles, but along orthogonal directions, one only finds correlations in the presence of shear flow. With the abbreviations

$$\lambda_{1,3} = 1 \pm 2\mu, \qquad \lambda_{2,4} = 1 \pm \mu, \qquad \mu = \frac{3a}{4d}, \tag{10}$$

and the connection vector $\mathbf{p}_{12}$ parallel to the flow two of the anti-cross-correlations in the shear plane are [24]

$$\langle x_1(t)y_2(0)\rangle = \frac{k_BT}{\mu k}\frac{W}{2}\left(e^{-\lambda_2 t/\tau} + e^{-\lambda_4 t/\tau} - \frac{2\lambda_2 e^{-\lambda_1 t/\tau}}{2+3\mu} - \frac{2\lambda_4 e^{-\lambda_3 t/\tau}}{2-3\mu}\right), \tag{11}$$

$$\langle x_1(0)y_2(t)\rangle = \frac{k_BT}{k}\frac{W}{2}\left(\frac{e^{-\lambda_2 t/\tau}}{2+3\mu} - \frac{e^{-\lambda_4 t/\tau}}{2-3\mu}\right). \tag{12}$$

The cross-correlation $\langle x_1(t)y_2(0)\rangle$ (triangles) in Fig. 4 and the fit (blue line) show a pronounced minimum at about the particles relaxation time $t \approx \tau$.

With a connection vector $\mathbf{p}_{12}$ perpendicular to the flow lines we obtain a cross-correlation $\langle x_2(t)y_1(0)$ in the limit of small values of μ,

$$\langle x_2(t)y_1(0)\rangle \approx -\frac{k_BT}{2k}\frac{W\mu}{2}e^{-t/\tau}\left(3 + 2\frac{t}{\tau} + 6\frac{t^2}{\tau^2}\right),$$

which exhibits in contrast to Eq. (11) two extrema.

Shear-induced cross-correlations between random displacements of a single particle in a potential were calcu-

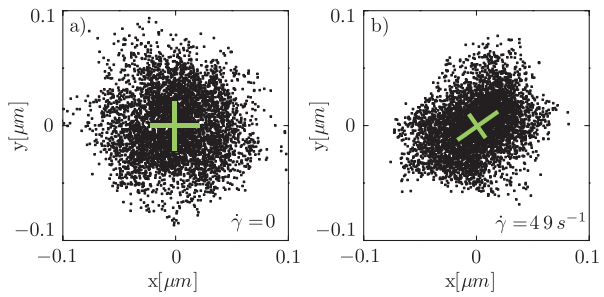

FIG. 3 (color online). The particle's distribution in the shear plane is shown in a) without flow and for a shear flow with $\dot\gamma = 49\ s^{-1}$ in b). The angle between the major and the x axis is $\phi \approx 38°$ and the ratio between the two principal axes is $R \approx 0.75$.

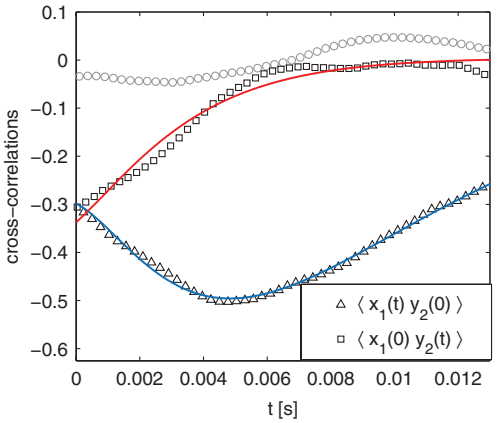

FIG. 4 (color). Correlations $\langle x_1(t)y_2(0)\rangle$ (triangles) and $\langle x_1(0)y_2(t)\rangle$ (squares) between random displacements of two particles. Colored lines are fits according to Eq. (11) and (12). Circles represent the same correlations in the absence of flow.

lated and measured here for the first time, to the best of our knowledge, cf. Fig. 2. At approximately half of the particle's relaxation time τ the correlation function in Eq. (6) exhibits with its maximum a typical signature of Brownian motion in shear flow, caused by the rotational part of the shear flow as well as the non-normal property of the linearized Navier-Stokes equation. Simultaneously, for a particle in a harmonic potential and shear flow an elliptical probability distribution was measured. Both independent measurements are described by a Langevin model for the same value of the Weissenberg number, which confirms the validity of our approach to shear-flow effects on the Brownian particle dynamics.

Theoretically, shear-induced correlations between perpendicular fluid velocity fluctuations have been investigated before [19,20]. Those are traced back to the non-normal property of the linearized Navier-Stokes equation [19] and they are important for the stability of shear flow and the onset of turbulence. The cross-correlations between these velocity fluctuations are based on the same mechanism as discussed here and they exhibit similar extrema as our experimental and analytical results.

Stochastic forces on a suspended particle are caused by velocity fluctuations of the surrounding fluid. Usually, they are assumed to be isotropic in related Langevin models with uncorrelated perpendicular components. However, cross-correlations of the velocity fluctuations in shear flow, as discussed in Refs. [19,20], will modify the cross-correlations between orthogonal particle displacements, as investigated here, but the related additional contributions to the particle displacement correlations are expected to be considerably smaller than the effects of isotropic random forces [24]. It is, however, an interesting and challenging future issue to separate these two nonequilibrium effects in experiments.

For two hydrodynamically interacting particles, each captured by an optical tweezer at the center of the shear flow, we find shear-induced anticorrelations between orthogonal particle displacements with one extremum if the vector connecting the mean particle positions is parallel to the streamlines and two extrema, if the connection vector is perpendicular to the flow lines. These properties may be relevant for further understanding of the dynamics of polymer models in shear flow.

This work was supported by the German science foundation via the priority program on micro- and nanofluidics SPP 1164 and the graduate school GRK 1276.

[1] A. Einstein, Ann. Phys. (Leipzig) **17**, 549 (1905).
[2] J. K. G. Dhont, *An Introduction to Dynamics of Colloids* (Elsevier, Amsterdam, 1996).
[3] H. A. Stone and S. Kim, AIChE J. **47**, 1250 (2001).
[4] J. M. Ottino and S. Wiggins, Phil. Trans. R. Soc. A **362**, 923 (2004).
[5] A. Ashkin, J. M. Dziedzic, J. E. Bjorkholm, and S. Chu, Opt. Lett. **11**, 288 (1986); D. G. Grier, Nature (London) **424**, 21 (2003).
[6] J.-C. Meiners and S. R. Quake, Phys. Rev. Lett. **82**, 2211 (1999).
[7] S. Henderson, S. Mitchell, and P. Bartlett, Phys. Rev. Lett. **88**, 088302 (2002).
[8] M. Atakhorrami, G. H. Koenderink, C. F. Schmidt, and F. C. MacKintosh, Phys. Rev. Lett. **95**, 208302 (2005).
[9] J. C. Crocker *et al.*, Phys. Rev. Lett. **85**, 888 (2000).
[10] M. Polin, D. G. Grier, and S. Quake, Phys. Rev. Lett. **96**, 088101 (2006).
[11] P. T. Korda, M. B. Taylor, and D. G. Grier, Phys. Rev. Lett. **89**, 128301 (2002); M. P. MacDonald, G. C. Spalding, and K. Dholakia, Nature (London) **426**, 421 (2003); J. Bammert and W. Zimmermann, Eur. Phys. J. E **28**, 331 (2009).
[12] G. I. Taylor, Proc. R. Soc. A **219**, 186 (1953).
[13] A. Groisman and V. Steinberg, Nature (London) **410**, 905 (2001).
[14] C. Lutz, M. Reichert, H. Stark, and C. Bechinger, Europhys. Lett. **74**, 719 (2006); L. Holzer and W. Zimmermann, Phys. Rev. E **73**, 060801(R) (2006).
[15] T. T. Perkins, D. E. Smith, and S. Chu, Science **276**, 2016 (1997).
[16] P. G. de Gennes, Science **276**, 1999 (1997).
[17] A. Groisman and V. Steinberg, Nature (London) **405**, 53 (2000).
[18] S. Grossmann, Rev. Mod. Phys. **72**, 603 (2000).
[19] B. Eckhardt and R. Pandit, Eur. Phys. J. B **33**, 373 (2003).
[20] G. Khujadze, M. Oberlack, and G. Chagelishvili, Phys. Rev. Lett. **97**, 034501 (2006); A. Jachens, J. Schuhmacher, B. Eckhardt, K. Knobloch, and H. H. Fernholz, J. Fluid Mech. **547**, 55 (2006).
[21] K. Miyazaki and D. Bedeaux, Physica (Amsterdam) **217A**, 53 (1995).
[22] T. B. Liverpool and F. C. MacKintosh, Phys. Rev. Lett. **95**, 208303 (2005).
[23] Y. Drossinos and M. W. Reeks, Phys. Rev. E **71**, 031113 (2005).
[24] L. Holzer, J. Bammert, and W. Zimmermann, arXiv:0911.3264v1.
[25] R. T. Foister and T. G. M. van der Ven, J. Fluid Mech. **96**, 105 (1980); G. G. Fuller, J. M. Rallison, R. L. Schmidt, and L. G. Leal, J. Fluid Mech. **100**, 555 (1980); M. Hoppenbrouwers and W. van de Water, Phys. Fluids **10**, 2128 (1998).
[26] M. K. Cheezum, W. F. Walker, and W. H. Guilford, Biophys. J. **81**, 2378 (2001).
[27] See EPAPS Document No. E-PRLTAO-103-061950 for more details on the experimental setup. For more information on EPAPS, see http://www.aip.org/pubservs/epaps.html.
[28] R. Rzehak and W. Zimmermann, Physica (Amsterdam) **324A**, 495 (2003).

Publication 4

Dynamics of a trapped Brownian particle in shear flows
L. Holzer, J. Bammert, R. Rzehak, and W. Zimmermann,
Physical Review E **81**, 041124 (2010)

Copyright by The American Physical Society 2010
DOI: 10.1103/PhysRevE.81.041124

Dynamics of a trapped Brownian particle in shear flows

Lukas Holzer,[1] Jochen Bammert,[1] Roland Rzehak,[2] and Walter Zimmermann[1]
[1]*Theoretische Physik I, Universität Bayreuth, D-95440 Bayreuth, Germany*
[2]*Störfallanalyse, Forschungszentrum Dresden, D-01328 Dresden, Germany*
(Received 16 November 2009; revised manuscript received 28 February 2010; published 20 April 2010)

The Brownian motion of a particle in a harmonic potential, which is simultaneously exposed either to a linear shear flow or to a plane Poiseuille flow is investigated. In the shear plane of both flows the probability distribution of the particle becomes anisotropic and the dynamics is changed in a characteristic manner compared to a trapped particle in a quiescent fluid. The particle distribution takes either an elliptical or a parachute shape or a superposition of both depending on the mean particle position in the shear plane. Simultaneously, shear-induced cross-correlations between particle fluctuations along orthogonal directions in the shear plane are found. They are asymmetric in time. In Poiseuille flow thermal particle fluctuations perpendicular to the flow direction in the shear plane induce a shift of the particle's mean position away from the potential minimum. Two complementary methods are suggested to measure shear-induced cross-correlations between particle fluctuations along orthogonal directions.

DOI: 10.1103/PhysRevE.81.041124 PACS number(s): 05.40.−a, 87.15.Ya, 83.50.Ax

I. INTRODUCTION

The Brownian motion of particles in a fluid is of central importance in chemical and biological physics as well as in material science and engineering [1–4]. Despite the long history of Brownian motion, especially in quiescent fluids, our understanding of thermally induced particle dynamics in flows is still far from complete.

Moreover, neutral colloidal particles moving relatively to each other interact via the fluid and these hydrodynamic interactions can cause a complex collective behavior [2–6]. In shear flows little is known about the dynamics of Brownian particles and the hydrodynamic interaction effects in spite of their fundamental relevance and importance in microfluidic applications. The Taylor dispersion [7] and fluid mixing issues [4,8] are well-known examples where fluctuations of particles and their hydrodynamic interaction effects in simple shear and Poiseuille flow play an important role. The interplay of shear gradients and thermal motion of polymers leads, even at low values of the Reynolds number, to the rich dynamics of polymers [9], the so-called molecular individualism [10]. Polymers tumbling in a shear flow cause elastic turbulence even in diluted polymer solutions [11] and spectacular mixing properties [8] in microchannels.

In shear flows, it is the contribution $(\mathbf{u}\cdot\nabla)\mathbf{u}$ of the flow field $\mathbf{u}(\mathbf{r})$ to the Navier-Stokes equation which causes interesting transient phenomena near the onset of turbulence [12], as well as amplifications of velocity fluctuations and their cross-correlations along and perpendicular to straight streamlines [13,14]. A cross-correlation is also expected between orthogonal particle fluctuations in the shear plane, because random jumps of a particle between neighboring streamlines of different velocity lead to a change in the particle's velocity and displacement along the streamlines, similar as via fluctuations. Nevertheless, there was no direct observation of these cross-correlations until recently [15]. Here we present the theoretical background for their determination.

The stochastic dynamics of free single spherical particles in linear shear flows have been studied in terms of the hydrodynamic fluctuation theory [16], and in combined Langevin and Fokker-Planck approaches, by taking inertia into account [17–19]. Even effects of nonequilibrium thermodynamics were included in Ref. [20]. Experiments for detecting shear-induced cross-correlations between perpendicular random displacements of free particles were described in Refs. [21,22]. Shear-induced cross-correlations between perpendicular fluid-velocity fluctuations and perpendicular fluctuations of particles are expected to be strongly asymmetric in time [13,18,23]. In dynamic light-scattering experiments certain aspects of this issue were observed indirectly [24], however, a direct measurement and characterization of related particle fluctuations in shear flows remained an open question.

Direct observations of particle fluctuations at the mesoscale became possible only quite recently by using optical tweezers. This rather young technique is a powerful experimental method for investigating the motion of a small number of particles [25–27], which contributes substantially to our understanding of the dynamics of particles and to a number of innovative applications. These include the inspiring studies on single polymers [28–35], the detection of anticorrelations between hydrodynamically interacting Brownian particles by Femto-Newton measurements [36], the propagation of hydrodynamic interactions [37], wall effects on Brownian motion [38,39], short-time inertial response of viscoelastic fluids [40], two-point microrheology [41], anomalous vibrational dispersion [42], particle sorting techniques [43–46], and a number of further investigations in microfluidics. The laser tweezer technique has also been applied to determine the force elongation relation of biopolymers [47] or the effective pair potential in colloidal suspensions [48].

Stochastic motions of a free particle moving along the streamlines of a sheared fluid and of a particle trapped in the minimum of a potential, while exposed to a shear flow, have common characteristic signatures. Since the trapped particles are more suited for a thorough statistical analysis of its Brownian dynamics, we present calculations for particles trapped by a harmonic potential and exposed to either a linear shear flow or to a plane Poiseuille flow. Our analytical

 ©2010 The American Physical Society

results show that shear flow causes characteristic signatures in the time dependence of the cross-correlation between particle displacements along orthogonal directions in the shear plane as well as an inclined elliptical particle distribution. Part of these results have already been applied and confirmed in a recent experimental study [15].

For our calculations, we utilize a Langevin model for the particle motion, where stochastic forces with different statistical properties may be used. Stochastic forces acting on suspended Brownian particles are caused by velocity fluctuations of the surrounding fluid. In a quiescent fluid the fluctuations of orthogonal velocity components are uncorrelated in the bulk [49]. Assuming such uncorrelated fluid-velocity fluctuations, and therefore uncorrelated stochastic forces in the particle Langevin model, we show how shear flow induces cross-correlations between particle fluctuations along orthogonal directions. Conversely, we show how the amplitudes of the stochastic forces acting on the particle can be determined by measuring the static correlations of the particle fluctuations.

In Sec. II the model equations of the Brownian particle motion and their formal analytical solutions are presented. The static correlation functions for the particle's position and velocity fluctuations are derived in Sec. III, where also the corresponding distributions are calculated in terms of the static correlations and under the assumption of Gaussian particle fluctuations. In addition, the ratio between the principal axes of both distributions are determined as well as the angle enclosed by each major axis and the flow direction. In Poiseuille flow the second derivative of the flow profile, as well as the fluctuations perpendicular to the flow lines, cause a shift of the particle's mean position in the potential via $\Delta\mathbf{u}(\mathbf{r}) \neq 0$. The latter contribution is usually not taken into account, if the effective particle radius is determined via Faxén's law from the particle displacement. In Sec. IV we present and discuss these results for the special cases of linear shear flow and plane Poiseuille flow. In addition, we compare the analytical results with numerical simulations of the Langevin equation given in Sec. II and we suggest experiments to measure some of the flow-induced effects determined in this work. The article closes with a discussion and possible further applications in Sec. V.

II. EQUATIONS OF MOTION AND THEIR SOLUTIONS

We consider a Brownian particle of mass m and effective radius R suspended at the position $\mathbf{r}=(x,y,z)$ in a flow field with parallel streamlines in the x-direction, $\mathbf{u}(\mathbf{r})=u_x(y)\hat{\mathbf{e}}_x$. We assume a velocity field

$$u_x(y) = (a + by + cy^2), \tag{1}$$

which corresponds for $b=c=0$ to a uniform flow, for $a=c=0$ to a linear shear flow with shear rate b, and for $c=-\frac{a}{l^2}$, $b=0$ to a plane Poiseuille flow between two parallel walls at a distance $2l$. The particle is trapped by a harmonic potential with its minimum at $\mathbf{r}_0=(x_0,y_0,z_0)=(0,0,0)$,

$$U(\mathbf{r}) = \frac{k}{2}\mathbf{r}^2. \tag{2}$$

The resulting linear restoring force is given by

$$\mathbf{F}^p = -\nabla U = -k\mathbf{r}, \tag{3}$$

in terms of the force constant k. Such a potential acting on a colloidal particle may be realized by an optical tweezer [25].

A particle moving with the speed $\mathbf{v}=\dot{\mathbf{r}}$ in a flow of velocity $\mathbf{u}$ experiences, according to Stokes' law, a hydrodynamic drag force $\mathbf{F}^h=6\pi\eta R(\mathbf{u}-\mathbf{v})$ proportional to the effective radius R, to the shear viscosity η and to the difference $\mathbf{u}-\mathbf{v}$ between the velocity of the particle and the local flow velocity [49,50]. If the flow velocity $\mathbf{u}(\mathbf{r})$ is a nonlinear function of the spatial coordinates, as in the case of a plane Poiseuille flow in Eq. (1), one has according to Faxén's theorems [51] an additional contribution to the drag force. This contribution includes the Laplacian of the velocity field and has in terms of the Stokes friction coefficient, $\zeta=6\pi\eta R$, the form

$$\mathbf{F}^h = -\zeta\left(\dot{\mathbf{r}} - \mathbf{u}(\mathbf{r}) - \frac{R^2}{6}\Delta\mathbf{u}(\mathbf{r})\right). \tag{4}$$

The Laplacian of the flow field in Eq. (1), with the abbreviation $\bar{a}=a+\frac{R^2}{3}c$, gives the following expression for the hydrodynamic drag force,

$$\mathbf{F}^h = -\zeta\dot{\mathbf{r}} + \zeta(\bar{a} + by + cy^2)\hat{\mathbf{e}}_x. \tag{5}$$

The stochastic motion of a Brownian particle is caused by the fluctuations $\tilde{\mathbf{u}}$ of the fluid-velocity field $\mathbf{u}(\mathbf{r},t)$ [52]. The effects of $\tilde{\mathbf{u}}$ on a particle can be taken into account in a Langevin model by a random force $\mathbf{F}^b(t)$. In uniform flows, namely with $b=c=0$ in Eq. (1), the cross-correlations of the velocity fluctuations of the fluid, $\langle\tilde{u}_i\tilde{u}_j\rangle$, lead to a vanishing cross-correlation of the random forces, $\langle F_i^b F_j^b\rangle=0$, $(i\neq j)$. The shear-induced contributions to $\tilde{u}_i$ and F_i^b are a matter of current research [13,14].

In our model we assume a Gaussian distribution of $\mathbf{F}^b(t)$ with vanishing correlation time and mean value

$$\langle F_i^b(t)\rangle = 0,$$

$$\langle F_i^b(t)F_j^b(t')\rangle = f_{ij}\delta(t-t') \quad \text{and} \quad i,j \in x,y,z. \tag{6}$$

For the moment we leave the fluctuation matrix f_{ij} unspecified, except to note that, according to time-translation and time-reversal invariance, it is symmetric. In uniform flows, namely, with $b=c=0$ in Eq. (1), the matrix f_{ij} is diagonal with $f_{ii}=2k_BT\zeta$ [53] as mentioned before, whereas in a shear flow the magnitude of the nondiagonal elements of f_{ij} depends on the shear rate, but shear-induced contributions are expected to be small [13,16,23]. However, we allow nondiagonal elements of f_{ij} for the moment to show in Sec. IV how these nondiagonal elements may be determined by measurements of the velocity fluctuations of the particle.

The net force acting on the particle,

$$\mathbf{F} = \mathbf{F}^h + \mathbf{F}^p + \mathbf{F}^b(t), \tag{7}$$

together with Newton's law gives the Langevin equations of motion for the translational degrees of freedom of the particle

$$m\ddot{x} = -\zeta\dot{x} - kx + \zeta(\bar{a} + by + cy^2) + F_x^b(t), \tag{8a}$$

$$m\ddot{y} = -\zeta\dot{y} - ky + F_y^b(t), \tag{8b}$$

$$m\ddot{z} = -\zeta\dot{z} - kz + F_z^b(t). \tag{8c}$$

Introducing the vectors $\mathbf{X}=(x,v_x)$, $\mathbf{Y}=(y,v_y)$, and $\mathbf{Z}=(z,v_z)$ one may express the second order differential Eq. (8) in terms of a system of coupled first-order equations

$$\dot{\mathbf{X}} = \mathrm{L}\mathbf{X} + \frac{F_x^b(t)}{m}\hat{\mathbf{e}}_v + 2\beta(\bar{a} + by + cy^2)\hat{\mathbf{e}}_v, \tag{9a}$$

$$\dot{\mathbf{Y}} = \mathrm{L}\mathbf{Y} + \frac{F_y^b(t)}{m}\hat{\mathbf{e}}_v, \tag{9b}$$

$$\dot{\mathbf{Z}} = \mathrm{L}\mathbf{Z} + \frac{F_z^b(t)}{m}\hat{\mathbf{e}}_v. \tag{9c}$$

Herein we have introduced the matrix

$$\mathrm{L} = \begin{pmatrix} 0 & 1 \\ -\omega^2 & -2\beta \end{pmatrix}, \tag{10}$$

the damping constant $\beta=\frac{\zeta}{2m}$, the squared frequency $\omega^2=\frac{k}{m}$ and the velocity unit-vector $\hat{\mathbf{e}}_v=(0,1)$. The rotational motion of the particle, which may provide further corrections to the leading order fluctuation effects discussed here, is not taken into account in this work.

The general solutions of the equations of motion (9) in terms of the initial conditions $\mathbf{X}(0)$, $\mathbf{Y}(0)$, and $\mathbf{Z}(0)$ are given by

$$\mathbf{X}(t) = e^{\mathrm{L}t}\mathbf{X}(0) + \int_0^t d\tau e^{\mathrm{L}(t-\tau)}\frac{F_x^b(\tau)}{m}\hat{\mathbf{e}}_v + 2\beta\int_0^t d\tau e^{\mathrm{L}(t-\tau)}(\bar{a} + by + cy^2)\hat{\mathbf{e}}_v, \tag{11a}$$

$$\mathbf{Y}(t) = e^{\mathrm{L}t}\mathbf{Y}(0) + \int_0^t d\tau e^{\mathrm{L}(t-\tau)}\frac{F_y^b(\tau)}{m}\hat{\mathbf{e}}_v, \tag{11b}$$

$$\mathbf{Z}(t) = e^{\mathrm{L}t}\mathbf{Z}(0) + \int_0^t d\tau e^{\mathrm{L}(t-\tau)}\frac{F_z^b(\tau)}{m}\hat{\mathbf{e}}_v. \tag{11c}$$

This system of coupled equations is the starting point of the following analysis, where the statistical properties of the particle's motion are characterized by the correlations of its position and velocity.

III. DISTRIBUTION FUNCTIONS AND STATIC CORRELATIONS

By taking the averages of Eq. (11) and using the vanishing mean of the stochastic forces in Eq. (6) we see that the mean velocity of a particle in a harmonic potential vanishes, $\langle\mathbf{v}\rangle=0$. In the case $\mathbf{r}_0=0$ the mean value of the deviations of the particle's position from the potential minimum in the directions perpendicular to the flow vanish too, $\langle y\rangle=\langle z\rangle=0$. However, the mean particle displacement in the direction of the flow given by Eq. (1) is nonzero

$$\langle x\rangle = \frac{\zeta}{k}\bar{a} + \frac{f_{yy}}{2k^2}c. \tag{12}$$

This equation is discussed in more detail in Sec. IV for specific flows. Since the spring constant k of the potential enters in different powers in Eq. (12), this formula might be employed for the experimental determination of the effective fluctuation magnitude f_{yy}.

With a combination of the coordinates of the particle and its velocities to a single six-dimensional vector, $\mathbf{q}=(\mathbf{r},\mathbf{v})=(x,y,z,v_x,v_y,v_z)$, the probability distribution function of the particle, $\mathcal{P}(\mathbf{q})$, may be formulated in a compact form in terms of the deviations $\tilde{\mathbf{q}}=\mathbf{q}-\langle\mathbf{q}\rangle=(\tilde{x},\tilde{y},\tilde{z},\tilde{v}_x,\tilde{v}_y,\tilde{v}_z)$ from the mean value $\langle\mathbf{q}\rangle$. If the fluctuations $\tilde{\mathbf{q}}$ are linear functions of Gaussian distributed stochastic forces, which is the case for uniform and linear shear flows, they can be expected to be themselves Gaussian variables [54] and can be described by a Gaussian distribution as follows:

$$\mathcal{P}(\tilde{\mathbf{q}}) = \frac{1}{\sqrt{(2\pi)^6\det(\mathrm{C})}}\exp\left(-\frac{1}{2}\tilde{\mathbf{q}}^T\mathrm{C}^{-1}\tilde{\mathbf{q}}\right). \tag{13}$$

Here the covariance matrix $\mathrm{C}=\langle\tilde{\mathbf{q}}\tilde{\mathbf{q}}^T\rangle$ is used, which includes second-order moments for the coordinates and the velocities at equal times (static correlations). The magnitudes of the elements C_{ij} depend on the correlation amplitudes of the stochastic forces, f_{ij}, and can be measured in experiments. Consequently, one may reconstruct the stochastic forces from the measurements, as discussed later.

For Poiseuille flow the relations between particle fluctuations and stochastic forces are nonlinear due to the contribution $\propto cy^2$ in Eq. (11a). Therefore, the particle distribution $\mathcal{P}(\tilde{\mathbf{q}})$ is not necessarily Gaussian. However, in the course of this work we use the formula in Eq. (13) also for particles in a potential, which are exposed to a Poiseuille flow, but with the covariance matrix C_{ij} now determined in terms of the parameters for the Poiseuille flow. The validity of this heuristic approach will be tested later in Sec. IV B by numerical simulations.

A. Covariance matrix and angular momentum

The covariance matrix C consists of four 3×3 submatrices

$$\mathrm{C} = \begin{pmatrix} \mathrm{C}_{rr} & \mathrm{C}_{rv} \\ \mathrm{C}_{vr} & \mathrm{C}_{vv} \end{pmatrix}, \tag{14}$$

that describe the autocorrelation for the positions C_{rr} and velocities C_{vv} and their cross-correlations C_{vr} and C_{rv} at equal times. The matrices

$$\mathrm{C}_{rr} = \begin{pmatrix} \langle \tilde{x}^2 \rangle & \langle \tilde{x}\tilde{y} \rangle & 0 \\ \langle \tilde{y}\tilde{x} \rangle & \langle \tilde{y}^2 \rangle & 0 \\ 0 & 0 & \langle \tilde{z}^2 \rangle \end{pmatrix}, \tag{15a}$$

$$\mathrm{C}_{vv} = \begin{pmatrix} \langle \tilde{v}_x^2 \rangle & \langle \tilde{v}_x\tilde{v}_y \rangle & 0 \\ \langle \tilde{v}_y\tilde{v}_x \rangle & \langle \tilde{v}_y^2 \rangle & 0 \\ 0 & 0 & \langle \tilde{v}_z^2 \rangle \end{pmatrix}, \tag{15b}$$

$$\mathrm{C}_{rv} = \mathrm{C}_{vr}^T = \begin{pmatrix} 0 & \langle \tilde{x}\tilde{v}_y \rangle & 0 \\ \langle \tilde{y}\tilde{v}_x \rangle & 0 & 0 \\ 0 & 0 & 0 \end{pmatrix}, \tag{15c}$$

may be calculated in terms of the expressions given by Eq. (11).

Under the Gaussian assumption, the four-point correlations of the stochastic forces, which occur due to the quadratic contribution y^2 of the flow in Eq. (11a), can be decomposed into two-point correlation functions according to Wick's theorem [54]:

$$\begin{aligned} \langle F_i^b(t_1)F_j^b(t_2)F_k^b(t_3)F_l^b(t_4) \rangle = {} & f_{ij}f_{kl}\delta(t_2 - t_1)\delta(t_4 - t_3) \\ & + f_{ik}f_{jl}\delta(t_3 - t_1)\delta(t_4 - t_3) \\ & + f_{il}f_{jk}\delta(t_4 - t_1)\delta(t_3 - t_2). \end{aligned} \tag{16}$$

Introducing the relaxation time of the particle in a harmonic potential

$$\tau_p = \frac{\zeta}{k}, \tag{17}$$

the nonzero components of the covariance matrices may be written in terms of the amplitudes of the stochastic forces and the flow parameters by the following set of equations:

$$\langle \tilde{v}_y^2 \rangle = \frac{1}{4}\frac{f_{yy}}{m^2\beta}, \quad \langle \tilde{y}^2 \rangle = \frac{\langle \tilde{v}_y^2 \rangle}{\omega^2}, \tag{18a}$$

$$\langle \tilde{v}_z^2 \rangle = \frac{1}{4}\frac{f_{zz}}{m^2\beta}, \quad \langle \tilde{z}^2 \rangle = \frac{\langle \tilde{v}_z^2 \rangle}{\omega^2}, \tag{18b}$$

$$\langle \tilde{v}_x\tilde{v}_y \rangle = \langle \tilde{v}_y\tilde{v}_x \rangle = \frac{1}{4}\frac{f_{xy}}{m^2\beta}, \tag{18c}$$

$$\langle \tilde{x}\tilde{y} \rangle = \langle \tilde{y}\tilde{x} \rangle = \frac{\langle \tilde{v}_x\tilde{v}_y \rangle}{\omega^2} + \frac{1}{2}b\tau_p\langle \tilde{y}^2 \rangle, \tag{18d}$$

$$\langle \tilde{x}\tilde{v}_y \rangle = -\langle \tilde{y}\tilde{v}_x \rangle = -\frac{b}{2}\langle \tilde{y}^2 \rangle, \tag{18e}$$

$$\langle \tilde{v}_x^2 \rangle = \frac{1}{4}\frac{f_{xx}}{m^2\beta} + \frac{1}{2}b^2\langle \tilde{y}^2 \rangle + \frac{8c^2\tau_p^2\omega^2}{3(1+2\tau_p^2\omega^2)}\langle \tilde{y}^2 \rangle^2, \tag{18f}$$

$$\langle \tilde{x}^2 \rangle = \frac{\langle \tilde{v}_x^2 \rangle}{\omega^2} + \tau_p b\langle \tilde{x}\tilde{y} \rangle + \frac{2}{3}\tau_p^2 c^2\langle \tilde{y}^2 \rangle^2. \tag{18g}$$

The nondiagonal elements of C_{vv}, namely, the correlations of the velocity fluctuations of the particle, $\langle \tilde{v}_x\tilde{v}_y \rangle$ and $\langle \tilde{v}_y\tilde{v}_x \rangle$, are directly proportional to the amplitude f_{xy} of the fluctuations given by Eq. (6). In contrast to this result for a fluctuating particle in a potential, one finds for a free particle in shear flow finite values for the cross-correlations $\langle \tilde{v}_x\tilde{v}_y \rangle$ and $\langle \tilde{v}_y\tilde{v}_x \rangle$ even in the case $f_{xy}=0$ [18]. However, as shown appendix A, in the presence of a harmonic potential these correlations decay on a time scale $1/(2\beta)$, which is very short for an overdamped particle motion. In the case of a weak laser tweezer potential the particle relaxation time $\tau_p=\zeta/k$ becomes rather large and one obtains according to Eqs. (A8) and (A10) for $f_{xy}=0$ a contribution to the velocity correlation $\langle \tilde{v}_x(t)\tilde{v}_y(t) \rangle \propto \exp[-2t/\tau_p]f_{yy}$, which decays slowly and gives in the limit of a vanishing potential $(k \to 0, \tau_p \to \infty)$ a constant contribution to the velocity-velocity correlation, which agrees with that in Ref. [18] for a free particle, cf. Appendix A. Therefore, finite values of $\langle \tilde{v}_x\tilde{v}_y \rangle$ and $\langle \tilde{v}_y\tilde{v}_x \rangle$ measured for particles trapped in a potential are a direct indication of cross-correlations of the stochastic forces along orthogonal directions, $\langle F_x^b F_y^b \rangle \neq 0$.

For $b \neq 0$ the contributions to the nondiagonal elements $\langle \tilde{x}\tilde{y} \rangle$ and $\langle \tilde{y}\tilde{x} \rangle$ of the positional correlations C_{rr}, which are related to $f_{xy} \propto b$, are expected to be small [14,23]. For this reason f_{xy} is neglected in the following. Both positional cross-correlations $\langle \tilde{x}\tilde{y} \rangle$ and $\langle \tilde{y}\tilde{x} \rangle$ are proportional to the local shear rate b and to the fluctuation strength f_{yy} in the y direction, cf. Eq. (18d).

The autocorrelation of the velocity fluctuations $\langle \tilde{v}_x^2 \rangle$ in the flow direction includes several contributions. It depends on the shear rate, the second derivative of the flow and the fluctuation strength f_{xx} and f_{yy}. The cross-correlations between velocity and position appear only in the shear plane and they are proportional to the local shear rate.

The submatrices C_{vr} and C_{rv}, describing the cross-correlations between the positional and the velocity fluctuations, are related to the mean angular momentum of the particle

$$\langle (m\mathbf{r} \times \mathbf{v})_z \rangle = m\langle \tilde{x}\tilde{v}_y - \tilde{y}\tilde{v}_x \rangle = -mb\langle \tilde{y}^2 \rangle. \tag{19}$$

B. Distribution of position and velocity

Integrating the particle distribution function $\mathcal{P}(\tilde{\mathbf{q}})$ in Eq. (13) with respect to its velocity degrees of freedom one obtains the particle's positional distribution function $\mathcal{P}(\tilde{\mathbf{r}})$, which may be expressed in terms of the covariance matrix C_{rr} as follows:

$$\mathcal{P}(\tilde{\mathbf{r}}) = \int d\tilde{\mathbf{v}}\mathcal{P}(\tilde{\mathbf{q}}) = \frac{1}{\sqrt{(2\pi)^3 \det(\mathrm{C}_{rr})}} \exp\left(-\frac{1}{2}\tilde{\mathbf{r}}^T\mathrm{C}_{rr}^{-1}\tilde{\mathbf{r}}\right). \tag{20}$$

A sketch of the distribution $\mathcal{P}(\tilde{\mathbf{r}})$ is shown in Fig. 1 for a linear shear flow $b \neq 0$ and $a=c=0$. The nondiagonal elements of the symmetric matrix C_{rr}, cf. Eq. (15a) and (18),

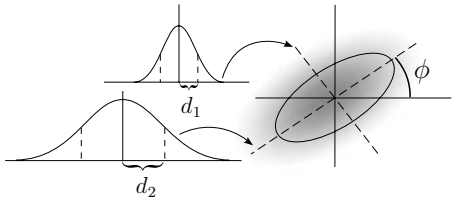

FIG. 1. The elliptical particle distribution in the xy shear plane is sketched for a nonzero shear rate. d_1 and d_2 are the two principal axes of an ellipse along which $\mathcal{P}(\tilde{\mathbf{r}})$ is constant. The Gaussian profiles along the two principal axes are also indicated.

describe the cross-correlations of the particle fluctuations in the x and y direction and therefore the deviation of $\mathcal{P}(\tilde{\mathbf{r}})$ from a spherically symmetric distribution to an ellipsoidal one in the shear plane. The principal axes of the particle's positional distribution are given by the eigenvectors $\mathbf{w}_{p;1,2,3}$ of the corresponding eigenvalues $c_{p;1,2,3}$ of the matrix C_{rr}.

In the z-direction one has $c_{p;3}=\langle\tilde{z}^2\rangle$ and $\mathbf{w}_{p;3}=(0,0,1)$. For the other two directions in the xy shear plane one obtains

$$c_{p;1,2}=\frac{1}{2}(\langle\tilde{x}^2\rangle+\langle\tilde{y}^2\rangle)\pm\frac{1}{2}\sqrt{4\langle\tilde{x}\tilde{y}\rangle^2+(\langle\tilde{x}^2\rangle-\langle\tilde{y}^2\rangle)^2},$$

$$\mathbf{w}_{p;1}=\left(\frac{c_{p;1}-\langle\tilde{y}^2\rangle}{\langle\tilde{x}\tilde{y}\rangle},1,0\right),$$

$$\mathbf{w}_{p;2}=\frac{\langle\tilde{x}\tilde{y}\rangle}{|\langle\tilde{x}\tilde{y}\rangle|}\left(-1,\frac{c_{p;1}-\langle\tilde{y}^2\rangle}{\langle\tilde{x}\tilde{y}\rangle},0\right). \tag{21}$$

With the orthogonal transformation matrix

$$\mathrm{D}=(\mathbf{w}_{p;1},\mathbf{w}_{p;2},\mathbf{w}_{p;3}), \tag{22}$$

the $\tilde{\mathbf{r}}$-dependence of the exponential function (20) can be rewritten as follows:

$$-\frac{1}{2}\tilde{\mathbf{r}}^T\mathrm{C}_{rr}^{-1}\tilde{\mathbf{r}}=-\frac{1}{2}(\mathrm{D}^T\tilde{\mathbf{r}})^T\mathrm{diag}(c_{p;1}^{-1},c_{p;2}^{-1},c_{p;3}^{-1})(\mathrm{D}^T\tilde{\mathbf{r}}). \tag{23}$$

The eigenvalues $c_{p;1}$ and $c_{p;2}$ determine the length of the principal axes $d_{p;1,2}=\sqrt{c_{p;1,2}}$ along the directions $\mathbf{w}_{p;1}$ and $\mathbf{w}_{p;2}$ of an ellipse, where the longer one is rotated counterclockwise with respect to the x-axis by an angle ϕ_p, which is given by the expression

$$\tan\phi_p=\frac{\langle\tilde{x}\tilde{y}\rangle}{c_{p,1}-\langle\tilde{y}^2\rangle}=\frac{1}{2}\left[\frac{\langle\tilde{x}\tilde{y}\rangle}{|\langle\tilde{x}\tilde{y}\rangle|}\sqrt{4+\left(\frac{\langle\tilde{x}^2\rangle-\langle\tilde{y}^2\rangle}{\langle\tilde{x}\tilde{y}\rangle}\right)^2}-\left(\frac{\langle\tilde{x}^2\rangle-\langle\tilde{y}^2\rangle}{\langle\tilde{x}\tilde{y}\rangle}\right)\right]. \tag{24}$$

The ratio between the minor and the major axis is given by

$$V_p:=\sqrt{\frac{c_{p;2}}{c_{p;1}}}=\left(\frac{\langle\tilde{x}^2\rangle+\langle\tilde{y}^2\rangle-\sqrt{4\langle\tilde{x}\tilde{y}\rangle^2+(\langle\tilde{x}^2\rangle-\langle\tilde{y}^2\rangle)^2}}{\langle\tilde{x}^2\rangle+\langle\tilde{y}^2\rangle+\sqrt{4\langle\tilde{x}\tilde{y}\rangle^2+(\langle\tilde{x}^2\rangle-\langle\tilde{y}^2\rangle)^2}}\right)^{1/2}. \tag{25}$$

Analogous to the particle distribution given above, one can also derive an expression for the probability distribution $\mathcal{P}(\tilde{\mathbf{v}})$ of the particle's velocity, which is obtained by integrating out the positional degrees of freedom in Eq. (13)

$$\mathcal{P}(\tilde{\mathbf{v}})=\int d\tilde{\mathbf{r}}\mathcal{P}(\tilde{\mathbf{r}},\tilde{\mathbf{v}})=\frac{1}{\sqrt{(2\pi)^3\det(\mathrm{C}_{vv})}}\exp\left(-\frac{1}{2}\tilde{\mathbf{v}}^T\mathrm{C}_{vv}^{-1}\tilde{\mathbf{v}}\right). \tag{26}$$

The eigenvalues $c_{v;1,2,3}$ and eigenvectors $\mathbf{w}_{v;1,2,3}$ of C_{vv} are determined in a similar manner as for C_{rr}. Again the eigenvalue $c_{v;3}=\langle\tilde{v}_z^2\rangle$ and the principal axis $\mathbf{w}_{v;3}=(0,0,1)$ perpendicular to the shear plane are obvious. The remaining two eigenvalues and eigenvectors are

$$c_{v;1,2}=\frac{1}{2}(\langle\tilde{v}_x^2\rangle+\langle\tilde{v}_y^2\rangle)\pm\frac{1}{2}\sqrt{4\langle\tilde{v}_x\tilde{v}_y\rangle^2+(\langle\tilde{v}_x^2\rangle-\langle\tilde{v}_y^2\rangle)^2},$$

$$\mathbf{w}_{v;1}=\left(\frac{c_{v;1}-\langle\tilde{v}_y^2\rangle}{\langle\tilde{v}_x\tilde{v}_y\rangle},1,0\right), \tag{27}$$

$$\mathbf{w}_{v;2}=\frac{\langle\tilde{v}_x\tilde{v}_y\rangle}{|\langle\tilde{v}_x\tilde{v}_y\rangle|}\left(-1,\frac{c_{v;1}-\langle\tilde{v}_y^2\rangle}{\langle\tilde{v}_x\tilde{v}_y\rangle},0\right). \tag{28}$$

They have the same structure like those for the covariance matrix C_{rr}. However, while the nondiagonal elements of C_{rr} are directly proportional to the local shear rate b, the nondiagonal elements of C_{vv} and therefore the angle enclosed between the principal axis of the distribution of the velocity fluctuations and the x axis,

$$\tan\phi_v=\frac{\langle\tilde{v}_x\tilde{v}_y\rangle}{c_{v,1}-\langle\tilde{v}_y^2\rangle}=\frac{1}{2}\left[\frac{\langle\tilde{v}_x\tilde{v}_y\rangle}{|\langle\tilde{v}_x\tilde{v}_y\rangle|}\sqrt{4+\left(\frac{\langle\tilde{v}_x^2\rangle-\langle\tilde{v}_y^2\rangle}{\langle\tilde{v}_x\tilde{v}_y\rangle}\right)^2}-\left(\frac{\langle\tilde{v}_x^2\rangle-\langle\tilde{v}_y^2\rangle}{\langle\tilde{v}_x\tilde{v}_y\rangle}\right)\right], \tag{29}$$

depends only weakly on the local shear rate, since the contribution of b to the shear-induced cross-correlation f_{xy} is small in magnitude, compared to f_{ii} [14,23]. From a measurement of the distribution of the particle's velocity one may calculate the eigenvalues $c_{v;1,2}$ and the angle ϕ_v, which may enable the determination of the stochastic force correlations f_{xx}, f_{yy}, and f_{xy}.

The mean kinetic energy of a trapped particle in shear flow is composed of two contributions, one induced by the distribution of the fluctuations and an additional one by virtue of the rotational part of the flow

$$E_{kin}=\frac{m}{2}\langle\tilde{v}_x^2+\tilde{v}_y^2+\tilde{v}_z^2\rangle=\frac{1}{4}\frac{f_{xx}+f_{yy}+f_{zz}}{m^2\beta}+\frac{b^2}{2}\langle\tilde{y}^2\rangle+\frac{8}{3}c^2\frac{\tau_p^2\omega^2}{1+2\tau_p^2\omega^2}\langle\tilde{y}^2\rangle^2. \tag{30}$$

If the correlations of the stochastic forces are assumed to be independent of the flow, the mean energy of the particle will be increased by the flow, since all terms in this equation are positive. But without knowing the explicit expressions for the force correlations, it is not clear how the energy is really changed. Recent calculations show that the mean kinetic energy of a fluid without an immersed particle increases in a

shear flow [55,56]. This indicates that the stochastic forces and the particle's mean energy, Eq. (30), may be amplified as well.

IV. RESULTS FOR SPECIFIC FLOWS

The results concerning the effects of a linear shear and a plane Poiseuille flow on the Brownian motion of a particle in a harmonic potential are presented in this section. Namely, the properties of the correlation functions and the particle's distribution are analyzed as a function of the flow parameters. They share common trends for both flows but there are also some characteristic differences, which are described in this section.

A. Linear shear flow

If the center of the harmonic potential at $\mathbf{r}_0=(0,y_0,0)$ does not coincide with the center of the linear shear flow of shear rate $\dot{\gamma}$, we may insert in Eq. (1) $y=y_0+\tilde{y}$, where $\tilde{y}$ describes the deviation from y_0. Consequently, in terms of the coordinates $\tilde{y}$, the three coefficients in Eq. (1) take the following form

$$b=\dot{\gamma}, \quad a=\bar{a}=\dot{\gamma}y_0 \quad \text{and} \quad c=0. \tag{31}$$

In the case $y_0\neq 0$ the flow velocity has a finite value at the center of the trap resulting in a nonzero mean position of the particle in flow direction, which is given via Eq. (12) by the formula

$$\langle x\rangle = \dot{\gamma}\tau_p y_0. \tag{32}$$

With the identifications (31) the elements of the covariance matrix C for the particle fluctuations around the potential minimum may be determined for a linear shear flow by Eq. (18) in terms of the noise amplitudes f_{xx}, f_{xy}, and f_{yy}.

An interesting question is how to detect the noise amplitudes f_{ij} in terms of the measured autocorrelations and cross-correlations of the particle's position- and velocity fluctuations. According to Eq. (18c) there is a direct relation between the velocity correlation $\langle\tilde{v}_x\tilde{v}_y\rangle$ and the noise magnitude f_{xy}. Therefore, a direct measurement of this velocity correlation, if experimentally possible, would give f_{xy}, or, the other way around, a nonzero value of $f_{xy}\neq 0$ is required in order to obtain nonzero values of the cross-correlations between these orthogonal velocity components.

As already mentioned in the introduction, it is favorable to investigate the particle fluctuations around a potential minimum rather than those of free particles since trapped particles can be investigated over a long period of time, as demonstrated by several experiments, see e. g., Ref. [36]. This opens the opportunity for the determination of the magnitudes of the noise f_{ij} in terms of the positional fluctuations via Eq. (18), which in the case of a linear shear flow take the following explicit form

$$f_{yy}=2k\zeta\langle\tilde{y}^2\rangle, \tag{33a}$$

$$f_{xy}=2k\zeta\left(\langle\tilde{x}\tilde{y}\rangle-\frac{1}{2}\dot{\gamma}\tau_p\langle\tilde{y}^2\rangle\right), \tag{33b}$$

$$f_{xx}=2k\zeta\left(\langle\tilde{x}^2\rangle-\frac{1}{2}\frac{\dot{\gamma}^2}{\omega^2}\langle\tilde{y}^2\rangle-\dot{\gamma}\tau_p\langle\tilde{x}\tilde{y}\rangle\right). \tag{33c}$$

In the case of isotropic stochastic forces with negligible cross-correlations, $f_{xx}=f_{yy}$ and $f_{xy}\propto\langle\tilde{v}_x\tilde{v}_y\rangle\approx 0$, one has in a linear shear flow still a nonvanishing positional cross-correlation $\langle\tilde{x}\tilde{y}\rangle=\dot{\gamma}\tau_p\langle\tilde{y}^2\rangle/2$. Its magnitude is determined by the shear rate $\dot{\gamma}$ and the noise strength via $\langle\tilde{y}^2\rangle$. According to this behavior and because $\langle\tilde{x}^2\rangle\neq\langle\tilde{y}^2\rangle$, we expect an anisotropic distribution of the positional fluctuations $\mathcal{P}(\tilde{\mathbf{r}})$, as sketched in Fig. 1 and as discussed below. For $f_{xy}\neq 0$ the anisotropy of the positional distribution has an additional contribution that depends on the magnitude of f_{xy}.

During the rest of the present Sec. IV A inertia effects are neglected and in addition, we assume an isotropic noise distribution with $f_{xy}=f_{yx}=0$ and $f_{xx}=f_{yy}=f_{zz}=2k_BT\zeta$. Both are good approximations for many experiments focusing on leading order effects of a shear flow on the fluctuations of particles. Taking into account the time dependence of the positional fluctuations, as given by Eq. (11), one obtains in terms of the dimensionless Weissenberg number,

$$\mathrm{Wi}=\tau_p\dot{\gamma}, \tag{34}$$

and the Heaviside step function $\Theta(t)$ the following time-dependent correlations:

$$\langle\tilde{x}(t)\tilde{x}(0)\rangle=\frac{k_BT}{k}\left[1+\frac{\mathrm{Wi}^2}{2}\left(1+\frac{|t|}{\tau_p}\right)\right]e^{-|t|/\tau_p}, \tag{35a}$$

$$\langle\tilde{y}(t)\tilde{y}(0)\rangle=\langle\tilde{z}(t)\tilde{z}(0)\rangle=\frac{k_BT}{k}e^{-|t|/\tau_p}, \tag{35b}$$

$$\langle\tilde{x}(t)\tilde{y}(0)\rangle=\frac{k_BT}{k}\frac{\mathrm{Wi}}{2}\left(1+2\frac{t}{\tau_p}\Theta(t)\right)e^{-|t|/\tau_p}. \tag{35c}$$

The cross-correlation between fluctuations along orthogonal directions, as given by the last equation, is shear induced and its asymmetry $\langle\tilde{x}(t)\tilde{y}(0)\rangle\neq\langle\tilde{x}(0)\tilde{y}(t)\rangle$ with respect to time reflection $t\to -t$ is one of the important effects of shear flow on the distribution of fluctuations.

For $t>0$, the algebraic prefactor in Eq. (35c) illustrates that a fluctuation $\tilde{y}(0)\neq 0$ of a particle is carried away by the flow along the x direction before the initial displacement starts to relax remarkably. This leads, during an initial period of time shorter than the relaxation time τ_p, to the growth of $\langle\tilde{x}(t)\tilde{y}(0)\rangle$, while $\langle\tilde{x}(0)\tilde{y}(t)\rangle$ decays monotonically (solid line in Fig. 2 corresponding to $t<0$). The predicted elementary signatures for the shear-induced cross-correlations, as shown in Fig. 2, are in agreement with experimental data as described recently in Ref. [15]. The expression $\langle\tilde{x}(t)\tilde{y}(0)\rangle$ is proportional to the Weissenberg number and takes its maximum at half of the particle's relaxation time $t_{max}=\tau_p/2$. For the correlations of the velocity fluctuations of the fluid in orthogonal directions a similar signature as in Eq. (35c) has been found [13], where however the mechanism is slightly different.

A comparison of the absolute values of the particle's fluctuations with experimental results may be difficult. However, one obtains from Eq. (35) and in terms of the dimensionless

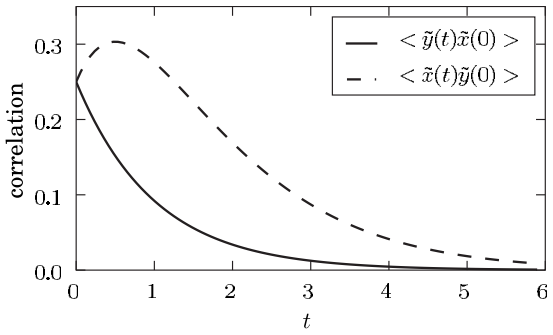

FIG. 2. Time dependence of the shear-induced cross-correlations $\langle \tilde{x}(t)\tilde{y}(0)\rangle$ (dashed line) and $\langle \tilde{x}(0)\tilde{y}(t)\rangle$ (solid line) as given by Eq. (35c) for the Weissenberg number Wi=1 and the relaxation time $\tau_p=1$.

Weissenberg number the following normalized ratios of the static correlations

$$\frac{\langle \tilde{x}(0)\tilde{y}(0)\rangle}{\langle \tilde{y}(0)\tilde{y}(0)\rangle} = \frac{\mathrm{Wi}}{2}, \tag{36a}$$

$$\frac{\langle \tilde{x}(0)\tilde{y}(0)\rangle}{\langle \tilde{x}(0)\tilde{x}(0)\rangle} = \frac{\mathrm{Wi}/2}{1+\mathrm{Wi}^2/2}. \tag{36b}$$

The left hand side and the right-hand side of Eq. (36) can be measured independently in different experiments and the results can be compared afterwards.

An anisotropic distribution of the particle's velocity $\mathcal{P}(\tilde{\mathbf{v}})$, as given by Eq. (26), is only obtained in the case of a finite cross-correlation f_{xy} of the stochastic forces. In contrast to this, the particle's distribution $\mathcal{P}(\tilde{\mathbf{r}})$ has in the overdamped limit an elliptical shape in the xy plane, even for a vanishing cross-correlation magnitude $f_{xy}=0$. In this limit an elliptical distribution $\mathcal{P}(\tilde{\mathbf{r}})$ is shown in Fig. 3 for the Weissenberg number Wi=2 and the relaxation time $\tau_p=1$. In Fig. 3 the time evolution of the particle's position, obtained by simulations of the basic Eq. (8), is plotted at equidistant times. This positional distribution can be characterized by the angle ϕ_p of the ellipsoid and the ratio V_p of its principal axis. The general expressions for ϕ_p and V_p, as given by Eqs. (24) and

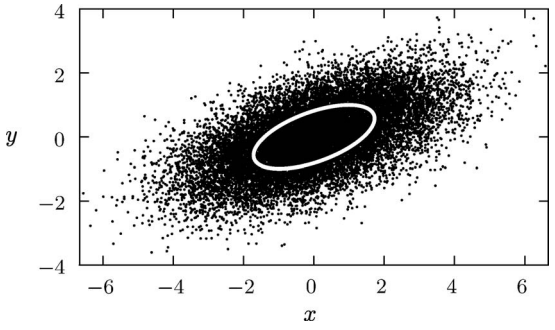

FIG. 3. Positional distribution of a particle in a harmonic potential with its minimum at $\mathbf{r}_0=(0,0,0)$ and exposed to a linear shear flow, as obtained by a stochastic simulation of the Eq. (8) in the overdamped limit for the Weissenberg number Wi=2 and the relaxation time $\tau_p=1$.

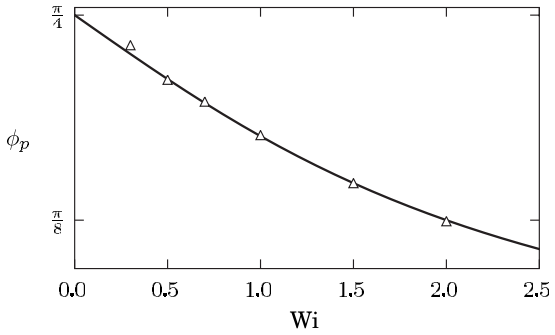

FIG. 4. The angle of the ellipse in the xy plane with respect to the flow lines as a function of the Weissenberg number Wi, as it is given by Eq. (37a). The triangles are the result of a simulation of Eq. (8) in the overdamped limit.

(25), can be further simplified in the case of a linear shear flow to functions of the dimensionless Weissenberg number Wi only

$$\tan\phi_p = \frac{1}{2}[\sqrt{4+\mathrm{Wi}^2}-\mathrm{Wi}], \tag{37a}$$

$$V_p = \left(\frac{\sqrt{4+\mathrm{Wi}^2}-\mathrm{Wi}}{\sqrt{4+\mathrm{Wi}^2}+\mathrm{Wi}}\right)^{1/2}. \tag{37b}$$

The two expressions in Eq. (37) suggest measurements of the shear-induced particle fluctuation effects, which are complementary to the measured static correlations. In experiments the particle positions may be recorded at equidistant times. By plotting these subsequent particle positions in the shear plane, a similar distribution is expected as shown by our numerical simulation in Fig. 3. From such an experimentally measured distribution for different shear rates the angle ϕ_p and the ratio between the principal axes, V_p, may be determined. If the determination of the Weissenberg number Wi is difficult or if the precision is not sufficient Eqs. (36) and (37) allow a consistency check between different aspects of the particle fluctuations, without a separate measurement of Wi. A cross-check has recently been performed in an experiment in which a good agreement between both approaches has been found, cf. Ref. [15].

In the limit of a vanishing Weissenberg number, $\mathrm{Wi}\to 0$, the angle ϕ_p of the ellipsoidal particle's distribution tends to $\phi_p=\pi/4$ and the positional variance becomes isotropic, $\langle \tilde{x}^2\rangle=\langle \tilde{y}^2\rangle$, corresponding to the ratio $V_p=1$. This trend is similar to the dependence of the orientation of vesicles in shear flow [57] or to the local orientation of the order parameter of nematic liquid crystals in plane shear flows [58].

If $\dot{\gamma}$ and therefore Wi is increased, the angle ϕ_p between the longer semiaxis and the x axis as well as the ratio V_p will decrease as shown in Figs. 4 and 5. The triangles in those figures have been obtained by numerical simulations of Eq. (8) for the same values of the Weissenberg number as used for the analytical curves. In our simulations of the Langevin model we have assumed an isotropic and Gaussian distributed white noise and vanishing cross-correlations $f_{xy}=0$. The simulation results confirm the assumption of a Gaussian dis-

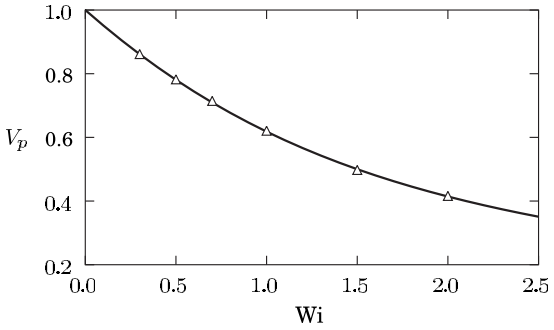

FIG. 5. The ratio V_p of the principal axis of the ellipse in Eq. (37b), as a function of the Weissenberg number Wi. The triangles are the result of a simulation of Eq. (8) in the overdamped limit.

tribution of the particle positions in the case of a shear flow in Sec. III. The analytical and numerical results on ϕ_p and V_p in Figs. 4 and 5 are in good agreement.

B. Plane Poiseuille flow

A Brownian particle is trapped by a harmonic potential close to $\mathbf{r}_0=(0,y_0,0)$ and exposed to a plane Poiseuille flow along the x direction,

$$\mathbf{u}(y) = u_p\left(1 - \frac{y^2}{l^2}\right)\hat{\mathbf{e}}_x. \tag{38}$$

The particle fluctuations $\tilde{x}$ and $\tilde{y}$ describe deviations with respect to the mean values y_0 and $\langle x\rangle$, which is not zero as determined below. The flow velocity along the x direction may be expressed for further analysis in terms of the fluctuations $\tilde{y}$ as follows

$$u_x(\tilde{y}) = u_p\left(1 - \frac{y_0^2}{l^2}\right) - 2\frac{u_p y_0}{l^2}\tilde{y} - \frac{u_p}{l^2}\tilde{y}^2. \tag{39}$$

Comparing this expression with Eq. (1) the coefficients in the latter equation are given by

$$c = -\chi := -\frac{u_p}{l^2},$$

$$a = u_p - \chi y_0^2,$$

$$b = -2\chi y_0. \tag{40}$$

Here χ describes the second derivative of the velocity profile, b the local shear rate and

$$\mathrm{Wi}(y_0) := -2\tau_p\chi y_0, \tag{41}$$

the local Weissenberg number $\mathrm{Wi}(y_0)$. With these identifications the elements of the covariance matrix C are again given via the expressions in Eq. (18) in terms of the strength of the noise, f_{xx}, f_{xy}, f_{yy}, and f_{zz} and the flow parameters.

The mean position of the particle in a plane Poiseuille flow can be determined via Eq. (12)

$$\langle x\rangle = \tau_p\left[u_p - \chi\left(y_0^2 + \frac{1}{3}R^2\right) - \chi\langle\tilde{y}^2\rangle\right]. \tag{42}$$

In contrast to a linear shear flow, it includes a contribution depending on the particle's radius R, which is a pure deterministic effect due to Faxén's theorem [2,51]. The last term on the right-hand side describes an additional shift based on the positional variance $\langle\tilde{y}^2\rangle$ in the y direction. Both contributions are proportional to the second derivative χ of the flow profile and are therefore not present in linear shear flows.

In experiments Eq. (42) may be used to measure the spatial variation in the flow profile by detecting the mean displacement of a particle of radius R out of the optical tweezer potential. For such a measurement usually deterministic formulas are used to describe the relation between the displacement and the flow velocity. But Eq. (42) indicates that a correction due to thermal motion has to be taken into account.

The relations given by Eq. (18) relate the fluctuations of the velocity and the position of a particle to the externally controlled flow properties and the magnitudes of the thermal fluctuations. Consequently they allow, in a similar manner as to the linear shear flow, a determination of the magnitudes of the stochastic forces in terms of the measured covariances of the particle fluctuations

$$f_{yy} = 2k\zeta\langle\tilde{y}^2\rangle, \tag{43a}$$

$$f_{xy} = 2k\zeta\left(\langle\tilde{x}\tilde{y}\rangle - \frac{1}{2}\mathrm{Wi}(y_0)\langle\tilde{y}^2\rangle\right), \tag{43b}$$

$$f_{xx} = 2k\zeta\left(\langle\tilde{x}^2\rangle - \frac{1}{2}\frac{\mathrm{Wi}(y_0)}{\tau_p\omega^2}\langle\tilde{y}^2\rangle - \frac{2}{3}\tau_p^2\chi^2\left(\frac{5+2\tau_p^2\omega^2}{1+2\tau_p^2\omega^2}\right)\langle\tilde{y}^2\rangle^2 - \mathrm{Wi}(y_0)\langle\tilde{x}\tilde{y}\rangle\right). \tag{43c}$$

The difference compared to Eq. (33) is an additional contribution to f_{xx}, which depends on the second derivative of the Poiseuille flow. Further comments made above for a linear shear flow hold as well.

Similar to the end of the previous Sec. IV A, we neglect from here on the particle inertia and we assume in addition isotropically distributed noise with $f_{xy}=0$ and $f_{ii}=2k_BT\zeta$. The static correlations of the particle's positional fluctuations in the shear plane, given by Eq. (18), then reduce to

$$\langle\tilde{x}^2\rangle = \frac{k_BT}{k}\left(1 + \frac{1}{2}\mathrm{Wi}(y_0)^2 + \frac{2}{3}\chi^2\tau_p^2\frac{k_BT}{k}\right), \tag{44a}$$

$$\langle\tilde{y}^2\rangle = \frac{k_BT}{k}, \tag{44b}$$

$$\langle\tilde{x}\tilde{y}\rangle = \langle\tilde{y}\tilde{x}\rangle = \frac{k_BT}{k}\frac{\mathrm{Wi}(y_0)}{2}. \tag{44c}$$

The static cross-correlation $\langle\tilde{x}\tilde{y}\rangle$ has the same dependence on the Weissenberg number as in the linear shear case Eq. (35c) at $t=0$, if the local shear rate of the Poiseuille flow at the

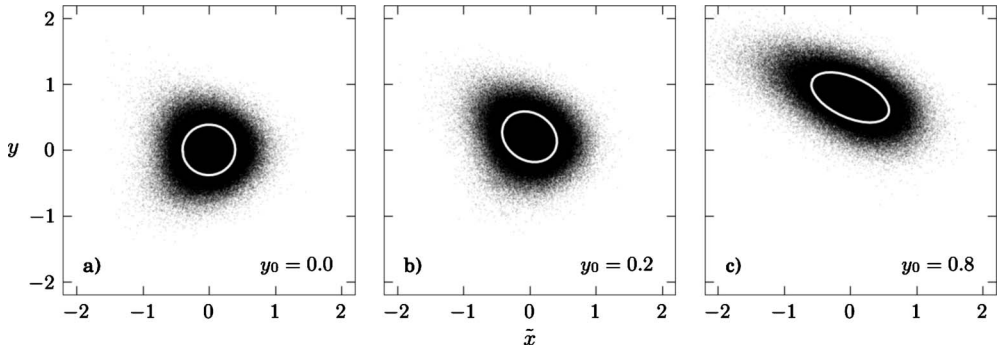

FIG. 6. Positional distribution of a Brownian particle in the xy plane captured by a harmonic potential with its minimum at $x_0=z_0=0$ and for different values of y_0. The particle is exposed to a Poiseuille flow and its dynamics have been calculated by stochastic simulations of the Eq. (8) in the overdamped limit for $\chi=1$, $k_BT=0.1$, and $\tau_p=1$.

potential center is taken. In contrast to a linear shear flow profile, the mean-square displacement of the particle in x direction, given by Eq. (44a), includes an additional constant contribution, $G:=2/3(\chi\tau_p k_B T/k)^2$, which is independent of the position of the potential minimum in the Poiseuille flow and therefore also independent of the local Weissenberg number. Besides the dependence on the second derivative χ of the flow profile, the contribution G is a direct function of the fluid temperature. Due to this contribution in Eq. (44a) one has $\langle\tilde{x}^2\rangle \neq \langle\tilde{y}^2\rangle$ and the isotropy of the particle's positional distribution in the shear plane is broken. This broken rotational symmetry also changes the analytically determined distribution function in Sec. III B along with the correlation matrix C_{ij} for a Poiseuille flow.

In addition to the calculations, we have performed simulations of the particle dynamics where we used isotropic and Gaussian distributed white noise in the overdamped version of Eq. (8). The resulting distributions for the particle's position are shown in Fig. 6 for three different positions y_0 of the potential center. With the potential minimum at the center of the flow ($y_0=0$) the numerical results show a broken mirror symmetry in x direction of the particle's positional distribution, cf. Fig. 6(a). One recognizes a parachute shape that is similar to the well-known conformation of vesicles and red blood cells in the center of a Poiseuille flow [59]. If one now makes the heuristic assumption of a Gaussian distribution for the particle's position in the case of a Poiseuille flow, as in Sec. III, but with the correlation matrix C_{ij} determined in terms of the Poiseuille flow parameters, one expects for the parameters in Fig. 6(a) an elliptical shape of the particle distribution. Indeed, the ratio between the principal axis in Fig. 6(a) is slightly smaller than 1.0. But within this analytical approximation, the $\pm x$ symmetry is not broken, which indicates the limitation of the heuristic approach.

Away from the center of the Poiseuille flow, for finite values of $y_0 \neq 0$, the $\pm y$ symmetry of the particle's positional distribution is also broken, as shown in Figs. 6(b) and 6(c). With increasing values of y_0 the local shear rate acting on the particle increases as well as the local Weissenberg number $\mathrm{Wi}(y_0)$. Consequently the cross-correlation $\langle\tilde{x}\tilde{y}\rangle$ in Eq. (44c) becomes nonzero and the particle's positional distribution in the xy plane approaches, according to our analytical results, an elliptic shape as indicated by the ellipses in Figs. 6(b) and 6(c). Again the full numerical simulations show deviations from the elliptical shape.

However, the inclination of the distribution and the inclination of the analytically determined ellipses agree rather well and therefore a determination of the angle ϕ_p for a Poiseuille flow according to Eq. (24), similar to that in the previous chapter, is reasonable and ϕ_p has the following form

$$\tan\phi_p = \frac{1}{2}\left[-\frac{y_0}{|y_0|}\sqrt{4+\left(\mathrm{Wi}(y_0)+\frac{4}{3}\frac{\tau_p^2\chi^2}{\mathrm{Wi}(y_0)}\langle\tilde{y}^2\rangle\right)^2} - \left(\mathrm{Wi}(y_0)+\frac{4}{3}\frac{\tau_p^2\chi^2}{\mathrm{Wi}(y_0)}\langle\tilde{y}^2\rangle\right)\right]. \tag{45}$$

We have shown in Sec. IV A, how the angle ϕ_p and the ratio V_p depend on the Weissenberg number of the linear shear flow. Since the local shear rate in a Poiseuille flow depends on the location y_0 of the minimum of the potential, one may plot ϕ_p and V_p [which is calculated via Eq. (25)] as a function of y_0 as shown in Fig. 7. Since the particle's distribution is anisotropic in the xy plane even for $y_0=0$, see Fig. 6(a), the corresponding principal axes are always unequal. This behavior is reflected in Fig. 7(b) where the inequality $V_p < 1$ holds for all values of y_0. The dependence of the angle ϕ_p on the local shear rate in a Poiseuille flow differs from the case of a linear shear flow: the function $\phi_p(y_0)$ is always well defined, even at the center of the flow, where it vanishes. This is one consequence of the asymmetry of the particle distribution. With increasing values of $|y_0|$ and therefore with increasing values of the local shear rate, the angle $|\phi_p|$ increases as well until it reaches some maximum value ϕ_{max} at $y_{0;max}$, as given by the following equations:

$$y_{0;max} = \pm\sqrt{\frac{\langle\tilde{y}^2\rangle}{3}}, \tag{46a}$$

$$\phi_{max} = \mp\arctan\left(\sqrt{1+\frac{4}{3}\tau_p^2\chi^2\langle\tilde{y}^2\rangle} - 2\tau_p\chi\sqrt{\frac{\langle\tilde{y}^2\rangle}{3}}\right). \tag{46b}$$

$y_{0,max}$ depends only on $\langle\tilde{y}^2\rangle$ and therefore on the width of the particle's distribution in y direction, which is determined by

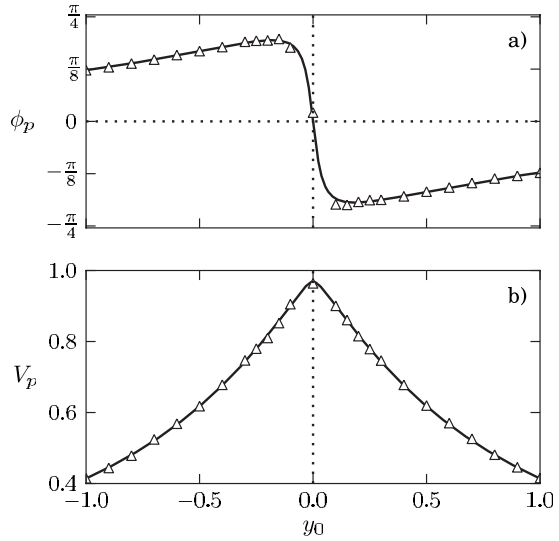

FIG. 7. The angle ϕ_p in the xy plane according to Eq. (45) is shown in (a) and the ratio V_p between the two principal axes, as determined by the Eq. (44) and Eq. (25), is shown in (b). Both are plotted as a function of the position of the potential minimum y_0 and for the parameters $\chi=\tau_p=1$, $\langle\tilde{y}^2\rangle=k_BT/k=0.1$. The triangles are the result of simulations of the Eq. (8) with the same parameter set.

the ratio between the thermal energy and the spring constant related to the harmonic potential acting on the particle. Increasing $|y_0|$ beyond $|y_{0,max}|$ the local shear rate, $\mathrm{Wi}(y_0)$, increases too, but ϕ_p starts to decrease; a similar behavior as seen in Sec. IV A. In the range $|y_0|>|y_{0,max}|$ the local shear dominates the curvature effects more and more and the Poiseuille flow resembles a linear shear flow. In addition, the particle's distribution approaches an ellipse as obtained by the heuristic approximation. As mentioned above, the heuristic analytical approach becomes exact in the case of a linear shear flow.

In Fig. 7 the analytical results on ϕ_p and V_p have been compared with our numerical simulations. In spite of the fact that we assumed for our analytical calculations a Gaussian distribution of the positional fluctuations $\tilde{x}$ and $\tilde{y}$, the results show surprisingly good agreement. The major reason for this good agreement is that we calculated the inertia tensor for the particle distribution, which includes only second order moments as assumed for the Gaussian distribution.

C. Pipe flow

For a flow profile in a pipe of radius d, cylindrical polar coordinates are appropriate. Similar to a plane Poiseuille flow the dependence of the velocity profile on the radial position ρ is also quadratic. Consequently, the ρ dependence corresponds now to the y dependence in the case of the plane Poiseuille flow. The velocity profile for the pipe flow, where the pipe axis coincides with the x axis, is of the following form,

$$u_x = u_p\left(1-\frac{\rho^2}{d^2}\right). \tag{47}$$

The results described above in Sec. IV B apply qualitatively also for the pipe flow.

With the potential minimum located at ρ_0 the coefficients in the Eq. (1) are $a=u_p(1-\frac{\rho_0^2}{d^2})$, $c=-\chi:=-\frac{u_p}{d^2}$, and $b=2\rho_0 c$. Moreover, one has to consider $\bar{a}=a+\frac{2}{3}R^2c$ in Eq. (5). The major difference to the plane Poiseuille flow is the prefactor $\frac{2}{3}$ instead of $\frac{1}{3}$. This is a consequence of the $2D$ Laplacian instead of a $1D$ second derivative in Eq. (4). The mean position of the particle is in terms of the pipe flow of the following form

$$\langle x\rangle = u_p\tau_p - \chi\tau_p\left(y_0^2+\frac{2}{3}R^2\right) - \chi\tau_p\langle y^2\rangle. \tag{48}$$

Besides the factor 2 in front of R^2 this expression corresponds to that in Eq. (42).

V. CONCLUSION

In this work, we have calculated analytically and numerically the autocorrelations and cross-correlations between different components of the velocity and the positional fluctuations of a Brownian particle in a harmonic potential, which is exposed to different shear flows. In addition, the particle's probability distribution in the harmonic potential has been determined as a function of the flow parameters. By solving an appropriate Langevin model, cross-correlations between velocity and positional fluctuations along orthogonal directions have been found and several suggestions for experimental measurements are made.

Cross-correlations between orthogonal velocity components occur only if there is already a cross-correlation between stochastic forces along orthogonal directions in the related Langevin model. On the other hand, we find cross-correlations between particle fluctuations along orthogonal directions without cross-correlations of orthogonal stochastic force components and their magnitude increases with the dimensionless shear rate, the Weissenberg number.

There are recent calculations on shear-induced cross-correlations between orthogonal fluctuations of freely floating particles [16,18]. They have the same origin as those discussed in this work. However, while measurements of the shear-induced cross-correlations of freely moving particles may be difficult, shear-induced cross-correlations for particles in a potential can be measured in a controlled manner. This insight was the basis of recent successful measurements on the cross-correlations between particle fluctuations along orthogonal directions as described in Ref. [15]. In this experiment, harmonic potentials for small latex spheres are induced by optical tweezers. The particle is simultaneously exposed to a linear shear flow in a special flow cell and its Brownian motion is investigated directly. In the same experiment and in a forthcoming work, the cross-correlations and anticorrelations between two particles captured in two neighboring potentials and exposed to shear flows are also investigated.

The measurements on the positional cross-correlation, $\langle x(t)y(0)\rangle$, presented in Ref. [15], exhibit a similar maximum as predicted by the expression in Eq. (35c) and as shown in Fig. 2. This maximum is a typical signature of Brownian motion in shear flow and it is found where the shear rate

approximately equals half of the particle's relaxation time. Also the elliptic shape of the particle's distribution, $P(\mathbf{r})$, as shown in Fig. 3, has been measured in Ref. [15]. The angle ϕ_p, enclosed by the major axis of the distribution $P(\mathbf{r})$ and the ratio V_p between the length of the two principal axes on the one hand and the magnitude of the static correlations on the other hand focus on different aspects of the dynamics of a particle in a potential exposed to a shear flow. The interrelation between these different aspects of the Brownian particle dynamics can be used for consistency checks in experiments; such cross-checks are described Ref. [15] for the case of a linear shear flow. They are also possible in experiments with Poiseuille flow as forthcoming measurements may demonstrate.

Shear-induced correlations of fluctuations of the fluid velocity with respect to a linear shear flow were found theoretically [13,14]. They are traced back to the non-normal property of the Navier-Stokes equation linearized around the linear shear profile [13] and these velocity fluctuations play an important role in a shear flow for its instability and the onset of turbulence. The cross-correlations between these velocity fluctuations exhibit a similar extremum as given by Eq. (35c), but it is a slightly different mechanism leading to this similar behavior on the level of the correlation function. This interrelation may be discussed in more detail in future work.

Stochastic forces acting on a particle in a fluid are caused by the velocity fluctuations of the fluid surrounding a particle. In quiescent fluids the correlations for velocity fluctuations are isotropically distributed. For reasons of simplicity, this is quite often assumed in models to investigate the Brownian motion of particles in shear flow. In that case, cross-correlations between stochastic forces along orthogonal directions vanish in the Langevin equation of motion. Shear-induced cross-correlations between orthogonal components of fluctuations of the fluid velocity are indeed small compared to the shear independent contributions [14,23] and hence this simplification is reasonable. However, to which extent such cross-correlations of the fluid velocity may quantitatively modify the presented results on the cross-correlations of particle displacements need further investigations.

In numerical simulations of the dynamics of a Brownian particle in a potential and exposed to a Poiseuille flow we found higher order correlations for the particle fluctuations of non-Gaussian behavior. However, for deriving our analytical results on the angle ϕ_p, which the major axis of the particle distribution encloses with the flow direction, and the ratio V_p between the lengths of the two principal axes, we assumed Gaussian distributed particle fluctuations also in Poiseuille flow. Accordingly, a perfect agreement between the results of the numerical simulations and the analytical calculations on ϕ_p and V_p could not be expected. Nevertheless, we find good agreement between both approaches, cf. Fig. 7, especially further away from the center of the Poiseuille flow, where the linear contribution in the flow profile dominates and where the assumptions are better fulfilled.

ACKNOWLEDGMENTS

We would like to thank A. Ziehl and C. Wagner for inspiring discussions. This work was supported by the German science foundation via the priority program on microfluids and nanofluidics Grant No. SPP 1164 and via the research unit Grant No. FOR 608.

APPENDIX A: CROSS-CORRELATION $\langle \tilde{v}_x(t)\tilde{v}_y(t)\rangle$

In this appendix, we discuss the correlation $\langle \tilde{v}_x(t)\tilde{v}_y(t)\rangle$ and we show that it includes, besides the contribution $\propto f_{xy}$ in Eq. (18c), in the limit $k\to 0$ an additional contribution $\propto f_{yy}$, which corresponds to the result described in Ref. [18] from Eq. (11) one obtains

$$\tilde{v}_x(t) = \int_0^t d\tau a_{vv}(t-\tau)\left[\frac{F_x^b(\tau)}{m} + 2\beta b\tilde{y}(\tau)\right], \tag{A1}$$

$$\tilde{v}_y(t) = \int_0^t d\tau a_{vv}(t-\tau)\frac{F_y^b(\tau)}{m}, \tag{A2}$$

$$\tilde{y}(\tau) = \int_0^t d\tau' a_{rv}(\tau-\tau')\frac{F_y^b(\tau)}{m}, \tag{A3}$$

with the abbreviations

$$a_{vv}(t) = \hat{\mathbf{e}}_v^T e^{\mathrm{L}(t)}\hat{\mathbf{e}}_v, \tag{A4}$$

$$a_{rv}(t) = \hat{\mathbf{e}}_r^T e^{\mathrm{L}(t)}\hat{\mathbf{e}}_v \quad \text{with} \quad \hat{\mathbf{e}}_r = \begin{pmatrix}1\\0\end{pmatrix}. \tag{A5}$$

The equal-time velocity correlation takes then the form

$$\langle \tilde{v}_x(t)\tilde{v}_y(t)\rangle = \int_0^t d\tau\int_0^t d\tau' a_{vv}(t-\tau)a_{vv}(t-\tau') \times\left\langle \frac{F_x^b(\tau)F_y^b(\tau')}{m^2}\right\rangle + 2\beta b\int_0^t d\tau a_{vv}(t-\tau) \times\langle \tilde{y}(\tau)\tilde{v}_y(t)\rangle. \tag{A6}$$

With the correlation between the position $\tilde{y}(t)$ and the velocity $\tilde{v}_y(t)$,

$$\langle \tilde{y}(\tau)\tilde{v}_y(t)\rangle = \frac{f_{yy}}{m^2}\int_0^{min(t,\tau)} d\tau'' a_{rv}(\tau-\tau'')a_{vv}(t-\tau''), \tag{A7}$$

one ends up with the expression

$$\langle \tilde{v}_x(t)\tilde{v}_y(t)\rangle = \frac{f_{xy}}{m^2}\int_0^t d\tau a_{vv}(t-\tau)^2 + 2\beta b\frac{f_{yy}}{m^2}\int_0^t d\tau\int_0^\tau d\tilde{\tau} a_{vv}(t-\tau)a_{rv}(\tau-\tilde{\tau})a_{vv}(t-\tilde{\tau}) = \frac{f_{xy}}{m^2}\frac{G_1(t)}{2} + 2\beta b\frac{f_{yy}}{m^2}\frac{G_2(t)}{4}, \tag{A8}$$

where we have introduced the functions $G_1(t)$ and $G_2(t)$ as well as the parameter δ

$$G_1(t) = \left[\frac{\beta \cos^2(\delta t)}{\delta^2} + \frac{\cos(\delta t)\sin(\delta t)}{\delta} - \frac{\delta^2 + 2\beta^2}{2\delta^2 \beta} \right] e^{-2\beta t} + \frac{1}{2\beta}, \tag{A9}$$

$$G_2(t) = \left[\frac{\sin(\delta t)\cos(\delta t)}{2\delta^3} - \frac{\beta \sin^2(\delta t)}{\delta^4} + \frac{t \sin^2(\delta t)}{2\delta^2} + \frac{\beta t \cos(\delta t)\sin(\delta t)}{\delta^3} - \frac{t \cos^2(\delta t)}{2\delta^2} \right] e^{-2\beta t}, \tag{A10}$$

$$\delta = \sqrt{\omega^2 - \beta^2}. \tag{A11}$$

In the limit $t \to \infty$ the contribution $G_1(t)$ remains finite, $\lim_{t\to\infty} G_1(t) = \frac{1}{2\beta}$. For finite values of $\tau_p = \zeta/k$ the function $G_2(t)$ vanishes on a time scale $t \gg 1/(2\beta)$ too. But in the limit of a vanishing laser tweezer potential, $k \sim \omega^2 \to 0$, one has $\delta \simeq \pm i[\beta - \omega^2/(2\beta) + \ldots]$ and in this limit some contributions of $G_2(t)$ cancel each other and the remaining terms are proportional to $\exp(-2t/\tau_p)$. These contributions do not decay in the limit $\tau_p \to \infty$ and one gets $G_2(t) = 1/(8\beta^3)$. In this case one obtains even for $f_{xy} = 0$ a nonzero cross-correlation $\langle \tilde{v}_x(t)\tilde{v}_y(t)\rangle = \frac{bf_{yy}}{4\zeta^2}$, which is exactly the same result as described in [18].

APPENDIX B: ANISOTROPIC TRAP

In experiments the force exerted by the optical tweezer on a colloidal particle may be anisotropic in the shear plane. For instance, the force constant may be different along and perpendicular to the laser beam. If the laser beam does not hit the shear plane perpendicularly the difference between the force constants in x and y direction increases with the deviation from the orthogonal direction to the shear plane. Let's assume in Eq. (3) a different force constant for each direction: k_x, k_y, and k_z.

The relaxation of the particle is now different along different directions around the potential minimum. In order to take this effect into account, we introduce three relaxation times in the same way as in Sec. III,

$$\tau_{p;i} = \frac{2\beta}{\omega_i^2} = \frac{\zeta}{k_i}, \tag{B1}$$

and we further define the fraction

$$\mu := \frac{\omega_y}{\omega_x} = \frac{k_y}{k_x}. \tag{B2}$$

between the eigenfrequencies in the shear plane, which is used to express k_y by k_x via $k_y = \mu k_x$.

The covariance matrix C from Sec. III depends now in a complex manner on the different force constants, but in the limit $\mu \to 1$ and $k_z = k_x$ the result from the previous sections are obtained again.

The different static correlations as given for the isotropic forces in Sec. III change as follows:

$$\langle \tilde{v}_y^2 \rangle = \frac{1}{4} \frac{f_{yy}}{m^2 \beta}, \tag{B3}$$

$$\langle \tilde{y}^2 \rangle = \frac{1}{4} \frac{f_{yy}}{m^2 \beta \omega_y^2} = \frac{\langle \tilde{v}_y^2 \rangle}{\omega_y^2}, \tag{B4}$$

$$\langle \tilde{v}_x^2 \rangle = \frac{1}{4} \frac{f_{xx}}{m^2 \beta} + \frac{1}{2} b^2 \langle \tilde{y}^2 \rangle \Theta_1 + \frac{8}{3} c^2 \frac{\omega_x^2 \tau_{p;x}^2}{(1 + 2\tau_{p;x}^2 \omega_x^2)} \langle \tilde{y}^2 \rangle^2 \Theta_2 - b \frac{1 - \mu^2}{1 + \mu^2} \frac{2\langle \tilde{v}_x \tilde{v}_y \rangle}{\tau_{p;x} \omega_x^2}, \tag{B5}$$

$$\langle \tilde{x}^2 \rangle = \frac{\langle \tilde{v}_x^2 \rangle}{\omega_x^2} + \frac{1}{2} \tau_{p;x}^2 b^2 \langle \tilde{y}^2 \rangle \Pi_1 + \frac{2}{3} \tau_{p;x}^2 c^2 \langle \tilde{y}^2 \rangle^2 \Pi_2 + b \tau_{p;x} \frac{2\langle \tilde{v}_x \tilde{v}_y \rangle}{\omega_x^2 (1 + \mu^2)}, \tag{B6}$$

$$\langle \tilde{v}_z^2 \rangle = \frac{1}{4} \frac{f_{zz}}{m^2 \beta}, \tag{B7}$$

$$\langle \tilde{z}^2 \rangle = \frac{1}{4} \frac{f_{zz}}{m^2 \beta \omega_y^2} = \frac{\langle \tilde{v}_z^2 \rangle}{\omega_z^2}, \tag{B8}$$

where the following abbreviations have been introduced:

$$\Theta_1 = 2 \frac{\mu^2}{1 + \mu^2},$$

$$\Theta_2 = 3\mu^2 \frac{\tau_{p;x}^2 \omega_x^2 + \frac{1}{6}(1 + 2\mu^2)}{(1 + 2\mu^2)\tau_{p;x}^2 \omega_x^2 + \frac{1}{6}(1 - 4\mu^2)^2},$$

$$\Pi_1 = 2 \frac{(1 + \mu^2)^2 + \frac{(1 - \mu^2)(1 + 2\mu^2)}{\tau_{p;x}^2 \omega_x^2} + \frac{1}{4} \frac{(1 - \mu^2)^3}{\tau_{p;x}^4 \omega_x^4}}{(1 + \mu^2)\left((1 + \mu^2) + \frac{1}{2} \frac{1}{\tau_{p;x}^2 \omega_x^2} (1 - \mu^2)^2 \right)^2},$$

$$\Pi_2 = \frac{1 + \frac{1}{3} \frac{1}{\tau_{p;x}^2 \omega_x^2} (2 + \mu^2) + \frac{1}{12} \frac{1}{\tau_{p;x}^4 \omega_x^4} (1 - 2\mu^2)(1 - 4\mu^2)}{1 + \frac{1}{2} \frac{1}{\tau_{p;x}^2 \omega_x^2} \left(\frac{(1 + 2\mu^2)}{3} + \frac{1}{2} \frac{1}{\tau_{p;x}^2 \omega_x^2} \frac{(1 - 4\mu^2)^2}{9} \right)}.$$

Since the y and z displacements are independent of any other direction, as can be seen in Eq. (11), their autocorrelations are functions of the individual force constant only and do not depend on μ. However, the autocorrelations for the velocity and the position in x direction depends in a complex manner on the different force constants. The same applies for the cross correlations in the shear plane as follows

$$\langle \tilde{v}_x \tilde{v}_y \rangle = \langle \tilde{v}_y \tilde{v}_x \rangle = \frac{1}{4} \frac{f_{xy}}{m^2 \beta} \frac{\tau_{p;x}^2 \omega_x^2 (1+\mu^2)}{\left[\tau_{p;x}^2 \omega_x^2 (1+\mu^2) + \frac{1}{2}(1-\mu^2)^2 \right]} + \frac{1}{4} b \langle \tilde{y}^2 \rangle \frac{\tau_{p;x} \omega_x^2 \mu^2 (1-\mu^2)}{\left[\tau_{p;x}^2 \omega_x^2 (1+\mu^2) + \frac{1}{2}(1-\mu^2)^2 \right]}, \quad \text{(B9)}$$

$$\langle \tilde{x}\tilde{y} \rangle = \langle \tilde{y}\tilde{x} \rangle = \left[\frac{\langle \tilde{v}_x \tilde{v}_y \rangle}{\omega_x^2} + \frac{1}{2} \tau_{p;x} b \langle \tilde{y}^2 \rangle \right] \frac{2}{(1+\mu^2)}, \quad \text{(B10)}$$

$$\langle \tilde{x}\tilde{v}_y \rangle = -\langle \tilde{y}\tilde{v}_x \rangle = -\frac{\mu^2 b \langle \tilde{y}^2 \rangle}{(1+\mu^2)} + \frac{(1-\mu^2)}{(1+\mu^2)} \frac{\langle \tilde{v}_x \tilde{v}_y \rangle}{\tau_{p;x} \omega_x^2}. \quad \text{(B11)}$$

[1] A. Einstein, Ann. Phys. **17**, 549 (1905).
[2] J. K. G. Dhont, *An Introduction to Dynamics of Colloids* (Elsevier, Amsterdam, 1996).
[3] H. Stone and S. Kim, AIChE J. **47**, 1250 (2001).
[4] J. Ottino and S. Wiggins, Philos. Trans. R. Soc. London, Ser. A **362**, 923 (2004).
[5] L. Holzer and W. Zimmermann, Phys. Rev. E **73**, 060801(R) (2006).
[6] C. Lutz, M. Reichert, H. Stark, and C. Bechinger, Europhys. Lett. **74**, 719 (2006).
[7] G. Taylor, Proc. R. Soc. London, Ser. A **219**, 186 (1953).
[8] A. Groisman and V. Steinberg, Nature (London) **410**, 905 (2001).
[9] T. Perkins, D. Smith, and S. Chu, Science **276**, 2016 (1997).
[10] P. G. deGennes, Science **276**, 1999 (1997).
[11] A. Groisman and V. Steinberg, Nature (London) **405**, 53 (2000).
[12] S. Grossmann, Rev. Mod. Phys. **72**, 603 (2000).
[13] B. Eckhardt and R. Pandit, Eur. Phys. J. B **33**, 373 (2003).
[14] G. Khujadze, M. Oberlack, and G. Chagelishvili, Phys. Rev. Lett. **97**, 034501 (2006).
[15] A. Ziehl, J. Bammert, L. Holzer, C. Wagner, and W. Zimmermann, Phys. Rev. Lett. **103**, 230602 (2009).
[16] K. Miyazaki and D. Bedeaux, Physica A **217**, 53 (1995).
[17] G. Subramanian and J. Brady, Physica A **334**, 343 (2004).
[18] Y. Drossinos and M. W. Reeks, Phys. Rev. E **71**, 031113 (2005).
[19] M. San Miguel and J. M. Sancho, Physica A **99**, 357 (1979).
[20] I. Santamaria-Holek, D. Reguera, and J. M. Rubi, Phys. Rev. E **63**, 051106 (2001).
[21] R. Foister and T. van de Ven, J. Fluid Mech. **96**, 105 (1980).
[22] G. Fuller, J. Rallison, R. Schmidt, and L. Leal, J. Fluid Mech. **100**, 555 (1980).
[23] L. Holzer, Ph. D thesis, Universität Bayreuth, 2009.
[24] M. Hoppenbrouwers and W. van de Water, Phys. Fluids **10**, 2128 (1998).
[25] D. G. Grier, Nature (London) **424**, 810 (2003).
[26] A. Ashkin, J. Dziedzic, J. Bjorkholm, and S. Chu, Opt. Lett. **11**, 288 (1986).
[27] S. Chu, Science **253**, 861 (1991).
[28] T. Perkins, S. Quake, D. Smith, and S. Chu, Science **264**, 822 (1994).
[29] T. Perkins, D. Smith, R. Larson, and S. Chu, Science **268**, 83 (1995).
[30] F. Brochard-Wyart, Europhys. Lett. **30**, 387 (1995).
[31] R. G. Larson, T. T. Perkins, D. E. Smith, and S. Chu, Phys. Rev. E **55**, 1794 (1997).
[32] R. Rzehak, D. Kienle, T. Kawakatsu, and W. Zimmermann, Europhys. Lett. **46**, 821 (1999).
[33] R. Rzehak, W. Kromen, T. Kawakatsu, and W. Zimmermann, Eur. Phys. J. E **2**, 3 (2000).
[34] D. Kienle and W. Zimmermann, Macromolecules **34**, 9173 (2001).
[35] R. Rzehak and W. Zimmermann, Europhys. Lett. **59**, 779 (2002).
[36] J. C. Meiners and S. R. Quake, Phys. Rev. Lett. **82**, 2211 (1999).
[37] S. Henderson, S. Mitchell, and P. Bartlett, Phys. Rev. Lett. **88**, 088302 (2002).
[38] E. Dufresne, D. Altman, and D. Grier, Europhys. Lett. **53**, 264 (2001).
[39] E. R. Dufresne, T. M. Squires, M. P. Brenner, and D. G. Grier, Phys. Rev. Lett. **85**, 3317 (2000).
[40] M. Atakhorrami, G. H. Koenderink, C. F. Schmidt, and F. C. MacKintosh, Phys. Rev. Lett. **95**, 208302 (2005).
[41] J. C. Crocker, M. T. Valentine, E. R. Weeks, T. Gisler, P. D. Kaplan, A. G. Yodh, and D. A. Weitz, Phys. Rev. Lett. **85**, 888 (2000).
[42] M. Polin, D. G. Grier, and S. Quake, Phys. Rev. Lett. **96**, 088101 (2006).
[43] P. T. Korda, M. B. Taylor, and D. G. Grier, Phys. Rev. Lett. **89**, 128301 (2002).
[44] J. Bammert, S. Schreiber, and W. Zimmermann, Phys. Rev. E **77**, 042102 (2008).
[45] J. Bammert and W. Zimmermann, Eur. Phys. J. E **28**, 331 (2009).
[46] M. P. MacDonald, G. C. Spalding, and K. Dholakia, Nature (London) **426**, 421 (2003).
[47] R. Simmons, J. Finer, S. Chu, and J. Spudich, Biophys. J. **70**, 1813 (1996).
[48] J. Crocker and D. Grier, J. Colloid Interface Sci. **179**, 298 (1996).
[49] L. D. Landau and E. M. Lifschitz, *Lehrbuch der Theoretischen Physik: Hydrodynamik*, 2nd ed. (Akademie Verlag, Berlin, 1987).
[50] G. G. Stokes, Trans. Cambridge Phil. Soc. **IX**, 8 (1850).
[51] H. Faxen, Z. Angew. Math. Mech. **7**, 79 (1927).
[52] L. E. Reichl, *A Modern Course in Statistical Physics*, 2nd ed. (Wiley, Berlin, 1998).
[53] L. D. Landau and E. M. Lifschitz, *Lehrbuch der Theoretischen Physik: Statistische Physik II* (Akademie Verlag, Berlin, 1980).
[54] N. G. van Kampen, *Stochastic Processes in Physics and Chemistry* (Elsevier, Amsterdam, 2004).
[55] B. Bamieh and M. Dahleh, Phys. Fluids **13**, 3258 (2001).

[56] J. M. Ortiz de Zárate and J. V. Sengers, Phys. Rev. E **77**, 026306 (2008).
[57] M. Kraus, W. Wintz, U. Seifert, and R. Lipowsky, Phys. Rev. Lett. **77**, 3685 (1996).
[58] P. G. deGennes and J. Prost, *The Physics of Liquid Crystals* (Clarendon Press, Oxford, 2006).
[59] G. Danker, P. M. Vlahovska, and C. Misbah, Phys. Rev. Lett. **102**, 148102 (2009).

Publication 5

Dynamics of two trapped Brownian particles: Shear-induced cross-correlations
J. Bammert, L. Holzer, and W. Zimmermann,
European Physical Journal E **33**, 313 (2010)

Copyright by EDP Sciences, Società Italiana di Fisica, Springer-Verlag 2010
DOI: 10.1140/epje/i2010-10675-2

Eur. Phys. J. E **33**, 313–325 (2010)
DOI 10.1140/epje/i2010-10675-2

THE EUROPEAN PHYSICAL JOURNAL E

Regular Article

Dynamics of two trapped Brownian particles: Shear-induced cross-correlations

J. Bammert, L. Holzer, and W. Zimmermann[a]

Theoretische Physik I, Universität Bayreuth, D-95440 Bayreuth, Germany

Received 8 June 2010 and Received in final form 7 September 2010
Published online: 1 December 2010 – © EDP Sciences / Società Italiana di Fisica / Springer-Verlag 2010

Abstract. The dynamics of two Brownian particles trapped by two neighboring harmonic potentials in a linear shear flow is investigated. The positional correlation functions in this system are calculated analytically and analyzed as a function of the shear rate and the trap distance. Shear-induced cross-correlations between particle fluctuations along orthogonal directions in the shear plane are found. They are linear in the shear rate, asymmetric in time, and occur for one particle as well as between both particles. Moreover, the shear rate enters as a quadratic correction to the well-known correlations of random displacements along parallel spatial directions. The correlation functions depend on the orientation of the connection vector between the potential minima with respect to the flow direction. As a consequence, the inter-particle cross-correlations between orthogonal fluctuations can have zero, one or two local extrema as a function of time. Possible experiments for detecting these predicted correlations are described.

1 Introduction

The Brownian dynamics of particles in fluids is of high relevance in many fields of natural and applied sciences. It is strongly affected by the interplay between the particles via the liquid, the so-called hydrodynamic interaction. Especially in the field of microfluidics this nonlinear interaction plays an important role in subjects such as Taylor dispersion [1] or fluid mixing [2,3]. In a quiescent fluid there is already a considerable understanding of the dynamics of Brownian particles and their interactions [4,5]. Investigations on the positional correlation functions of two trapped particles give further insight in the coupling between thermal motion and the hydrodynamic interaction among them [6,7]. However, the understanding of this interplay in typical laminar flows, like in a linear shear flow or in a Poiseuille flow, is still far from complete although it is the origin of a number of interesting phenomena. For example, polymers exhibit in shear flows already at small values of the Reynolds number the so-called molecular individualism [8,9], elastic turbulence, and spectacular mixing properties in the dilute regime [10]. The complex interplay between Brownian motion and hydrodynamic interaction also affects considerably the conformational distribution functions of tethered polymers in flows and their dynamics [11–19]. When polymers are attached to a wall and subjected to a flow, an additional time-periodic behavior influences the dynamics [20–24], which shows similar features as tumbling polymers in shear flows [8,25–27].

Recent theoretical investigations on the fluid velocity fluctuations in shear flows show that in contrast to quiescent fluids or uniform flows, cross-correlations between velocity fluctuations along and perpendicular to the streamlines occur [28,29]. For free Brownian particles in a linear shear flow in the x-direction, where the shear plane is parallel to the xy-plane, one also expects a cross-correlation between the orthogonal positional fluctuations $\tilde{x}$ and $\tilde{y}$ of the particles, *i.e.* $\langle\tilde{x}\tilde{y}\rangle \neq 0$ [30–32]. In this case, random jumps of a particle between neighboring parallel streamlines lead to a change of the particle's velocity. For example, a positional fluctuation, $\tilde{y}$, perpendicular to the streamlines may cause a fluctuation, $\tilde{x}$, along the streamlines and contributes in this way to the correlation function $\langle\tilde{x}\tilde{y}\rangle$, which reflects the shear-induced coupling between fluctuations along orthogonal directions.

The theoretical considerations described in ref. [33] show that shear-induced cross-correlations between perpendicular random particle displacements, like $\langle\tilde{x}\tilde{y}\rangle \neq 0$, survive if a particle experiences some constraints such as a harmonic potential. This is important from various points of view. First, these cross-correlations are inherently present in bead-spring models, which are used to describe polymer dynamics in shear flows, because the individual beads along the chain are bound to their neighbors. Second, this knowledge facilitates the experimental detection of these cross-correlations, because measurements of particle fluctuations in the spatially limited area of the trapping potential can be performed in a controlled manner compared to tracing free Brownian particles. According to this strategy, the cross-correlations $\langle\tilde{x}\tilde{y}\rangle$ of trapped

[a] e-mail: walter.zimmermann@uni-bayreuth.de

particles in a linear shear flow have been measured directly for the first time and the results are in good agreement with the theoretical predictions [34].

The optical tweezer technique, employed in ref. [34], triggered a number of further direct observations of particle fluctuations. These include inspiring studies on single polymers [11–13,35], the propagation of hydrodynamic interactions [36], wall effects on Brownian motion [37,38], two-point microrheology [39], particle sorting techniques [40–43], the determination of the effective pair potential in colloidal suspensions [44], and many other investigations in microfluidics, cf. [45,46]. By femto-Newton measurements anti-correlations have been detected between two hydrodynamically interacting and neighboring particles in a quiescent fluid, each one captured by a laser tweezer potential [6]. This was recently extended in ref. [34], where shear-induced inter-particle anti-correlations between orthogonal motions of the two particles have been found.

The present work focuses on the question, which kind of cross-correlations can be expected between hydrodynamically interacting particles in linear shear flows. Such inter-particle correlations along a single polymer and between different polymers in flows influence their dynamics. This paper is an extension of the theoretical work on the single-particle dynamics described in ref. [33] to a pair of two hydrodynamically interacting point-particles with an effective hydrodynamic radius and trapped in a linear shear flow. It provides the theoretical background for the experimental results on the two-particle correlations presented in ref. [34]. The correlation functions between the different particle displacements are calculated analytically and we show how a second Brownian particle influences the stochastic motion and the positional probability distribution of its neighbor compared to the single-particle case [34,33]. In addition, we find that the anti cross-correlations between two fluctuating particles in a quiescent fluid, as described in ref. [6], experience shear-induced corrections. We also describe the occurrence of shear-induced anti cross-correlations between the fluctuations of the two particles along two orthogonal directions. The results depend significantly on the orientation of the connection vector between the two traps with respect to the flow direction. We focus on the leading-order contributions to the correlation functions and neglect the effects of finite size and rotations of the particles.

The structure of the paper is as follows: In sect. 2, the model equations are introduced and their formal analytical solution is presented, which results in the calculation of the correlation functions for the random particle displacements. In sect. 3, the results for three representative setups of the two-particle system are discussed in detail, where the connection vector between the two potential minima is either parallel, perpendicular, or oblique to the shear flow direction. In addition, the results are compared with direct simulations of the Langevin equation for representative examples. For the parallel case, a few experimental and theoretical results have already been described in ref. [34], where a good agreement between experiment and theory was found. The article closes with a discussion and further possible applications in sect. 4.

2 Equations of motion and their solution

The basis of our investigation is a Langevin model that describes the over-damped dynamics of two particles, each held by a harmonic potential in a linear shear flow. In this section the equation of motion is introduced and solved in order to calculate the correlation functions analytically. They consist of different eigenmodes, which are discussed briefly.

2.1 Model equations

We consider two Brownian point-particles with effective hydrodynamic radius a, immersed in a Newtonian fluid of viscosity η at the positions $\mathbf{r}_i = (x_i, y_i, z_i)$ with $i = 1, 2$. Each particle is held by a linear restoring force,

$$\mathbf{f}_i^V = -\nabla V_i = -k\left(\mathbf{r}_i - \mathbf{q}_i\right), \tag{1}$$

close to the minimum $\mathbf{q}_i$ of a corresponding harmonic potential,

$$V_i = \frac{k}{2}\left(\mathbf{r}_i - \mathbf{q}_i\right)^2, \tag{2}$$

with the spring constant k. The distance between the potential minima is labeled with d. Uncharged polystyrene latex beads of micrometer size that are trapped by laser tweezers experience such a potential as described by eq. (2) [6,47,48].

Both trapped particles are exposed to a linear shear flow in the x-direction with the shear plane parallel to the xy-plane and the shear rate $\dot{\gamma}$:

$$\mathbf{u}(\mathbf{r}) = \dot{\gamma} y \mathbf{e}_x. \tag{3}$$

This flow causes a drag force on the hydrodynamically interacting Brownian particles, which is in competition with the restoring force (1). In a recent experiment the interplay between these two forces has been studied [34], where the size of the particles was about $5\,\mu$m and the shear rate about $50\,\mathrm{s}^{-1}$. At the length scale of the excursions of the particles from their potential minima and the distance between the two beads, the Reynolds number is small and therefore, we can describe the fluid motion around the beads in the Stokes limit. Consequently, the over-damped particle dynamics is described by the Langevin equations,

$$\dot{\mathbf{r}}_i = \mathbf{u}(\mathbf{r}_i) + \mathsf{H}_{ij}\mathbf{f}_j^V + \mathbf{f}_i^S, \tag{4}$$

with the four 3×3 mobility matrices

$$\mathsf{H}_{11} = \mathsf{H}_{22} = \frac{1}{\zeta}\mathsf{I}, \tag{5a}$$

$$\mathsf{H}_{12} = \mathsf{H}_{21} = \frac{1}{\zeta}\frac{3a}{4r_{12}}\left[\mathsf{I} + \frac{\mathbf{r}_{12} \otimes \mathbf{r}_{12}}{r_{12}^2}\right], \tag{5b}$$

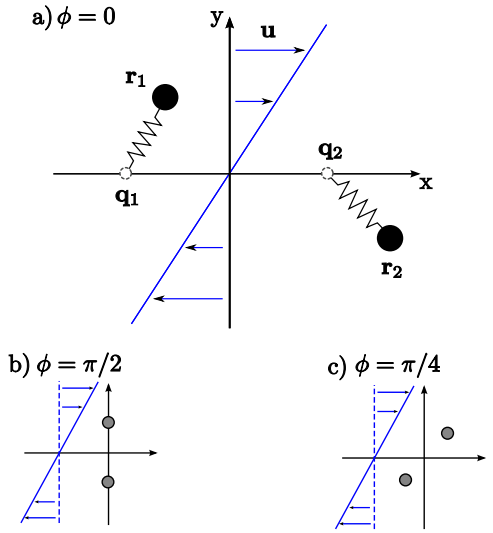

Fig. 1. Two Brownian particles are kept by linear spring forces $\mathbf{f}^V_{1,2}$ close to the minima of two corresponding harmonic potentials at $\mathbf{q}_{1,2}$. Both particles are simultaneously exposed to a linear shear flow $\mathbf{u}(\mathbf{r})$. The angle ϕ between the flow direction $\mathbf{u}(\mathbf{r})$ and the vector $\mathbf{q}_{12} = \mathbf{q}_1 - \mathbf{q}_2$ connecting the potential minima at the distance $d = |\mathbf{q}_{12}|$ is either zero, as in part a), or $\phi = \pi/2$ as in b), or $\phi = \pi/4$ as in c).

including the Stokes friction coefficient $\zeta = 6\pi\eta a$ for a single point-particle [49]. The latter two matrices describe the hydrodynamic interaction between two point-particles in terms of the Oseen tensor [5] and I represents the unity matrix. The dyadic product (tensor product) $\otimes$ has been used as well as the distance vector $\mathbf{r}_{12} := \mathbf{r}_1 - \mathbf{r}_2$ between the beads, with $r_{12} = |\mathbf{r}_{12}|$.

The stochastic forces in the Langevin model have their origin in the velocity fluctuations of the surrounding liquid. In a quiescent fluid these random forces are uncorrelated along orthogonal directions in the bulk [50]. This assumption is kept in our Langevin model, because shear-induced cross-correlations between the stochastic forces along orthogonal directions are expected to be small [29,51,52]. So, for the contribution $\mathbf{f}^S_i(t)$ in eq. (4) we assume a zero mean and a vanishing correlation time [5]

$$\left\langle \mathbf{f}^S_i(t) \right\rangle = 0, \tag{6a}$$

$$\left\langle \mathbf{f}^S_i(t) \otimes \mathbf{f}^S_j(t') \right\rangle = 2k_BT\mathsf{H}_{ij}\delta(t-t'). \tag{6b}$$

The strength of the stochastic forces is proportional to the thermal energy k_BT.

The orientation of the connection vector between the potential minima, $\mathbf{q}_{12} := \mathbf{q}_1 - \mathbf{q}_2$, with respect to the flow direction is described by the angle ϕ. It has a strong influence on the correlation functions of the positional fluctuations of the particles. For this reason, we investigate three characteristic setups, where $\mathbf{q}_{12}$ is either parallel to the external flow $\mathbf{u}$ ($\phi = 0$), or perpendicular ($\phi = \pi/2$), or oblique ($\phi = \pi/4$) as sketched in fig. 1.

2.2 Solutions and relaxation times

There are two characteristic time scales in the system. One is determined by the inverse shear rate $\dot\gamma^{-1}$ and the other one is given by the relaxation time $\tau := \zeta/k$ of the particles in the two identical potentials. Their ratio gives the dimensionless Weissenberg number,

$$\mathrm{Wi} := \dot\gamma\tau, \tag{7}$$

which will be useful for the further discussion.

The first step in the solution of eq. (4) is to rewrite the equation of motion in a more compact form by introducing the positional vector $\mathbf{R} = (\mathbf{r}_1, \mathbf{r}_2)$ with six components and the 6×6 mobility matrix H,

$$\mathsf{H} = \begin{pmatrix} \mathsf{H}_{11} & \mathsf{H}_{12} \\ \mathsf{H}_{12} & \mathsf{H}_{22} \end{pmatrix}, \tag{8}$$

composed of the sub-matrices H_{ij} from eqs. (5). The shear flow in eq. (3) can be written in an analogous manner with the 6×6 shear rate tensor U,

$$\mathbf{U}(\mathbf{R}) = \mathsf{U}\mathbf{R}, \tag{9}$$

with $\mathsf{U}_{12} = \mathsf{U}_{45} = \dot\gamma$ and all other $\mathsf{U}_{kl} = 0$. The equation of motion (4) then takes the form,

$$\dot{\mathbf{R}} = \mathsf{U}\mathbf{R} + k\mathsf{H}\left(\mathbf{Q} - \mathbf{R}\right) + \mathbf{F}, \tag{10}$$

where the vector $\mathbf{Q} = (\mathbf{q}_1, \mathbf{q}_2)$ describes the positions of the two potential minima being separated by the distance d. The stochastic contribution $\mathbf{F}$ in eq. (10) is obtained from eqs. (6)

$$\langle \mathbf{F}(t) \rangle = 0, \tag{11a}$$

$$\langle \mathbf{F}(t) \otimes \mathbf{F}(t') \rangle = 2k_BT\mathsf{H}\delta(t-t'). \tag{11b}$$

We assume two well-separated point-particles with small values of a/d and small fluctuations around their mean positions, *i.e.* $k_BT/(ka^2) \ll 1$. The experimental results described in ref. [34], which were obtained for $a/d \approx 1/4$ and a magnitude of the fluctuations below $a/10$, are well described within this approximation.

Since we investigate the particle fluctuations, the mean position $\mathbf{R}_\phi := \langle \mathbf{R}(t) \rangle$ has to be determined first. In the case $\phi = 0$ the mean positions are identical with the locations of the potential minima: $\mathbf{R}_0 = \mathbf{Q}$. For $\phi = \pi/2$ and $\phi = \pi/4$, $\mathbf{R}_\phi$ is obtained numerically by determining the stationary solution of eq. (10) in the absence of noise. Disregarding the hydrodynamic interaction between the two particles, one finds the analytical expressions

$$\mathbf{R}^a_{\pi/2} = \frac{d}{2}\left(\mathrm{Wi}, 1, 0, -\mathrm{Wi}, -1, 0\right), \tag{12a}$$

$$\mathbf{R}^a_{\pi/4} = \frac{d}{4}\left(\sqrt{2} + \mathrm{Wi}, \sqrt{2}, 0, -\sqrt{2} - \mathrm{Wi}, -\sqrt{2}, 0\right), \tag{12b}$$

which may serve as an approximation of the stationary solution and as the starting point of the numerical iteration.

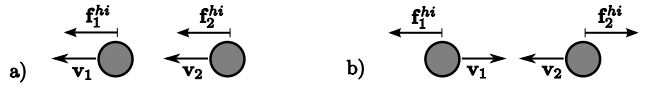

Fig. 2. The motion of particle 1 causes, via the hydrodynamic interaction, a force $\mathbf{f}_2^{hi}$ on particle 2 and vice versa. In part a), where the two particles move in the same direction, the resulting hydrodynamic forces accelerate the motion. This situation corresponds to the parallel relaxation. Part b) shows the anti-parallel case, where the forces $\mathbf{f}_i^{hi}$ decelerate the motion.

The equation of motion for the particle fluctuations $\bar{\mathbf{R}} = (\bar{x}_1, \bar{y}_1, \bar{z}_1, \bar{x}_2, \bar{y}_2, \bar{z}_2)$ are obtained by the ansatz $\mathbf{R} = \mathbf{R}_\phi + \bar{\mathbf{R}}$ and the linearization of eq. (10) with respect to $\bar{\mathbf{R}}$

$$\dot{\bar{\mathbf{R}}} = \mathsf{U}\bar{\mathbf{R}} - k\mathsf{H}\bar{\mathbf{R}} + k\left[\nabla \mathsf{H}\bar{\mathbf{R}}\right](\mathbf{Q} - \mathbf{R}_\phi) + \mathbf{F}. \tag{13}$$

Here the mobility matrix H and its derivative are evaluated at the exact mean positions $\mathbf{R}_\phi$. For $\phi = 0$ one has $\mathbf{R}_\phi = \mathbf{Q}$ and the third contribution on the right-hand side vanishes. Introducing the matrix $\mathsf{K} := [\nabla \otimes (\mathsf{H}(\mathbf{Q} - \mathbf{R}_\phi))]^T$, eq. (13) can be rewritten to

$$\dot{\bar{\mathbf{R}}} = -\left(k\mathsf{H} - \mathsf{U} - k\mathsf{K}\right)\bar{\mathbf{R}} + \mathbf{F} = -\mathsf{M}\bar{\mathbf{R}} + \mathbf{F}, \tag{14}$$

and this linear equation has the formal solution

$$\bar{\mathbf{R}}(t) = e^{-t\mathsf{M}}\bar{\mathbf{R}}(0) + \int_0^t \mathrm{d}t' e^{(t'-t)\mathsf{M}}\mathbf{F}. \tag{15}$$

By introducing the scaled deviation

$$\tilde{\mathbf{R}} = \frac{\bar{\mathbf{R}}}{\sqrt{B}}, \quad \text{with} \quad B = \frac{2k_BT}{k}, \tag{16}$$

and taking into account the statistical properties of the stochastic forces as given by eq. (11), one can determine by a straightforward calculation, assisted by computer algebra, the correlation matrix $\mathsf{C}(t)$ defined by

$$\mathsf{C}(t) := \langle \tilde{\mathbf{R}}(0) \otimes \tilde{\mathbf{R}}(t) \rangle, \quad \text{for} \quad t \geq 0. \tag{17}$$

The brackets $\langle \cdot \rangle$ denote the ensemble average over a large number of particle trajectories. The elements $\mathsf{C}_{kl}(t)$ of the Matrix $\mathsf{C}(t)$ can be represented as a sum of six exponentially decaying contributions,

$$\mathsf{C}_{kl}(t) = \sum_\alpha g_{\alpha,kl} e^{-\lambda_\alpha t} \qquad (\alpha, k, l = 1 \ldots 6), \tag{18}$$

where the coefficients $g_{\alpha,kl}$ depend on the Weissenberg number $\mathrm{Wi} = \dot{\gamma}\tau$ and on the distance between the potential minima d.

The origin of the relaxation times $1/Re(\lambda_\alpha)$, given by the eigenvalues λ_α of the matrix $\mathsf{M} := k\mathsf{H} - \mathsf{U} - k\mathsf{K}$, can be explained as follows: After a stochastic kick that pushes the particles away from their mean positions, the potential forces start to pull them back. During this relaxation the particle motion can be decomposed into parallel or anti-parallel translations as illustrated in fig. 2. It is the hydrodynamic interaction between the particles which accelerates or damps this process, since the resulting hydrodynamic forces depend on the relative particle motions. The beads relax faster, if they move in the same direction. The whole relaxation process is described by six relaxation rates, λ_α, two for each spatial direction and in the two cases $\phi = \pi/2$ and $\phi = \pi/4$ some of them may even be complex. For the configuration $\phi = 0$, cf. fig. 1a), two relaxation modes coincide, so there are only four instead of six different relaxation times.

3 Correlation functions

In the two-particle system, the fluctuation statistics of one particle is influenced by its neighbor. We call the corresponding correlation functions "one-particle correlations" and for the inter-particle cross-correlations between the random displacements of two different particles we use the notation "inter-particle correlations".

In a previous study on hydrodynamic interactions between two trapped Brownian particles in a quiescent fluid, anti cross-correlations between their random motions along parallel spatial directions were found [6]. We show that the shear flow alters these correlations and additionally induces inter-particle cross-correlations along orthogonal directions in the shear plane.

In this section the exact expressions and the approximations of the correlation functions $\mathsf{C}_{kl}(t)$, as defined by eq. (17), are discussed in detail and they are also compared with numerically obtained solutions of the Langevin equation (10). The behavior of $\mathsf{C}_{kl}(t)$ depends on the trap distance d, and in the limit $d \to \infty$, our formulas become identical to the recently presented results for a single trapped particle in a linear shear flow [33]. Since our results depend on the angle ϕ between the connection vector $\mathbf{q}_{12}$ and the flow direction, the three characteristic configurations, as sketched in fig. 1, are analyzed.

3.1 Parallel case: $\phi = 0$

At first, we consider the two-particle configuration with the connection vector $\mathbf{q}_{12}$ parallel to the flow lines $\mathbf{u}$ as sketched in fig. 1a), *e.g.* $\mathbf{Q} = d/2(1, 0, 0, -1, 0, 0)$. The discussion of the one-particle correlations in sect. 3.1.1 is complemented by the analysis of the inter-particle correlations in sect. 3.1.2.

Similar to the case of two trapped particles in a quiescent fluid in ref. [6] there are four different relaxation rates describing the four relaxation times in the system, cf. sect. 2.2

$$\lambda_1 = \frac{1+2\mu}{\tau}, \qquad \lambda_3 = \frac{1-2\mu}{\tau}, \tag{19a}$$

$$\lambda_2 = \frac{1+\mu}{\tau}, \qquad \lambda_4 = \frac{1-\mu}{\tau}\ . \tag{19b}$$

The parameter $0 < \mu := 3a/(4d) < 3/8$ is a measure for the distance between the traps. λ_1 and λ_3 correspond

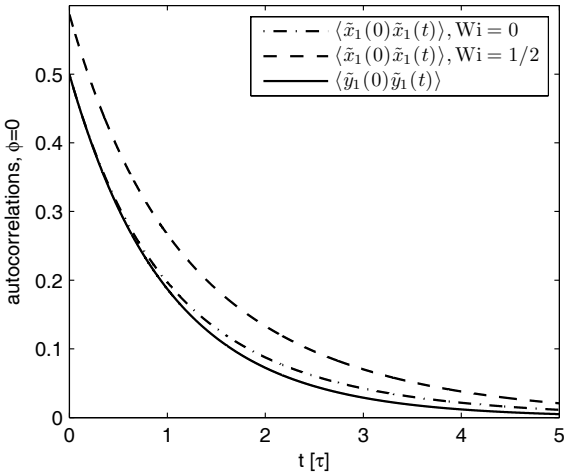

Fig. 3. The autocorrelations, $\langle\tilde{x}_1(0)\tilde{x}_1(t)\rangle = \langle\tilde{x}_2(0)\tilde{x}_2(t)\rangle$, along the flow direction are shown for Wi = 0 (dash-dotted line) and for Wi = 1/2 (dashed line). The correlation functions perpendicular to the flow direction, $\langle\tilde{y}_i(0)\tilde{y}_i(t)\rangle = \langle\tilde{z}_i(0)\tilde{z}_i(t)\rangle$ with $i = 1, 2$ (solid line), do not depend on the Weissenberg number. All curves are obtained for a distance $d = 4a$ and t is given in units of τ.

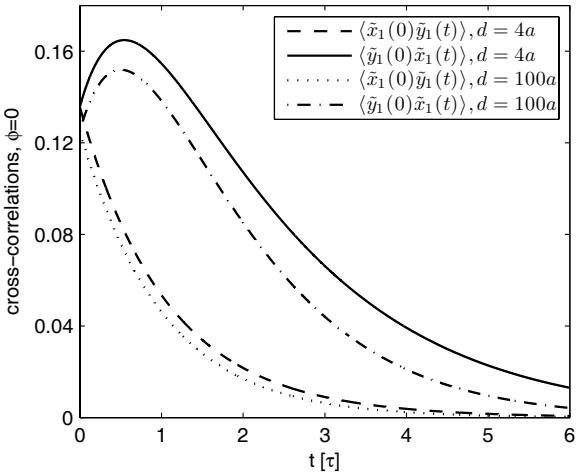

Fig. 4. Shear-induced cross-correlations of a single particle in the parallel case for Wi = 1/2 and $d = 4a$, respectively $d = 100a$. $\langle\tilde{x}_1(t)\tilde{y}_1(0)\rangle$ has a maximum around $t' \approx \tau$, which does not depend on Wi and only very weakly on d.

to the particle motions parallel and anti-parallel to the connection vector $\mathbf{q}_{12}$ (longitudinal displacements), while λ_2 and λ_4 belong to the particle relaxations perpendicular to $\mathbf{q}_{12}$ (transversal displacements).

3.1.1 One-particle correlations

The autocorrelations are identical for both particles but they are different for the longitudinal and transversal displacements: $\langle\tilde{x}_1(0)\,\tilde{x}_1(t)\rangle = \langle\tilde{x}_2(0)\,\tilde{x}_2(t)\rangle$ and $\langle\tilde{y}_1(0)\tilde{y}_1(t)\rangle = \langle\tilde{y}_2(0)\tilde{y}_2(t)\rangle = \langle\tilde{z}_1(0)\tilde{z}_1(t)\rangle = \langle\tilde{z}_2(0)\tilde{z}_2(t)\rangle$. The expressions

$$\begin{aligned}\langle\tilde{x}_1(0)\tilde{x}_1(t)\rangle = {} & \frac{1}{4}\left(e^{-\lambda_1 t} + e^{-\lambda_3 t}\right) \\ & + \frac{\mathrm{Wi}^2}{4\mu}\left(\frac{-(1+\mu)e^{-\lambda_1 t}}{6\mu^2+7\mu+2} + \frac{e^{-\lambda_2 t}}{2+3\mu}\right) \\ & + \frac{\mathrm{Wi}^2}{4\mu}\left(\frac{(1-\mu)e^{-\lambda_3 t}}{6\mu^2-7\mu+2} - \frac{e^{-\lambda_4 t}}{2-3\mu}\right), \quad (20a)\end{aligned}$$

$$\langle\tilde{y}_1(0)\tilde{y}_1(t)\rangle = \langle\tilde{z}_1(0)\tilde{z}_1(t)\rangle = \frac{1}{4}\left(e^{-\lambda_2 t} + e^{-\lambda_4 t}\right), \quad (20b)$$

are exponentially decaying in time and both functions are plotted in fig. 3 for different values of the Weissenberg number Wi. Due to the scaling (16) the value of $\langle\tilde{y}_1(0)\tilde{y}_1(0)\rangle$ is 1/2. The correlation functions (20) depend via μ on the trap distance d, which leads to interesting corrections to the autocorrelations compared to the case of one isolated particle in ref. [33].

The distinct relaxation rates given by eqs. (19) lead to different autocorrelations of particle displacements along and perpendicular to $\mathbf{q}_{12}$, independent of the parameter Wi. This is also indicated in fig. 3 by the difference between the correlations $\langle\tilde{x}_1(0)\tilde{x}_1(t)\rangle$ (dash-dotted line) and $\langle\tilde{y}_1(0)\tilde{y}_1(t)\rangle$ (solid line). The latter one is independent of the Weissenberg number, which is similar to the case of an isolated trapped particle, where only the autocorrelation in flow direction (20a) depends on Wi^2 [33].

Any translation of a particle in the y-direction is coupled via the flow profile (3) to a change of the particle's velocity in the x-direction, which leads to a change of the particle's positional fluctuation along the x-direction. Consequently, the particle fluctuations in the x- and y-directions become correlated due to the shear flow. The resulting cross-correlations between the displacements along orthogonal directions in the shear plane are linear functions of the parameter Wi, similar to the single-particle case in refs. [33,34]. However, compared to these results, we obtain for the two-particle system an additional dependence on the trap distance d. The time dependence of the cross-correlations is given by the following expressions:

$$\langle\tilde{x}_1(0)\tilde{y}_1(t)\rangle = \frac{\mathrm{Wi}}{4}\left(\frac{e^{-\lambda_2 t}}{2+3\mu} + \frac{e^{-\lambda_4 t}}{2-3\mu}\right), \quad (21a)$$

$$\begin{aligned}\langle\tilde{y}_1(0)\tilde{x}_1(t)\rangle = {} & \frac{\mathrm{Wi}}{4\mu}\left(e^{-\lambda_2 t} - e^{-\lambda_4 t}\right) \\ & + \frac{\mathrm{Wi}}{2\mu}\left(\frac{(1-\mu)e^{-\lambda_3 t}}{2-3\mu} - \frac{(1+\mu)e^{-\lambda_1 t}}{2+3\mu}\right). \quad (21b)\end{aligned}$$

Both functions are plotted in fig. 4 for two different distances. The two sets of curves indicate that the magnitude of the cross-correlation increases weakly with decreasing values of d. The cross-correlation functions involving the z coordinate vanish as in ref. [33].

The time asymmetry of the shear-induced cross-correlations, namely $\langle\tilde{y}_1(0)\tilde{x}_1(t)\rangle \neq \langle\tilde{x}_1(0)\tilde{y}_1(t)\rangle$ with $t > 0$, can be explained in the following way: A random particle displacement at $t = 0$ in the y-direction leads immediately after the kick to a linear growth of the particle's x coordinate due to the larger flow velocity $\mathbf{u}(\mathbf{r})$ at a larger

value of the y coordinate. Consequently, for small values of t, the product $\tilde{y}_1(0)\tilde{x}_1(t)$ grows in time until the particle is pulled back by the linear spring force, which happens on the time scale $\tau = \zeta/k$. The result is a maximum in the correlation function $\langle \tilde{y}_1(0)\tilde{x}_1(t)\rangle$ at a time of the order of τ. Considering the effect of a random kick in the x-direction at $t = 0$, the particle does not jump between streamlines of different velocity and therefore the cross-correlation $\langle \tilde{x}_1(0)\tilde{y}_1(t)\rangle$ does not show this maximum and decays exponentially.

By replacing the time t by $-t$ in eq. (21a) the two functions (21a) and (21b) can be combined to one correlation function $\langle \tilde{x}_1(0)\tilde{y}_1(t)\rangle$, where t can now take positive and negative values. This function is asymmetric with respect to time reflections $t \to -t$. A similar behavior was previously found for the fluctuations of the fluid velocity in a shear flow [28].

The static correlation functions given by eqs. (20a)–(21b) for $t = 0$ determine also the positional distribution function $P(\mathbf{r})$ of a Brownian particle in a potential as described in more detail in ref. [33]. It is an interesting question, how the single-particle distribution in a shear flow is changed by the presence of a second one.

In a linear shear flow $P(\mathbf{r})$ has an elliptical shape in the shear plane and the angle θ between the major axis of the ellipse and the flow direction is determined by the equation

$$\tan\theta = \frac{1}{2}\left[\frac{\langle \tilde{x}_1\tilde{y}_1\rangle}{|\langle \tilde{x}_1\tilde{y}_1\rangle|}\sqrt{4+G^2} - G\right], \tag{22}$$

with

$$G = \frac{\langle \tilde{x}_1^2\rangle - \langle \tilde{y}_1^2\rangle}{\langle \tilde{x}_1\tilde{y}_1\rangle}. \tag{23}$$

Using the d-dependent static correlations from eqs. (20) and (21), we obtain

$$G = \mathrm{Wi}\,\frac{1+3\mu^2}{1-4\mu^2}. \tag{24}$$

Consequently the inclination angle θ is a function of the parameter d too. In fig. 5 $\tan(\theta)$ is shown as a function of $\mu = 3a/(4d)$ for three different values of the Weissenberg number Wi and in all three cases $\tan(\theta)$ decreases considerably when the two particles approach. Since θ changes in the same manner by decreasing d or increasing Wi, the shear flow effects can be considered to be amplified by the presence of the second particle.

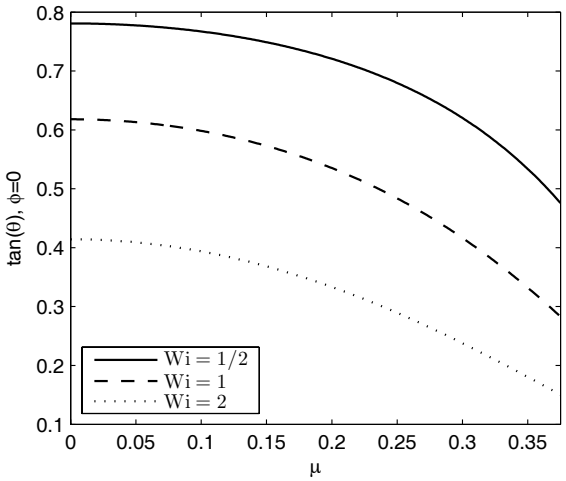

Fig. 5. The inclination angle θ of the single-particle distribution is shown as function of $\mu = 3a/(4d)$ for three different values of the Weissenberg number Wi.

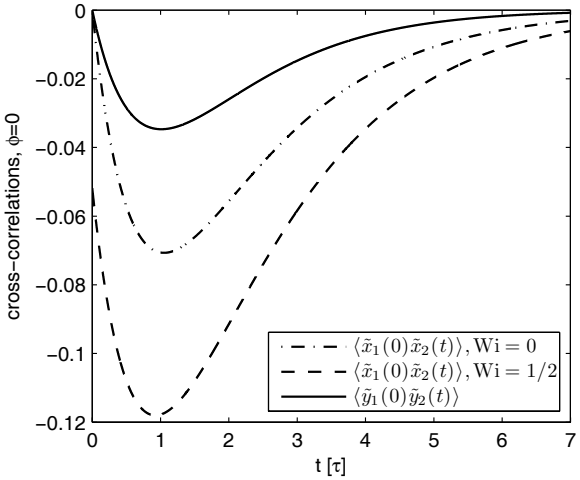

Fig. 6. The cross-correlation functions between the two beads along parallel directions are shown for $\phi = 0$ and $d = 4a$. The minimum of $\langle \tilde{x}_1(0)\tilde{x}_2(t)\rangle = \langle \tilde{x}_2(0)\tilde{x}_1(t)\rangle$ increases with the Weissenberg number Wi and is always deeper than the one of the function $\langle \tilde{y}_1(0)\tilde{y}_2(t)\rangle = \langle \tilde{z}_1(0)\tilde{z}_2(t)\rangle$, which is independent of Wi.

3.1.2 Inter-particle correlations

The motion of the two trapped Brownian particles is coupled via the hydrodynamic interaction. In a quiescent fluid this coupling leads to a cross-correlation between the thermal fluctuations of the two particles along the same direction [6]. Since this cross-correlation is negative as a function of time, cf. fig. 6, the notion "anti cross-correlation" is used. For the anti cross-correlation of the longitudinal displacements we obtain a shear-induced correction, similar to the one-particle autocorrelation in eq. (20a), which is proportional to Wi^2

$$\begin{aligned}\langle \tilde{x}_1(0)\tilde{x}_2(t)\rangle = {} & \frac{1}{4}\left(e^{-\lambda_1 t} - e^{-\lambda_3 t}\right) \\ & + \frac{\mathrm{Wi}^2}{4\mu}\left(\frac{-(1+\mu)e^{-\lambda_1 t}}{6\mu^2+7\mu+2} + \frac{e^{-\lambda_2 t}}{2+3\mu}\right), \\ & + \frac{\mathrm{Wi}^2}{4\mu}\left(\frac{-(1-\mu)e^{-\lambda_3 t}}{6\mu^2-7\mu+2} + \frac{e^{-\lambda_4 t}}{2-3\mu}\right). \end{aligned} \tag{25}$$

The cross-correlations between random particle displacements perpendicular to $\mathbf{q}_{12}$ are independent of the

Weissenberg number Wi

$$\langle \tilde{y}_1(0)\tilde{y}_2(t)\rangle = \langle \tilde{z}_1(0)\tilde{z}_2(t)\rangle = \frac{1}{4}\left(e^{-\lambda_2 t} - e^{-\lambda_4 t}\right). \quad (26)$$

Both correlation functions are plotted in fig. 6.

As indicated in fig. 2, the relaxation processes of the displacements of the two particles along the same spatial direction can be decomposed into a parallel and an anti-parallel translation. In the present case the eigenvalue λ_1 (λ_2) in eqs. (19) corresponds to the parallel relaxation modes along (perpendicular to) the connection vector $\mathbf{q}_{12}$. For the parallel motions, the signs of the particle displacements are always equal for both particles $(+,+$ or $-,-)$, whereas for the anti-parallel ones the corresponding displacements have opposite signs $(+,-$ or $-,+)$. As a consequence, the product of the two displacements is always positive for the parallel case and negative for the anti-parallel case, as indicated by the prefactors of the corresponding contributions in the correlation functions in eq. (25) and eq. (26). As the magnitudes of the anti-parallel translations are larger than the parallel ones, the superposition of the two different modes is negative and has a pronounced minimum at a time $t' \approx \tau$, as shown in fig. 6. The value of t' in case of eq. (25) depends only weakly on the distance d between the two traps. For the cross-correlation $\langle \tilde{y}_1(0)\tilde{y}_2(t)\rangle$ an analytical expression for t' and its magnitude can be given:

$$t' = \frac{\tau}{2\mu}\ln\left(\frac{1+\mu}{1-\mu}\right), \quad (27)$$

$$\langle \tilde{y}_1(0)\tilde{y}_2(t')\rangle = \frac{1}{4}\left(\left(\frac{1-\mu}{1+\mu}\right)^{\frac{1+\mu}{2\mu}} - \left(\frac{1-\mu}{1+\mu}\right)^{\frac{1-\mu}{2\mu}}\right). \quad (28)$$

For finite values of the Weissenberg number Wi the cross-correlation of the longitudinal displacements, $\langle \tilde{x}_1(0)\tilde{x}_2(t)\rangle$, also includes contributions describing relaxation processes perpendicular to $\mathbf{q}_{12}$ with the eigenvalues λ_2 and λ_4. These additional contributions cause larger shear-induced corrections to the cross-correlation in eq. (25) than for the autocorrelation function in eq. (20a), which can be seen by comparing the deviations between the dash-dotted and the dashed curves in fig. 3 and in fig. 6.

For a single particle in a linear shear flow shear-induced cross-correlations between displacements along perpendicular directions in the shear plane were found, which are proportional to the Weissenberg number [33]. In the two-particle system, one also obtains cross-correlations between the displacements of two different particles along orthogonal directions in the shear plane as described by

$$\langle \tilde{x}_1(0)\tilde{y}_2(t)\rangle = \frac{\mathrm{Wi}}{4}\left(\frac{e^{-\lambda_2 t}}{2+3\mu} - \frac{e^{-\lambda_4 t}}{2-3\mu}\right), \quad (29a)$$

$$\langle \tilde{y}_2(0)\tilde{x}_1(t)\rangle = \frac{\mathrm{Wi}}{4\mu}\left(e^{-\lambda_2 t} + e^{-\lambda_4 t}\right) - \frac{\mathrm{Wi}}{2\mu}\left(\frac{(1+\mu)e^{-\lambda_1 t}}{2+3\mu} + \frac{(1-\mu)e^{-\lambda_3 t}}{2-3\mu}\right). \quad (29b)$$

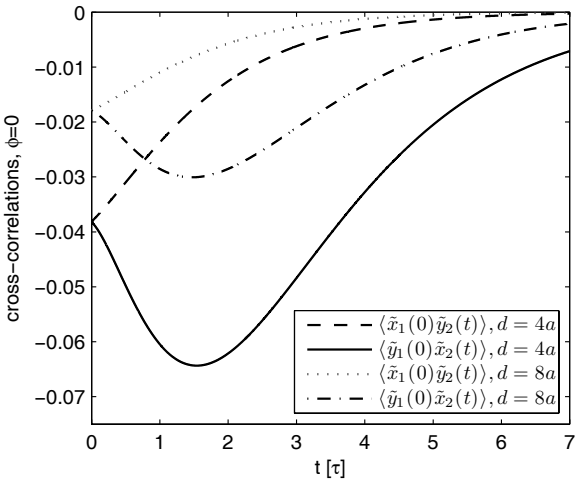

Fig. 7. Shear-induced cross-correlations between orthogonal fluctuations of different particles in the case where $\mathbf{q}_{12}$ is parallel to the streamlines, for $\mathrm{Wi} = 1/2$ and different distances.

Both functions are plotted for different values of the trap distance in fig. 7 and one can see that the magnitudes of the correlations are larger for smaller values of d. Note that in general the particle index in the previous equations can be interchanged: $\langle \tilde{x}_1(0)\tilde{y}_2(t)\rangle = \langle \tilde{x}_2(0)\tilde{y}_1(t)\rangle$.

The ratio between the two shear-induced cross-correlations at $t = 0$ is independent of the Weissenberg number Wi and given by

$$\frac{\langle \tilde{x}_1(0)\tilde{y}_2(0)\rangle}{\langle \tilde{x}_1(0)\tilde{y}_1(0)\rangle} = \frac{-3\mu}{2} = \frac{-9a}{8d}. \quad (30)$$

This relation is reasonable for a sufficiently large ratio d/a. It might serve in an experiment as a consistency check, since the bead radius a and the particle distance d are usually well known. If the two beads come close to each other, additional effects related to their shear-induced rotation may come into play. This is in general a limitation of our Langevin model (4) for point-like particles with an effective hydrodynamic radius. In ref. [7] particle rotations caused by an external torque have been taken into account in a Langevin model for two trapped particles in a quiescent fluid. This work describes a coupling between translational and rotational particle motions, which was confirmed by experiments [53].

The asymmetry in eqs. (29) with respect to time, $t \to -t$, has a similar origin as explained above for the shear-induced one-particle correlations (21). The location of the minimum is again mainly determined by the relaxation time τ of the beads in the harmonic potentials.

Note that for all described correlation functions the single-particle case is recovered in the limit $d \to \infty$, which corresponds to $\mu \to 0$, for example

$$\lim_{\mu\to 0}\langle \tilde{y}_1(0)\tilde{x}_1(t)\rangle = \frac{\mathrm{Wi}}{4}\left(1 + 2\frac{t}{\tau}\right)e^{-t/\tau}. \quad (31)$$

All the correlation functions presented in this subsection have already been measured in experiments [34,54].

3.2 Perpendicular case: $\phi = \pi/2$

For $\phi = \pi/2$ the time dependence of the correlation functions and their magnitudes are changed compared to the parallel orientation $\phi = 0$. This subsection focuses on these differences.

Formulas (19) for the eigenvalues of the matrix M were derived for the identity $\mathbf{R}_0 = \mathbf{Q}$. This allows the determination of exact analytical formulas for the correlations. In the present case, $\mathbf{R}_{\pi/2}$ has to be determined numerically as well as the relaxation rates λ_i and the exact functions $\mathsf{C}_{kl}(t)$. However, if we use the approximation $\mathbf{R}_{\pi/2} = \mathbf{Q} = d/2(0,1,0,0,-1,0)$, which is valid for small Weissenberg numbers, we obtain analytical formulas for the correlations that also describe quantitatively the characteristics of the functions $\mathsf{C}_{kl}(t)$ at large values of Wi. Within this assumption eqs. (19) remain, but the eigenvalues exchange their meanings: Now λ_1 and λ_3 belong to the longitudinal fluctuations in the y-direction, whereas λ_2 and λ_4 describe the transversal motions in x- and z-direction, perpendicular to $\mathbf{q}_{12}$. We also compare the numerical solutions with direct simulations of the Langevin equation (4).

3.2.1 One-particle correlation

For the perpendicular configuration the one-particle autocorrelations are given for the approximation $\mathbf{R}_{\pi/2} = \mathbf{Q}$ by the following expressions:

$$\langle \tilde{x}_1(0)\tilde{x}_1(t)\rangle = \frac{1}{4}\left(e^{-\lambda_2 t} + e^{-\lambda_4 t}\right) + \frac{\mathrm{Wi}^2}{4\mu}\left(\frac{(2\mu-1)e^{-\lambda_4 t}}{3\mu^2-5\mu+2} + \frac{e^{-\lambda_3 t}}{2-3\mu}\right) + \frac{\mathrm{Wi}^2}{4\mu}\left(\frac{(2\mu+1)e^{-\lambda_2 t}}{3\mu^2+5\mu+2} - \frac{e^{-\lambda_1 t}}{2+3\mu}\right), \quad (32a)$$

$$\langle \tilde{y}_1(0)\tilde{y}_1(t)\rangle = \frac{1}{4}\left(e^{-\lambda_1 t} + e^{-\lambda_3 t}\right), \quad (32b)$$

$$\langle \tilde{z}_1(0)\tilde{z}_1(t)\rangle = \frac{1}{4}\left(e^{-\lambda_2 t} + e^{-\lambda_4 t}\right). \quad (32c)$$

While the correlations $\langle \tilde{y}_1(0)\tilde{y}_1(t)\rangle$ and $\langle \tilde{z}_1(0)\tilde{z}_1(t)\rangle$ of the displacements perpendicular to the flow lines were identical in the case $\phi = 0$, they are different in the present case, because they describe positional fluctuations either parallel or perpendicular to $\mathbf{q}_{12}$. Only for a vanishing Weissenberg number one obtains $\langle \tilde{x}_1(0)\tilde{x}_1(t)\rangle = \langle \tilde{z}_1(0)\tilde{z}_1(t)\rangle$, but for a finite shear rate the correlation functions are all different —for the approximations in eqs. (32) as well as for the numerical solutions shown in fig. 8.

The shear-induced cross-correlations between particle displacements along orthogonal directions in the shear plane behave qualitatively similar as in the case $\phi = 0$. For the approximation $\mathbf{R}_{\pi/2} = \mathbf{Q}$ they are described by

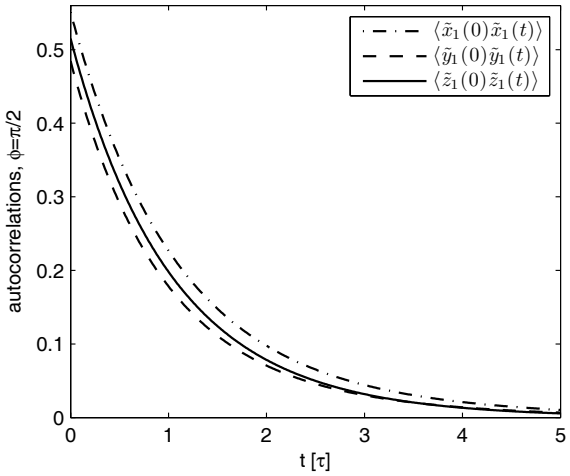

Fig. 8. Autocorrelations for $\phi = \pi/2$, $d = 4a$ and $\mathrm{Wi} = 1/2$. $\langle \tilde{x}_1(0)\tilde{x}_1(t)\rangle$, $\langle \tilde{y}_1(0)\tilde{y}_1(t)\rangle$ and $\langle \tilde{z}_1(0)\tilde{z}_1(t)\rangle$ are different, because of the different relaxation rates and additional Wi^2 contributions in the x-direction. One has $\langle \tilde{x}_1(0)\tilde{x}_1(t)\rangle = \langle \tilde{z}_1(0)\tilde{z}_1(t)\rangle$ only for $\mathrm{Wi} = 0$.

the formulas

$$\langle \tilde{x}_1(0)\tilde{y}_1(t)\rangle = \frac{\mathrm{Wi}}{4}\left(\frac{e^{-\lambda_1 t}}{2+3\mu} + \frac{e^{-\lambda_3 t}}{2-3\mu}\right), \quad (33a)$$

$$\langle \tilde{y}_1(0)\tilde{x}_1(t)\rangle = \frac{\mathrm{Wi}}{4\mu}\left(e^{-\lambda_3 t} - e^{-\lambda_1 t}\right) + \frac{\mathrm{Wi}}{2\mu}\left(\frac{(1+2\mu)e^{-\lambda_2 t}}{2+3\mu} - \frac{(1-2\mu)e^{-\lambda_4 t}}{2-3\mu}\right). \quad (33b)$$

The magnitudes of the different contributions in eqs. (33) changed compared to the expressions in eqs. (21), which influences the positional probability distribution $P(\mathbf{r})$ of one particle. The dependence of the inclination angle θ on the distance d is weaker in the present case than for $\phi = 0$, see fig. 13 in the next section. Possible consequences of this difference for the dynamics of beads-spring models for polymers in shear flows are discussed in the concluding remarks.

The magnitudes of the correlation functions given by eqs. (33) are smaller than those determined numerically for the exact distance $\mathbf{R}_{\pi/2}$, which are plotted in fig. 9. In the same figure these exact solutions are compared with the results of a Brownian dynamics simulation of eq. (4), where $2 \cdot 10^6$ ensemble averages were made. This example illustrates the good agreement between both approaches, which is not affected by the choice of the Rotne-Prager tensor instead of the Oseen tensor in the simulation. The analytical expressions (33) turn out to be a good approximation for the parameters $d \geq 8a$ and $\mathrm{Wi} \leq 0.1$. Especially for smaller values of the trap distance d deviations in the relaxation times occur.

3.2.2 Inter-particle correlations

The cross-correlations of the random displacements between the two particles in the same direction are given for

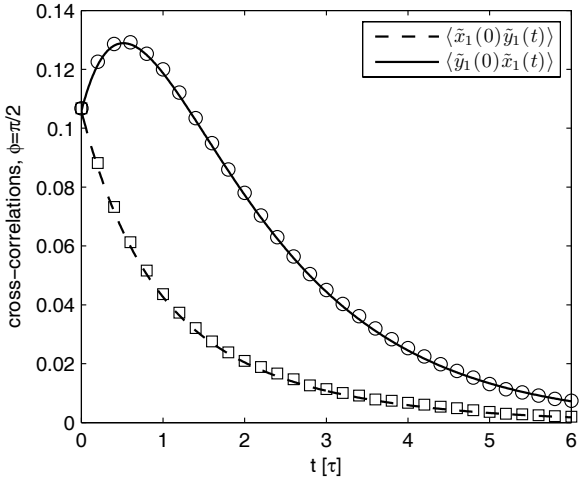

Fig. 9. Comparison of the numerically determined one-particle cross-correlations (lines) with the results from the direct simulation of eq. (4) (circles, squares). The error bars are smaller than the symbols. Parameters: $d = 4a, \mathrm{Wi} = 1/2$.

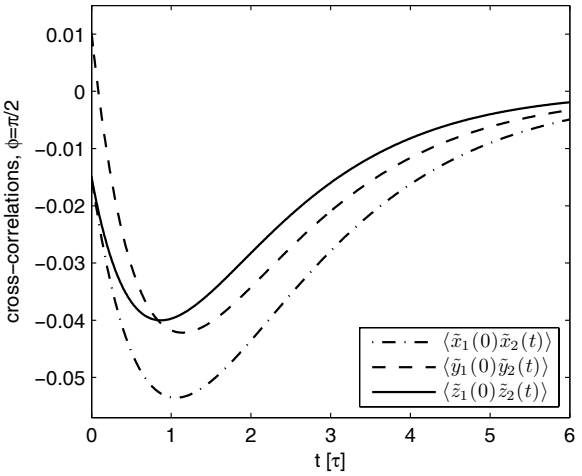

Fig. 10. Inter-particle cross-correlations in the orthogonal case for $d = 4a$ and $\mathrm{Wi} = 1/2$. $\langle\tilde{x}_1(0)\tilde{x}_2(t)\rangle$, $\langle\tilde{y}_1(0)\tilde{y}_2(t)\rangle$ and $\langle\tilde{z}_1(0)\tilde{z}_2(t)\rangle$ are all different and anti-correlated with pronounced minima. One obtains $\langle\tilde{x}_1(0)\tilde{x}_2(t)\rangle = \langle\tilde{z}_1(0)\tilde{z}_2(t)\rangle$ for $\mathrm{Wi} = 0$.

$\mathbf{R}_{\pi/2} = \mathbf{Q}$ by

$$\langle\tilde{x}_1(0)\tilde{x}_2(t)\rangle = \frac{1}{4}\left(e^{-\lambda_2 t} - e^{-\lambda_4 t}\right) + \frac{\mathrm{Wi}^2}{4\mu}\left(\frac{(1-2\mu)e^{-\lambda_4 t}}{3\mu^2-5\mu+2} - \frac{e^{-\lambda_3 t}}{2-3\mu}\right) + \frac{\mathrm{Wi}^2}{4\mu}\left(\frac{(1+2\mu)e^{-\lambda_2 t}}{3\mu^2+5\mu+2} - \frac{e^{-\lambda_1 t}}{2+3\mu}\right), \quad (34a)$$

$$\langle\tilde{y}_1(0)\tilde{y}_2(t)\rangle = \frac{1}{4}\left(e^{-\lambda_1 t} - e^{-\lambda_3 t}\right), \quad (34b)$$

$$\langle\tilde{z}_1(0)\tilde{z}_2(t)\rangle = \frac{1}{4}\left(e^{-\lambda_2 t} - e^{-\lambda_4 t}\right). \quad (34c)$$

Similar to the one-particle correlations in sect. 3.2.1 and in contrast to the case $\phi = 0$ in sect. 3.1.2, all three correlation functions are different for finite values of the Weissenberg number. This is indicated by the expression in eqs. (34) as well as by the numerical correlation functions displayed in fig. 10, and they are again all anti-correlated.

The most striking difference between the case $\phi = 0$ and $\phi = \pi/2$ is found by looking at the shear-induced inter-particle correlations between orthogonal directions in the shear plane, which are given for $\mathbf{R}_{\pi/2} = \mathbf{Q}$ by the following expressions:

$$\langle\tilde{x}_1(0)\tilde{y}_2(t)\rangle = \frac{\mathrm{Wi}}{4}\left(\frac{e^{-\lambda_1 t}}{2+3\mu} - \frac{e^{-\lambda_3 t}}{2-3\mu}\right), \quad (35a)$$

$$\langle\tilde{y}_1(0)\tilde{x}_2(t)\rangle = \frac{-\mathrm{Wi}}{4\mu}\left(e^{-\lambda_1 t} + e^{-\lambda_3 t}\right) + \frac{\mathrm{Wi}}{2\mu}\left(\frac{(1+2\mu)e^{-\lambda_2 t}}{2+3\mu} + \frac{(1-2\mu)e^{-\lambda_4 t}}{2-3\mu}\right). \quad (35b)$$

A Taylor expansion of the correlation function $\langle\tilde{y}_1(0)\tilde{x}_2(t)\rangle$ with respect to small values of μ reveals the difference between the parallel and the perpendicular orientations. For $\phi = 0$ one obtains up to the linear order of μ

$$\langle\tilde{y}_1(0)\tilde{x}_2(t)\rangle \sim \mu\left(3 + 4\frac{t}{\tau} + 6\frac{t^2}{\tau^2}\right)e^{-t/\tau}, \quad (36)$$

whereas for $\phi = \pi/2$ one obtains

$$\langle\tilde{y}_1(0)\tilde{x}_2(t)\rangle \sim \mu\left(3 + 2\frac{t}{\tau} + 6\frac{t^2}{\tau^2}\right)e^{-t/\tau}. \quad (37)$$

The first expression has only *one* extremum as a function of time. The different prefactor of $te^{-t/\tau}$ in the second expression is the origin of an additional extremum in the case $\phi = \pi/2$.

For $\mathbf{Q} = d/2(0,1,0,0,-1,0)$ the angle between the vector connecting the resulting mean positions of the particles, $\langle\mathbf{r}_{12}\rangle$, and the y axis increases as a function of Wi. In this configuration the numerical solution for $\langle\tilde{y}_1(0)\tilde{x}_2(t)\rangle$ does not show a second extremum. However, if $\mathbf{Q}$ is tilted against the flow direction, like

$$\mathbf{Q} = \frac{d}{2\sqrt{1+\mathrm{Wi}^2}}(-\mathrm{Wi}, 1, 0, \mathrm{Wi}, -1, 0), \quad (38)$$

the resulting vector $\langle\mathbf{r}_{12}\rangle$ becomes nearly parallel to the y axis and the second extremum of $\langle\tilde{y}_1(0)\tilde{x}_2(t)\rangle$ is obtained again, as predicted by the approximation in eq. (37). The result for the tilted trap is shown in fig. 11 for two different values of d. Moreover, the extrema are now stronger pronounced than predicted by eq. (37). Comparing this with fig. 7, where the results for $\phi = 0$ are plotted, it can be clearly seen that the correlation $\langle\tilde{y}_1(0)\tilde{x}_2(t)\rangle$ now has an additional local maximum, cf. solid and dash-dotted line in fig. 7, and that $\langle\tilde{x}_1(0)\tilde{y}_2(t)\rangle$ has a minimum at small values of the time t, cf. dashed and dotted lines in fig. 7.

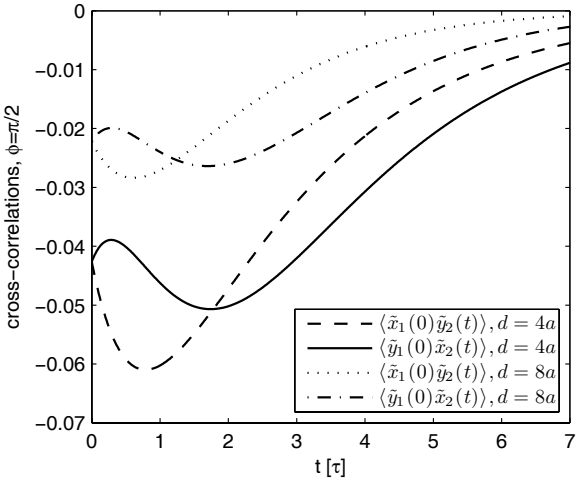

Fig. 11. Shear-induced inter-particle correlations in case of a tilted trap for a Weissenberg number Wi = 1/2 and for the two distances $d = 4a$ and $d = 8a$. The time dependence is different from the case $\phi = 0$, cf. fig. 7.

3.3 Oblique case: $\phi = \pi/4$

If the connection vector $\mathbf{q}_{12}$ between the two potential minima is oblique to the flow direction, further aspects for the correlation functions may come into play. In principle, the matrix $\mathsf{C}_{kl}(t)$ can be calculated for any angle ϕ. However, we focus on the special case $\phi = \pi/4$ as an example. This has the advantage that analytical expressions can be obtained under the assumption $\mathbf{R}_{\pi/4} = \mathbf{Q}$. These approximate solutions remain rather compact and may serve as a guide for the qualitative behavior of the correlation functions.

Since the linear shear flow (3) dictates a preferred direction in the system, the particle fluctuations are decomposed into eigenmodes parallel and perpendicular to the x axis as described in sect. 2.2. That is why in the oblique configuration the longitudinal displacements consist of a superposition of the eigenmodes in the shear plane. If $\phi = \pi/4$, the eigenvalues of the matrix M are given for $\mathbf{R}_{\pi/4} = \mathbf{Q} = d\sqrt{2}/4(1, 1, 0, -1, -1, 0)$ by the following expressions:

$$\lambda_1 = \frac{2 + 3\mu + \sqrt{\mu^2 - 2\mu\mathrm{Wi}}}{2\tau}\,, \tag{39a}$$

$$\lambda_2 = \frac{2 + 3\mu - \sqrt{\mu^2 - 2\mu\mathrm{Wi}}}{2\tau}\,, \tag{39b}$$

$$\lambda_3 = \frac{1 + \mu}{\tau}\,, \tag{39c}$$

$$\lambda_4 = \frac{2 - 3\mu - \sqrt{\mu^2 + 2\mu\mathrm{Wi}}}{2\tau}\,, \tag{39d}$$

$$\lambda_5 = \frac{2 - 3\mu + \sqrt{\mu^2 + 2\mu\mathrm{Wi}}}{2\tau}\,, \tag{39e}$$

$$\lambda_6 = \frac{1 - \mu}{\tau}\,. \tag{39f}$$

While λ_1 and λ_4 describe the parallel and anti-parallel relaxation modes in the x-direction, λ_2 and λ_5 belong to the y-direction, and λ_3 and λ_6 to the z-direction. In contrast to the parallel case, the relaxation processes along the x- and y-direction in the shear plane are now affected by the shear rate. So the corresponding eigenvalues depend directly on the Weissenberg number. This was not the case in the previous section for $\mathbf{R}_{\pi/2} = \mathbf{Q}$. As long as $\mathrm{Wi} \neq 0$, the six relaxation parameters are different and can partly become complex numbers, causing oscillatory contributions to the functions $\mathsf{C}_{kl}(t)$.

In order to write down the full expressions for the correlations in a compact form, we introduce the following notions similar to eq. (18):

$$g_{1,1} = \mu + \frac{\mathrm{Wi}(\lambda_1 - \lambda_2)}{2\lambda_1}\,, \tag{40a}$$

$$g_{2,1} = \mu - \frac{\mathrm{Wi}(\lambda_1 - \lambda_2)}{2\lambda_2}\,, \tag{40b}$$

$$g_{4,1} = \mu + \frac{\mathrm{Wi}(\lambda_5 - \lambda_4)}{2\lambda_4}\,, \tag{40c}$$

$$g_{5,1} = \mu - \frac{\mathrm{Wi}(\lambda_5 - \lambda_4)}{2\lambda_5}\,, \tag{40d}$$

$$g_{1,2} = \mu - \frac{\mathrm{Wi}(3\lambda_1 + \lambda_2)}{2\lambda_1}\,, \tag{40e}$$

$$g_{2,2} = \mu - \frac{\mathrm{Wi}(3\lambda_2 + \lambda_1)}{2\lambda_2}\,, \tag{40f}$$

$$g_{4,2} = \mu + \frac{\mathrm{Wi}(3\lambda_4 + \lambda_5)}{2\lambda_4}\,, \tag{40g}$$

$$g_{5,2} = \mu + \frac{\mathrm{Wi}(3\lambda_5 + \lambda_4)}{2\lambda_5}\,. \tag{40h}$$

Analogous to the previous subsections, we discuss the one-particle correlations first. The autocorrelations of a single particle show the same behavior as in the case $\phi = \pi/2$. They are different in distinct directions as long as $\mathrm{Wi} \neq 0$ and decay exponentially in time. For $\mathbf{R}_{\pi/4} = \mathbf{Q}$ the analytical formulas read

$$\begin{aligned}\langle \tilde{x}_1(0)\tilde{x}_1(t)\rangle = {} & \frac{g_{1,1}e^{-\lambda_1 t}}{8\mu} + \frac{g_{2,1}e^{-\lambda_2 t}}{8\mu} \\ & + \frac{g_{4,1}e^{-\lambda_4 t}}{8\mu} + \frac{g_{5,1}e^{-\lambda_5 t}}{8\mu}\,,\end{aligned} \tag{41a}$$

$$\begin{aligned}\langle \tilde{y}_1(0)\tilde{y}_1(t)\rangle = {} & \frac{g_{1,2}e^{-\lambda_1 t}}{8(\mu - 2\mathrm{Wi})} + \frac{g_{2,2}e^{-\lambda_2 t}}{8(\mu - 2\mathrm{Wi})} \\ & + \frac{g_{4,2}e^{-\lambda_4 t}}{8(\mu + 2\mathrm{Wi})} + \frac{g_{5,2}e^{-\lambda_5 t}}{8(\mu + 2\mathrm{Wi})}\,,\end{aligned} \tag{41b}$$

$$\langle \tilde{z}_1(0)\tilde{z}_1(t)\rangle = \frac{1}{4}\left(e^{-\lambda_3 t} + e^{-\lambda_6 t}\right). \tag{41c}$$

However, in contrast to eqs. (32) one can see that the two autocorrelation functions for the particle displacements in the shear plane, namely $\langle \tilde{x}_1(0)\tilde{x}_1(t)\rangle$ and $\langle \tilde{y}_1(0)\tilde{y}_1(t)\rangle$, include the four corresponding relaxation modes and depend in a complex way on the Weissenberg number.

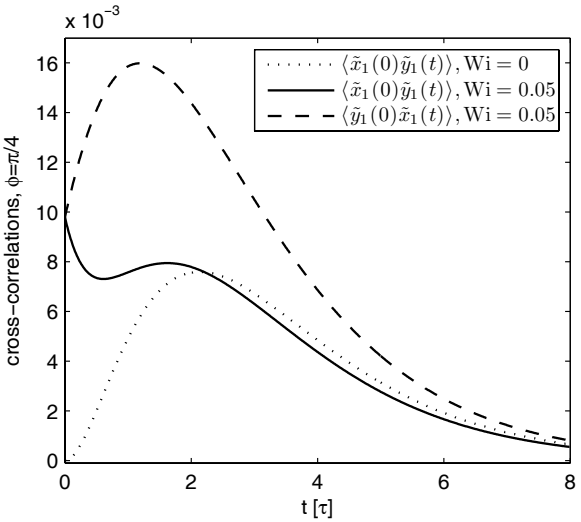

Fig. 12. Single-particle correlations between orthogonal displacements in the shear plane for different Weissenberg numbers, $\phi = \pi/4$ and $d = 4a$. In contrast to the parallel or the perpendicular case, $\langle \tilde{x}_1(0)\tilde{y}_1(t)\rangle$ and $\langle \tilde{y}_1(0)\tilde{x}_1(t)\rangle$ remain finite for $\mathrm{Wi} = 0$.

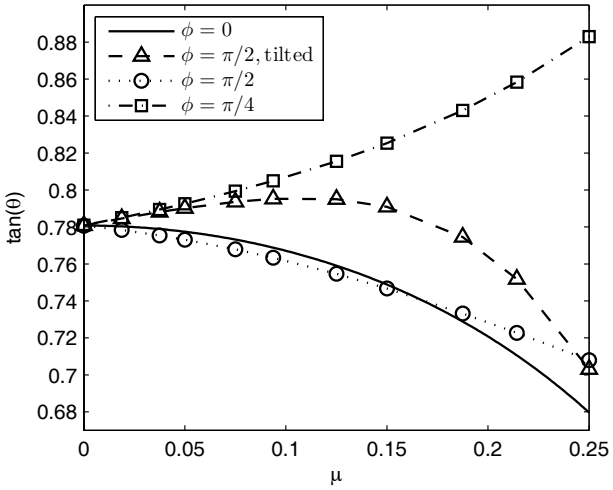

Fig. 13. The inclination angle of the single-particle distribution, as given by eq. (22), is shown as a function of the parameter μ. For $\mathrm{Wi} = 1/2$ the exact results for the different setups described in the text are compared.

The one-particle cross-correlations between orthogonal positional fluctuations in the shear plane, like $\langle \tilde{x}_1(0)\tilde{y}_1(t)\rangle$, are purely shear-induced in the parallel and in the perpendicular case. They are linear functions of the parameter Wi, which means that they vanish in the limit of zero shear rate. This is different in the orthogonal configuration. For $\phi = \pi/4$ and $\mathbf{R}_{\pi/4} = \mathbf{Q}$ the correlation functions are given by the following expressions:

$$\langle \tilde{x}_1(0)\tilde{y}_1(t)\rangle = \frac{g_{1,1}e^{-\lambda_1 t}}{8\sqrt{\mu^2 - 2\mu\mathrm{Wi}}} - \frac{g_{2,1}e^{-\lambda_2 t}}{8\sqrt{\mu^2 - 2\mu\mathrm{Wi}}} + \frac{g_{4,1}e^{-\lambda_4 t}}{8\sqrt{\mu^2 + 2\mu\mathrm{Wi}}} - \frac{g_{5,1}e^{-\lambda_5 t}}{8\sqrt{\mu^2 + 2\mu\mathrm{Wi}}}\,, \quad (42a)$$

$$\langle \tilde{y}_1(0)\tilde{x}_1(t)\rangle = \frac{g_{1,2}e^{-\lambda_1 t}}{8\sqrt{\mu^2 - 2\mu\mathrm{Wi}}} - \frac{g_{2,2}e^{-\lambda_2 t}}{8\sqrt{\mu^2 - 2\mu\mathrm{Wi}}} + \frac{g_{4,2}e^{-\lambda_4 t}}{8\sqrt{\mu^2 + 2\mu\mathrm{Wi}}} - \frac{g_{5,2}e^{-\lambda_5 t}}{8\sqrt{\mu^2 + 2\mu\mathrm{Wi}}}\,. \quad (42b)$$

In the limit of very large particle distances, when $\mu \to 0$, $\langle \tilde{x}_1(0)\tilde{y}_1(t)\rangle$ and $\langle \tilde{y}_1(0)\tilde{x}_1(t)\rangle$ resemble the one-particle case given by eq. (31), whereas in the limit $\mathrm{Wi} \to 0$ the two functions become equal but do not vanish in contrast to the previous subsections. Instead of the approximate expressions (42) we display in fig. 12 the full numerical solution for these correlation functions. If $\mathrm{Wi} = 0$, the identity $\langle \tilde{x}_1(0)\tilde{y}_1(t)\rangle = \langle \tilde{y}_1(0)\tilde{x}_1(t)\rangle$ is obtained, cf. dotted line in fig. 12. For larger values of Wi the two functions resemble the curves shown in fig. 4.

According to eq. (22) and eq. (23) the inclination angle θ of the elliptical positional probability distribution is determined by the static single-particle correlation functions, which depend on the trap distance d. In fig. 13 $\tan(\theta)$ is shown as a function of the parameter $\mu = 3a/(4d)$ for different trap configurations. The analytical expression from the parallel case (solid line) is compared with the full numerical solutions for the other setups. For $\phi = \pi/2$ (circles) the monotonous decrease of $\tan(\theta)$ is weaker than for $\phi = 0$. For the tilted configuration given by eq. (38) θ has a broad maximum (triangles), whereas in the oblique case, $\phi = \pi/4$, the inclination angle is increasing continuously with increasing μ (squares).

The inter-particle cross-correlations in parallel directions are again anti-correlated in the present case. For the approximation $\mathbf{R}_{\pi/4} = \mathbf{Q}$, we obtain

$$\langle \tilde{x}_1(0)\tilde{x}_2(t)\rangle = \frac{g_{1,1}e^{-\lambda_1 t}}{8\mu} + \frac{g_{2,1}e^{-\lambda_2 t}}{8\mu} - \frac{g_{4,1}e^{-\lambda_4 t}}{8\mu} - \frac{g_{5,1}e^{-\lambda_5 t}}{8\mu}\,, \quad (43a)$$

$$\langle \tilde{y}_1(0)\tilde{y}_2(t)\rangle = \frac{g_{1,2}e^{-\lambda_1 t}}{8(\mu - 2\mathrm{Wi})} + \frac{g_{2,2}e^{-\lambda_2 t}}{8(\mu - 2\mathrm{Wi})} - \frac{g_{4,2}e^{-\lambda_4 t}}{8(\mu + 2\mathrm{Wi})} - \frac{g_{5,2}e^{-\lambda_5 t}}{8(\mu + 2\mathrm{Wi})}\,, \quad (43b)$$

$$\langle \tilde{z}_1(0)\tilde{z}_2(t)\rangle = \frac{1}{4}\left(e^{-\lambda_3 t} - e^{-\lambda_6 t}\right). \quad (43c)$$

Equations (43) indicate that these correlations are different from each other, similar to the perpendicular case. The correlation functions for the correct $\mathbf{R}_{\pi/4}$ are shown in fig. 14.

The cross-correlations $\langle \tilde{x}_1(0)\tilde{y}_2(t)\rangle$ and $\langle \tilde{y}_1(0)\tilde{x}_2(t)\rangle$ show the strongest dependence on the orientation of the trapped particles with respect to the flow direction. If $\phi = \pi/4$, they have one minimum each, which is different from the case $\phi = 0$ and from the tilted configuration (38).

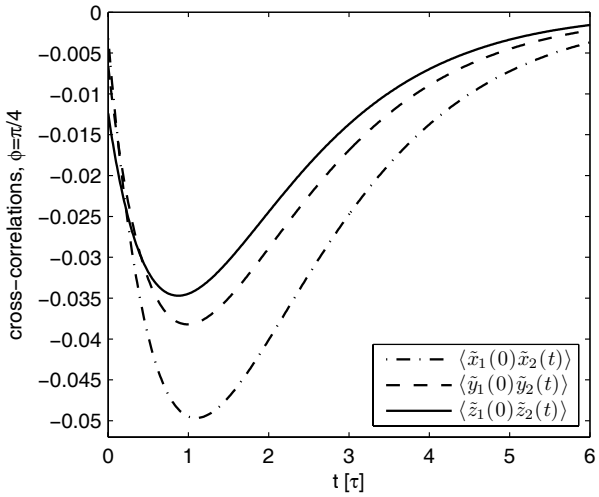

Fig. 14. Inter-particle cross-correlations in the oblique case for $d = 4a$ and $\mathrm{Wi} = 1/2$. In the limit $\mathrm{Wi} = 0$, $\langle\tilde{x}_1(0)\tilde{x}_2(t)\rangle$ and $\langle\tilde{y}_1(0)\tilde{y}_2(t)\rangle$ become equal.

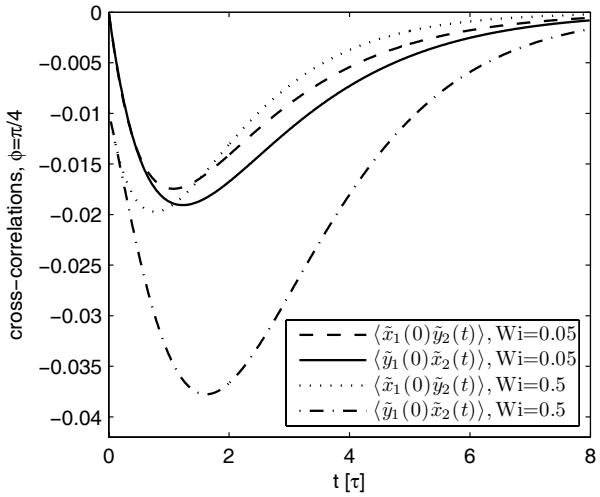

Fig. 15. Cross-correlations in the oblique case for $d = 4a$ and different Weissenberg numbers. The amplitude of $\langle\tilde{y}_1(0)\tilde{x}_2(t)\rangle$ increases more strongly with increasing values of Wi than the amplitude of $\langle\tilde{x}_1(0)\tilde{y}_2(t)\rangle$.

Within the approximation, the functions are given by

$$\langle\tilde{x}_1(0)\tilde{y}_2(t)\rangle = \frac{g_{1,1}e^{-\lambda_1 t}}{8\sqrt{\mu^2-2\mu\mathrm{Wi}}} - \frac{g_{2,1}e^{-\lambda_2 t}}{8\sqrt{\mu^2-2\mu\mathrm{Wi}}} - \frac{g_{4,1}e^{-\lambda_4 t}}{8\sqrt{\mu^2+2\mu\mathrm{Wi}}} + \frac{g_{5,1}e^{-\lambda_5 t}}{8\sqrt{\mu^2+2\mu\mathrm{Wi}}}, \quad (44a)$$

$$\langle\tilde{y}_1(0)\tilde{x}_2(t)\rangle = \frac{g_{1,2}e^{-\lambda_1 t}}{8\sqrt{\mu^2-2\mu\mathrm{Wi}}} - \frac{g_{2,2}e^{-\lambda_2 t}}{8\sqrt{\mu^2-2\mu\mathrm{Wi}}} - \frac{g_{4,2}e^{-\lambda_4 t}}{8\sqrt{\mu^2+2\mu\mathrm{Wi}}} + \frac{g_{5,2}e^{-\lambda_5 t}}{8\sqrt{\mu^2+2\mu\mathrm{Wi}}}. \quad (44b)$$

As illustrated by the numerical results for the correct $\mathbf{R}_{\pi/4}$ in fig. 15, it is remarkable that $\langle\tilde{x}_1(0)\tilde{y}_2(t)\rangle$ does not change very much with the Weissenberg number, while the amplitude of $\langle\tilde{y}_1(0)\tilde{x}_2(t)\rangle$ increases with Wi. Their asymptotic behavior for $\mathrm{Wi} \to 0$ is similar to the single-particle correlations given by eqs. (42).

4 Conclusion

In this work we investigated the dynamics of two Brownian particles, each trapped by a harmonic potential and exposed to a linear shear flow. The one-particle and the inter-particle positional correlation functions, which can be measured in an experiment, were calculated by solving an appropriate Langevin model. We discussed the correlations in detail as a function of the distance between the two traps, as a function of the Weissenberg number Wi, and for three different configurations, where the vector connecting the two potential minima was either parallel, perpendicular, or oblique with respect to the flow direction. This relative orientation strongly affects the time dependence of the correlation functions. For the parallel configuration exact analytical expressions were presented. Otherwise, we provided numerical solutions and analytical approximations for the correlation functions.

Although the stochastic forces in our model were assumed to be uncorrelated along orthogonal directions, we found a coupling between perpendicular particle displacements caused by the shear flow, similar to that in ref. [33]. The resulting shear-induced cross-correlations depend linearly on the Weissenberg number, Wi, and occur also between orthogonal fluctuations of different particles. These inter-particle correlations have zero, one, or two extrema as a function of time, depending on the particle configuration. Besides generating new cross-correlations, the shear flow causes a contribution proportional to Wi^2 in the correlation functions of particle fluctuations along parallel directions.

Due to the hydrodynamic interaction between the two particles, the magnitudes of the one-particle correlations are enhanced with decreasing trap distance d, while in the limit of large distances the single-particle results presented in ref. [33] were recovered. Moreover, we found a significant impact of the parameter d on the positional probability distribution of each particle in the shear flow. The shape of the elliptical distribution is tilted and stretched when the two particles approach each other in the parallel configuration. The same effect is observed when the shear rate is increased. So the shear flow effects are enhanced by the presence of a second particle. In the oblique configuration the opposite effect is observed.

The shear-induced cross-correlations investigated in this work are of the same origin as the correlations between orthogonal fluctuations of a single freely floating particle as discussed in refs. [30,32]. However, if the Brownian particles are trapped, a direct experimental detection of these correlations becomes possible. This has been achieved recently in ref. [34], where two polystyrene latex spheres were trapped by optical tweezers and exposed to a linear shear flow in a special microfluidic device. With

this setup the cross-correlations of the positional fluctuations for the parallel case, as shown in fig. 7, were measured directly for the first time. Moreover, we predict an additional extremum for the shear-induced inter-particle correlations, if the two particles are trapped perpendicular to the flow lines, cf. fig. 11.

The two hydrodynamically interacting beads are treated as point-particles. In forthcoming works, the presented results on the shear-induced correlations are extended by taking the finite particle extension into account. Preliminary investigations show that the effects of particle rotations do not change the major trends in this work [55], and for small Wi the rotation can be neglected anyhow.

The present article provides insight on the Brownian motion of two trapped particles that might be useful for the analysis of the stochastic dynamics of a bead-spring model for polymers too, where the Brownian particles are connected along a chain and fluctuate around some mean distance to their next neighbors. The fluctuations along and perpendicular to the connection vector between two neighboring beads may exhibit similar correlations as for the three model configurations investigated in this work, cf. fig. 1. In this spirit, a profound analysis of the stochastic motion of a bead-spring model in a linear shear flow is an interesting task and may contribute further to the understanding of polymer dynamics.

We would like to thank C. Wagner, A. Ziehl, S. Schreiber and D. Kienle for instructive discussions and the anonymous referee for very useful questions and suggestions. This work has been supported by the German Science Foundation (DFG) through the priority program on nano- and microfluidics SPP 1164 and by the Bayerisch-Französisches Hochschulzentrum (BFHZ).

References

1. G. Taylor, Proc. R. Soc. London, Ser. A **219**, 186 (1953).
2. J. Ottino, S. Wiggins, Philos. Trans. R. Soc. London, Ser. A **362**, 923 (2004).
3. A. Groisman, V. Steinberg, Nature **410**, 905 (2001).
4. J.K.G. Dhont, *An Introduction to Dynamics of Colloids* (Elsevier, Amsterdam, 1996).
5. M. Doi, S.F. Edwards, *The Theory of Polymer Dynamics* (Clarendon Press, Oxford, 1986).
6. J.C. Meiners, S.R. Quake, Phys. Rev. Lett. **82**, 2211 (1999).
7. M. Reichert, H. Stark, Phys. Rev. E **69**, 031407 (2004).
8. D. Smith, H. Babcock, S. Chu, Science **283**, 1724 (1999).
9. P.G. deGennes, Science **276**, 1999 (1997).
10. A. Groisman, V. Steinberg, Nature **405**, 53 (2000).
11. T. Perkins, D. Smith, R. Larson, S. Chu, Science **268**, 83 (1995).
12. F. Brochard-Wyart, Europhys. Lett. **23**, 105 (1993).
13. R.G. Larson, T.T. Perkins, D.E. Smith, S. Chu, Phys. Rev. E **55**, 1794 (1997).
14. R. Rzehak, D. Kienle, T. Kawakatsu, W. Zimmermann, Europhys. Lett. **46**, 821 (1999).
15. R. Rzehak, W. Kromen, T. Kawakatsu, W. Zimmermann, Eur. Phys. J. E **2**, 3 (2000).
16. D. Kienle, W. Zimmermann, Macromolecules **34**, 9173 (2001).
17. R. Rzehak, W. Zimmermann, Phys. Rev. E **68**, 021804 (2003).
18. P. Szymczak, M. Cieplak, J. Chem. Phys. **125**, 164903 (2006).
19. D. Kienle, R. Rzehak, W. Zimmermann, submitted (2010).
20. P. Doyle, B. Ladoux, J. Viovy, Phys. Rev. Lett. **84**, 4769 (2000).
21. M. Webster, J. Yeomans, J. Chem. Phys. **122**, 164903 (2005).
22. R. Delgado-Buscalioni, Phys. Rev. Lett. **96**, 088303 (2006).
23. C.A. Lueth, E.S.G. Shaqfeh, Macromolecules **42**, 9170 (2009).
24. Y. Zhang *et al.*, J. Chem. Phys. **130**, 234902 (2009).
25. J. Hur, E. Shaqfeh, R. Larson, J. Rheol. **44**, 713 (2000).
26. C. Schroeder, R. Teixeira, E. Shaqfeh, S. Chu, Phys. Rev. Lett. **95**, 018301 (2005).
27. S. Gerashchenko, V. Steinberg, Phys. Rev. Lett. **96**, 038304 (2006).
28. B. Eckhardt, R. Pandit, Eur. Phys. J. B **33**, 373 (2003).
29. G. Khujadze, M. Oberlack, G. Chagelishvili, Phys. Rev. Lett. **97**, 034501 (2006).
30. K. Miyazaki, D. Bedeaux, Physica A **217**, 53 (1995).
31. G. Subramanian, J. Brady, Physica A **334**, 343 (2004).
32. Y. Drossinos, M.W. Reeks, Phys. Rev. E **71**, 031113 (2005).
33. L. Holzer, J. Bammert, R. Rzehak, W. Zimmermann, Phys. Rev. E **81**, 041124 (2010).
34. A. Ziehl *et al.*, Phys. Rev. Lett. **103**, 230602 (2009).
35. R. Simmons, J. Finer, S. Chu, J. Spudich, Biophys. J. **70**, 1813 (1996).
36. S. Henderson, S. Mitchell, P. Bartlett, Phys. Rev. Lett. **88**, 088302 (2002).
37. E.R. Dufresne, T.M. Squires, M. Brenner, D.G. Grier, Phys. Rev. Lett. **85**, 3317 (2000).
38. T. Franosch, S. Jeney, Phys. Rev. E **79**, 031402 (2009).
39. J. Crocker *et al.*, Phys. Rev. Lett. **85**, 888 (2000).
40. P.T. Korda, M.B. Taylor, D.G. Grier, Phys. Rev. Lett. **89**, 128301 (2002).
41. M.P. MacDonald, G.C. Spalding, K. Dholakia, Nature **426**, 421 (2003).
42. J. Bammert, S. Schreiber, W. Zimmermann, Phys. Rev. E **77**, 042102 (2008).
43. J. Bammert, W. Zimmermann, Eur. Phys. J. E **28**, 331 (2009).
44. J. Crocker, D. Grier, J. Colloid Interface Sci. **179**, 298 (1996).
45. B. Lukic *et al.*, Phys. Rev. Lett. **95**, 160601 (2005).
46. M. Atakhorrami, G.H. Koenderink, C.F. Schmidt, F.C. MacKintosh, Phys. Rev. Lett. **95**, 208302 (2005).
47. S. Chu, Science **253**, 861 (1991).
48. M. Polin, Y. Roichman, D.G. Grier, Phys. Rev. E **77**, 051401 (2008).
49. G.G. Stokes, Trans. Cambridge Philos. Soc. **IX**, 8 (1850).
50. L.D. Landau, E.M. Lifschitz, *Lehrbuch der Theoretischen Physik: Hydrodynamik*, 2nd edition (Akademie Verlag, Berlin, 1987).
51. L. Holzer, Ph.D. Thesis, Universität Bayreuth (2009).
52. R. Rzehak, W. Zimmermam, Physica A **324**, 495 (2003).
53. S. Martin, M. Reichert, H. Stark, T. Gisler, Phys. Rev. Lett. **97**, 248301 (2006).
54. A. Ziehl, Ph.D. Thesis, Universität des Saarlandes (2010).
55. S. Schreiber, J. Bammert, P. Peyla, W. Zimmermann, in preparation (2010).

Publication 6

The probability distribution of a trapped Brownian particle in plane shear flows
J. Bammert and W. Zimmermann,
Physical Review E **82**, 052102 (2010)

Copyright by The American Physical Society 2010
DOI: 10.1103/PhysRevE.82.052102

Probability distribution of a trapped Brownian particle in plane shear flows

Jochen Bammert and Walter Zimmermann
Theoretische Physik I, Universität Bayreuth, 95440 Bayreuth, Germany
(Received 16 August 2010; published 4 November 2010)

We investigate the statistical properties of an overdamped Brownian particle that is trapped by a harmonic potential and simultaneously exposed to a linear shear flow or to a plane Poiseuille flow. Its probability distribution is determined via the corresponding Smoluchowski equation, which is solved analytically for a linear shear flow. In the case of a plane Poiseuille flow, analytical approximations for the distribution are obtained by a perturbation analysis and are substantiated by numerical results. There is good agreement between the two approaches for a wide range of parameters.

DOI: 10.1103/PhysRevE.82.052102 PACS number(s): 05.40.−a, 05.10.Gg, 83.50.Ax

The dynamics of Brownian particles in fluids is of central importance in many areas of science [1,2]. There is a profound understanding of Brownian motion in quiescent fluids, but the situation is different for particles in flows. Several statistical properties of free Brownian particles in open flows have been investigated, for instance, in terms of the corresponding Langevin and Fokker-Planck equations [3]. Recent works also consider inertia effects on diffusion in shear flows [4,5] and the relation between the Gaussian nature of noise and time reversibility in driven systems [6]. It has also been shown that shear flow causes, compared to a quiescent fluid, additional correlations of the particle's velocity and positional fluctuations [4,7,8]. However, the detection of statistical properties of free particles in a flow is an intricate issue.

To overcome part of these problems, three recent works focused on the dynamics of Brownian particles trapped by harmonic potentials and exposed to shear flows [9–11]. It was shown that the shear-induced correlations between the positional fluctuations of a captured particle along orthogonal directions are essentially the same as in the free-particle case [10]. Furthermore, surprisingly good agreement was found between the predictions and the measurements of these correlations [9].

In Ref. [10] the probability distribution of a trapped Brownian particle in shear flows was obtained by simulations of the Langevin equation. In this brief report the related Smoluchowski equation for the probability distribution is presented and for a linear shear flow an exact analytical solution is given. For a plane Poiseuille flow we determine approximate analytical solutions, which are in good agreement for a wide parameter range with numerical solutions of the Smoluchowski equation and with simulations of the Langevin equation as well.

We consider a Brownian particle trapped by a harmonic potential with the spring constant k at the origin of the Cartesian coordinate frame $(\bar{x},\bar{y},\bar{z})$,

$$V(\bar{\mathbf{r}}) = \frac{k}{2}\bar{\mathbf{r}}^2. \tag{1}$$

The particle is exposed to a flow along the $\bar{x}$ direction with a $\bar{y}$-dependent magnitude,

$$\mathbf{u}(\bar{\mathbf{r}}) = (a + b\bar{y} + c\bar{y}^2)\hat{\mathbf{e}}_x. \tag{2}$$

Since the Brownian motion perpendicular to the shear plane is decoupled from the one in the shear plane, we consider the quasi-two-dimensional problem with $\bar{\mathbf{r}}=(\bar{x},\bar{y})$ and $\bar{\nabla}=(\partial_{\bar{x}},\partial_{\bar{y}})$.

For a plane Poiseuille flow the position of the potential minimum can be different from the center of the flow. In the shifted coordinate frame, $(\tilde{x},\tilde{y})=(\bar{x},\bar{y}+\tilde{y}_0)$, where $\tilde{y}_0$ describes the y coordinate of the potential minimum, the flow profile is given by $\mathbf{u}(\tilde{y})=u_p(1-\tilde{y}^2/l^2)\hat{\mathbf{e}}_x$ with the flow velocity u_p at its center and the confining plane boundaries at $\tilde{y}=\pm l$. If a particle is trapped at $\tilde{y}_0\neq 0$, one obtains with $\tilde{y}=\tilde{y}_0+\bar{y}$ the coefficients $a=u_p(1-\tilde{y}_0^2/l^2)$, $b=-2u_p\tilde{y}_0/l^2$, and $c=-u_p/l^2$ in Eq. (2). This work focuses on situations where the particle positions are sufficiently far away from the boundaries, so that hydrodynamic interactions with the wall, as discussed in [3] for instance, can be neglected.

The particle dynamics are determined by thermal motion, potential forces and drag forces caused by the flow. The thermal motion is characterized by the diffusion constant $D=k_BT/\zeta$, which is given by the Einstein relation in terms of the temperature T, the Boltzmann constant k_B and the Stokes friction coefficient $\zeta=6\pi\eta R$, where η is the viscosity of the fluid and R is the effective radius of the particle. The external flow $\mathbf{u}$ is the origin of the Stokes drag force $\zeta\mathbf{u}$ on the pointlike particle, which is balanced by the restoring force $-\bar{\nabla}V=-k\bar{\mathbf{r}}$.

The diffusion and the two deterministic forces drive the probability current $\mathbf{j}(x,y,t)$ of the Smoluchowski equation (SE) for the particle's positional distribution function $\mathcal{P}(\bar{x},\bar{y},\bar{t})$ [12],

$$\partial_{\bar{t}}\mathcal{P} = -\bar{\nabla}\mathbf{j}, \tag{3}$$

$$\mathbf{j} = -D\bar{\nabla}\mathcal{P} + \left(\mathbf{u} - \frac{1}{\zeta}\nabla V\right)\mathcal{P}. \tag{4}$$

With the expressions in Eqs. (1)–(4) the SE of a Brownian particle trapped in a harmonic potential and exposed to a shear flow reads

$$\partial_{\bar{t}}\mathcal{P} = D\bar{\nabla}^2\mathcal{P} + \frac{D}{\delta^2}(2 + \bar{x}\partial_{\bar{x}} + \bar{y}\partial_{\bar{y}})\mathcal{P}$$

$$-(a + b\bar{y} + c\bar{y}^2)\partial_{\bar{x}}\mathcal{P}. \tag{5}$$

 ©2010 The American Physical Society

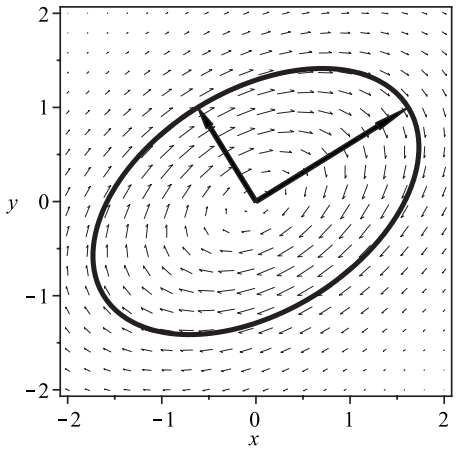

FIG. 1. An elliptical contour line of the distribution of a trapped particle in a linear shear flow is shown, cf. Eq. (8) with $\alpha=0$, $\beta=1$, as well as the vector field $\mathbf{j}(x,y)$. The broad arrows indicate the two principal axes of the ellipse.

The two spatial coordinates may be rescaled by the length $\delta=\sqrt{k_BT/k}$, $\bar{x}=\delta x$ and $\bar{y}=\delta y$, alike the time, $\bar{t}=\zeta/kt$. This results in the dimensionless SE

$$\partial_t \mathcal{P} = [\nabla^2 + 2 + y\partial_y + (x - \alpha - \beta y - \gamma y^2)\partial_x]\mathcal{P}, \tag{6}$$

with the parameters $\alpha=a\delta/D$, $\beta=b\delta^2/D$ and $\gamma=c\delta^3/D$ describing the flow profile and $y\in[(-l-\tilde{y}_0)/\delta,(l-\tilde{y}_0)/\delta]$. β is the so-called Weissenberg number. We note here, that a modified Smoluchowski equation including inertia in shear flows is presented in [4,5]. In comparison to these works, the presence of the potential [Eq. (1)] ensures a stationary solution $\mathcal{P}(x,y)$.

For a uniform flow, i.e., $\alpha\neq 0$ and $\beta=\gamma=0$, the static solution of Eq. (6) is the shifted Boltzmann distribution

$$\mathcal{P}_n(x,y) = P_0 e^{-(1/2)x^2-(1/2)y^2+\alpha x}, \tag{7}$$

where $P_0=(2\pi e^{\alpha^2/2})^{-1}$ is determined by $\int\int dxdy P_n(x,y)=1$. A superposition of a uniform flow and a linear shear flow, i.e., $\alpha\neq 0$, $\beta\neq 0$ and $\gamma=0$, leads to the expected Gaussian distribution

$$\mathcal{P}_{ab}(x,y) = P_0 e^{-(a_1x^2+a_2y^2+a_3xy+a_4x+a_5y)}, \tag{8}$$

with the coefficients

$$a_1 = \frac{2}{\beta^2+4}, \quad a_2 = \frac{\beta^2+2}{\beta^2+4}, \quad a_3 = \frac{-2\beta}{\beta^2+4}, \tag{9a}$$

$$a_4 = \frac{-4\alpha}{\beta^2+4}, \quad a_5 = \frac{2\alpha\beta}{\beta^2+4}, \tag{9b}$$

and the norm $P_0=(\pi\sqrt{\beta^2+4}e^{2\alpha^2/(\beta^2+4)})^{-1}$. In the case of a finite Weissenberg number β the contour lines of the probability distribution $\mathcal{P}_{ab}(x,y)$ are elliptical, as shown in Fig. 1. The probability current $\mathbf{j}(x,y)$, indicated by the vector field in the same figure, characterizes the mean particle motion.

The parameter α, describing the contribution of the uniform flow, causes essentially a shift of the distribution $\mathcal{P}_{ab}(x,y)$ in the x direction. In the following we consider the case $\alpha=0$, where $a_4=a_5=0$ and the resulting distribution function is denoted by $\mathcal{P}_a(x,y)$. Its elliptical contour lines can be characterized by two principal axes. The ratio between their lengths as well as the angle between the major principal axis and the flow direction are a function of the Weissenberg number β. This was already discussed in Ref. [10], where shear-induced corrections to the autocorrelations as well as a cross-correlation between orthogonal particle fluctuations in the shear plane were found. These correlations can also be calculated in terms of the probability distribution $\mathcal{P}_a(x,y)$ via the expression $\langle r_i r_j\rangle=\int\int dxdy\mathcal{P}_a(x,y)r_i r_j$,

$$\langle xx\rangle = 1 + \frac{\beta^2}{2}, \quad \langle xy\rangle = \langle yx\rangle = \frac{\beta}{2}, \quad \langle yy\rangle = 1. \tag{10}$$

After rescaling to dimensional units, $x\to\bar{x}$, the results given in Ref. [10] are recovered.

In a plane Poiseuille flow all three parameters α, β and γ in the SE [Eq. (6)] may be nonzero and no exact analytical solution was found in this case. Similar to [3], the probability distribution is calculated perturbatively and compared with numerical solutions of Eq. (6).

First, we consider a Brownian particle which is trapped at the center of a plane Poiseuille flow, with $\tilde{y}_0=0$. In this case of vanishing β, the parameter $\alpha=u_p\delta\zeta/(k_BT)$ describes the ratio between the drag force imposed by the flow and the potential force on the particle. If α is fixed, the parameter $\gamma=-\alpha(\delta/l)^2$ depends on the ratio between the two characteristic lengths l and δ. Note, the hydrodynamic interactions between the particle and the walls are small in the range $\delta/l<1/2$.

Our ansatz for the perturbation expansion of the solution of Eq. (6) up to the second order in γ reads

$$\mathcal{P}(x,y) = \mathcal{P}_n(x,y)e^{\gamma f_1(x,y)+\gamma^2 g_1(x,y)}, \tag{11}$$

with the two polynomials

$$f_1(x,y) = b_1x + b_2y^2 + b_3xy^2, \tag{12a}$$

$$g_1(x,y) = (c_1x + c_2x^2)(1+y^2) + c_3y^2 + c_4y^4. \tag{12b}$$

The SE [Eq. (6)] may then be rewritten,

$$[p_0(x,y) + \gamma p_1(x,y) + \gamma^2 p_2(x,y)]\mathcal{P}(x,y) = 0. \tag{13}$$

Since γ is an arbitrary, but small number, the polynomials $p_{0,1,2}(x,y)$ in Eq. (13) have to vanish separately. According to Eq. (8) the condition $p_0(x,y)=0$ is automatically fulfilled. The second condition, $p_1(x,y)=0$, provides the first-order coefficients

$$b_1 = \frac{2}{3}, \quad b_2 = \frac{-\alpha}{3}, \quad b_3 = \frac{1}{3}, \tag{14}$$

whereas the third condition, $p_2(x,y)=0$, determines the coefficients at $\mathcal{O}(\gamma^2)$,

$$c_1 = \frac{-2\alpha}{9}, \quad c_2 = \frac{1}{9}, \quad c_3 = \frac{\alpha^2}{9} - \frac{1}{3}, \quad c_4 = \frac{-1}{18}. \tag{15}$$

With the potential minimum off the center of the Poiseuille flow, one has $\tilde{y}_0\neq 0$, a finite Weissenberg number $\beta\neq 0$

and no longer $\pm y$ symmetry. Again we use an ansatz of the form,

$$\mathcal{P}(x,y) = \mathcal{P}_{ab}(x,y)e^{\gamma f_2(x,y)+\gamma^2 g_2(x,y)}. \tag{16}$$

Due to the loss of the $\pm y$ symmetry, the polynomial $f_2(x,y)$ has nine different contributions,

$$f_2(x,y) = d_1 x + d_2 y + d_3(x-3\alpha)x^2 + d_4(x-\alpha)y^2 + d_5(x-2\alpha)xy + d_6 y^3. \tag{17}$$

The condition that the $\mathcal{O}(\gamma)$-terms in Eq. (6) have to vanish determines the coefficients in the ansatz [Eq. (17)]. With $B=\beta^2+4$ and $E=2/(9B^3)$ they are given by

$$d_1 = 4E[(12-\beta^2)B + 16\alpha^2\beta^2],$$

$$d_2 = -2E\beta[(20+\beta^2)B + 8\alpha^2(\beta^2-4)],$$

$$d_3 = \frac{64}{3}E\beta^2, \quad d_4 = 2E(3\beta^4 - 8\beta^2 + 48),$$

$$d_5 = 16E\beta(4-\beta^2),$$

$$d_6 = \frac{-E\beta}{3}(5\beta^4 + 24\beta^2 + 144). \tag{18}$$

In the limit $\beta \to 0$ the coefficients [Eq. (14)] are recovered. The polynomial $g_2(x,y)$ for the order γ^2 includes 14 lengthy contributions, which we do not list here.

In order to estimate the validity range of the approximations presented above, we determine stationary solutions of the SE [Eq. (6)] numerically. To this end a simple Jacobi-relaxation method, cf. Ref. [13], or a direct integration of the rescaled Eq. (3) is sufficient. The probability current is determined via

$$\mathbf{j} = -\nabla\mathcal{P} + \left[\begin{pmatrix}\alpha+\beta y+\gamma y^2\\ 0\end{pmatrix} - \begin{pmatrix}x\\ y\end{pmatrix}\right]\mathcal{P}. \tag{19}$$

Figure 2 shows the contour lines of the numerically obtained probability distribution $\mathcal{P}(x,y)$ in the case with the minimum of the trapping potential at the center of a plane Poiseuille flow. This distribution has similarities with the parachute or bulletlike shape of vesicles in a Poiseuille flow [14–16]. In comparison to similar numerical results, obtained via the related Langevin equation and presented in Ref. [10], we additionally show the probability current $\mathbf{j}(x,y)$. As indicated in Fig. 2, the vector field $\mathbf{j}(x,y)$ includes two counter-rotating vortices that are symmetric with respect to the x axis.

In Fig. 3 contour lines of the numerically obtained probability distribution are compared with those obtained from the perturbative solution [Eq. (11)] for the parameters $\alpha=6$ and $\gamma=-\alpha(\delta/l)^2=-3/8$. In spite of this rather large $|\gamma|$-value, beyond the expected validity range of the perturbation expansion, the differences between both solutions in Fig. 3 are surprisingly small. As expected, for decreasing values of $|\gamma|$ these differences become even smaller, but the analytical formula (11) may be useful for fitting experimental data up to $|\gamma| \simeq 3/8$.

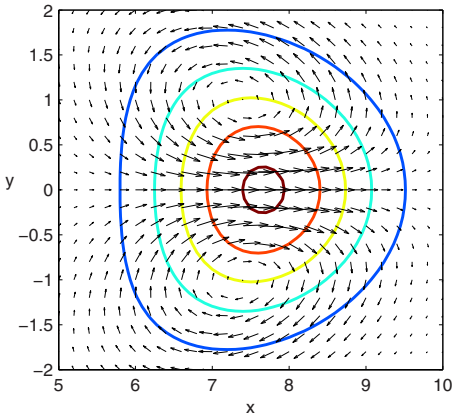

FIG. 2. (Color online) Contour lines of the numerical solution of Eq. (6) as well as the vector field $\mathbf{j}(x,y)$ are shown for the case where the potential minimum is at the center of a plane Poiseuille flow. Parameters: $\alpha=8$, $\gamma=-\alpha(\delta/l)^2=-1/2$.

The symmetrical shape of the distribution is lost if the particle is trapped away from the center of the plane Poiseuille flow. With increasing values of $\tilde{y}_0$ and β, the shape of the probability distribution deforms from a parachute or bullet toward an ellipse. Simultaneously one vortex of the probability current is enhanced while the other one is weakened. For the values $\tilde{y}_0=l/4$, $\delta/l=1/4$ and $\alpha=7$, with $\beta=-2\alpha/15$ and $\gamma=-\alpha/15$, the contour lines of $\mathcal{P}(x,y)$ as well as the current $\mathbf{j}(x,y)$ are displayed in Fig. 4. In this case the lower vortex in $\mathbf{j}(x,y)$ has already vanished and the distribution $\mathcal{P}(x,y)$ shares similarities with the slipper shape of vesicles in capillary flows [17]. Again the results are in good agreement with the simulations in Ref. [10].

In conclusion, we investigated the positional distribution of a Brownian particle, which is trapped by a harmonic potential and simultaneously exposed to different shear flows. A complete analytical solution of the corresponding Smoluchowski equation is given in the case of a linear shear flow. For a plane Poiseuille flow, we presented approximate analytical formulas, which are in good agreement with numeri-

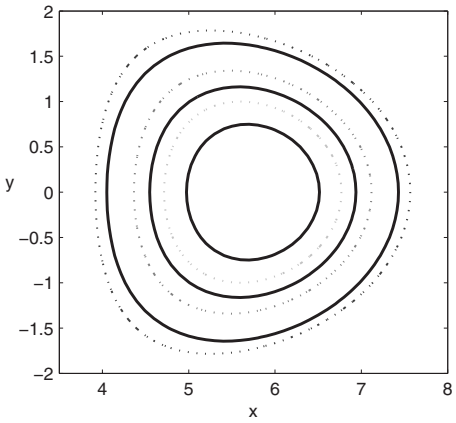

FIG. 3. Comparison of the numerically determined distribution (solid lines) with the analytical approximations, given by Eq. (11) (dashed lines). The contour lines of both types are plotted at different heights in order to distinguish them to compare their shapes. Parameters: $\alpha=6$, $\gamma=-3/8$.

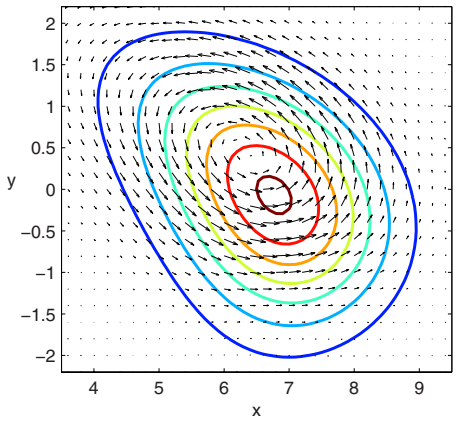

FIG. 4. (Color online) Contour lines of $\mathcal{P}(x,y)$ and vector field $\mathbf{j}(x,y)$ for the case where the potential minimum is off the center of the Poiseuille flow. Parameters: $\alpha=7$, $\beta=-14/15$, $\gamma=-7/15$.

cal solutions for a wide range of parameters. Some of our results confirm earlier ones obtained in Ref. [10] on the basis of simulations of the related Langevin equation.

Our predictions of the particle's probability distribution in a Poiseuille flow may be measured in an experiment similar to that in Ref. [9]. In this work, a micron-sized polystyrene bead was trapped by an optical tweezer and the fluctuating particle positions were recorded by a high speed camera in a stroboscopic manner. For the positions of a trapped particle in Poiseuille flow one expects probability distributions as predicted in this work. The presented analytical approximations for the particle distribution may be useful for fitting the experimental data.

Experiments with particles placed near the center of a Poiseuille flow, where the flow velocity takes its maximum value, may require large laser intensities in order to keep the particles trapped by the potential. This constraint reduces the flexibility for variations of the typical length scale δ of the particle's positional fluctuations. Since the flow profile determines the shape of the particle distribution and not the flow velocity near the potential minimum, one may reduce the drag force by moving the trap along with the flow.

The statistical properties of trapped Brownian particles, as investigated in [9,10,18], share similarities with those of tethered polymers exposed to uniform flows [19–22] or to shear flows [23]. The related theoretical explorations are mainly based on Brownian dynamics simulations. An interesting question is, how far can the analysis described here be applied to tethered bead-spring models in shear flows? Do such investigations exhibit temporal oscillations as found for instance for deterministic models [24]?

We thank M. Burgis for inspiring discussions. This work was supported by DFG via the priority program on micro- and nanofluidics SPP 1164, and by the Bayerisch-Französisches Hochschulzentrum.

[1] J. K. G. Dhont, *An Introduction to Dynamics of Colloids* (Elsevier, Amsterdam, 1996).
[2] H. Berg, *Random Motions in Biology* (Princeton University Press, Princeton, 1993).
[3] R. T. Foister and T. G. M. van de Ven, J. Fluid Mech. **96**, 105 (1980).
[4] Y. Drossinos and M. W. Reeks, Phys. Rev. E **71**, 031113 (2005).
[5] D. C. Swailes, Y. Ammar, M. W. Reeks, and Y. Drossinos, Phys. Rev. E **79**, 036305 (2009).
[6] M. H. Vainstein and J. M. Rubi, Phys. Rev. E **75**, 031106 (2007).
[7] K. Miyazaki and D. Bedeaux, Physica A **217**, 53 (1995).
[8] G. Subramanian and J. F. Brady, Physica A **334**, 343 (2004).
[9] A. Ziehl, J. Bammert, L. Holzer, C. Wagner, and W. Zimmermann, Phys. Rev. Lett. **103**, 230602 (2009).
[10] L. Holzer, J. Bammert, R. Rzehak, and W. Zimmermann, Phys. Rev. E **81**, 041124 (2010).
[11] J. Bammert, L. Holzer, and W. Zimmermann, Eur. Phys. J. E (in print), e-print arXiv:1006.1560.
[12] H. Risken, *The Fokker-Planck Equation: Methods of Solution and Applications* (Springer-Verlag, Berlin, 1989).
[13] W. H. Press, S. A. Teukolsky, W. T. Vetterling, and B. P. Flannery, *Numerical Recipes in Fortran: The Art of Scientific Computing*, 2nd ed. (Cambridge University Press, Cambridge, England, 1992).
[14] R. Skalak and P. I. Branemar, Science **164**, 717 (1969).
[15] H. Noguchi and G. Gompper, Proc. Natl. Acad. Sci. U.S.A. **102**, 14159 (2005).
[16] G. Danker, P. M. Vlahovska, and C. Misbah, Phys. Rev. Lett. **102**, 148102 (2009).
[17] B. Kaoui, G. Biros, and C. Misbah, Phys. Rev. Lett. **103**, 188101 (2009).
[18] J. C. Meiners and S. R. Quake, Phys. Rev. Lett. **84**, 5014 (2000).
[19] T. Perkins, D. Smith, R. Larson, and S. Chu, Science **268**, 83 (1995).
[20] F. Brochard-Wyart, EPL **23**, 105 (1993).
[21] R. Rzehak, D. Kienle, T. Kawakatsu, and W. Zimmermann, EPL **46**, 821 (1999).
[22] R. Rzehak, W. Kromen, T. Kawakatsu, and W. Zimmermann, Eur. Phys. J. E **2**, 3 (2000).
[23] P. S. Doyle, B. Ladoux, and J. L. Viovy, Phys. Rev. Lett. **84**, 4769 (2000).
[24] L. Holzer and W. Zimmermann, Phys. Rev. E **73**, 060801(R) (2006).

Publication 7

Dynamics and rheology of dumbbell suspensions: a numerical study
J. Bammert, P. Peyla, and W. Zimmermann,
preprint

Dynamics and rheology of dumbbell suspensions: a numerical study

J. Bammert[1], P. Peyla[2], W. Zimmermann[1]
[1] *Theoretische Physik I, Universität Bayreuth, 95440 Bayreuth, Germany*
[2] *Laboratoire de Spectrométrie Physique, Université Joseph Fourier, F-38402 Grenoble, France*
(Dated: Received: December 19, 2010/ Revised version: (date))

The rheological and dynamical behavior of a dumbbell suspension in a linear shear flow is investigated by using Fluid Particle Dynamics simulations. By exploring the motion of a single dumbbell in shear flow, we identify three different effects which contribute to the effective viscosity: the volume fraction, elastic correlation effects, and the hydrodynamic interaction between pairs of beads. For a suspension of dumbbells, we observe a significant enhancement of the viscosity compared to the case of independent spheres. This increase depends on the volume fraction and on the size of the dumbbells.

PACS numbers: 83.50.Ax – Steady shear flows, viscometric flow, 47.15.G- – Low-Reynolds-number (creeping) flows, 47.57.E- – Suspensions

I. INTRODUCTION

Complex fluid flows reveal a variety of astonishing and not yet completely understood effects [1]. Two famous examples are shear thinning, where the effective viscosity of a polymer solution decreases with increasing shear stress [2], and elastic turbulence [3], a type of turbulence at small values of the Reynolds number caused by polymer dynamics. The latter effect enables an efficient fluid mixing at low values of the Weissenberg number [4]. In both cases, a detailed explanation of the underlying mechanisms is still missing.

One possibility to model complex fluids is the use of constitutive equations for the stress tensor σ in the Navier-Stokes equations [5]. Very often, the derived expressions are motivated by dumbbell models for the suspended polymer, which leads to a continuum description of the complex fluid. Several examples for this procedure can be found in literature [6–12]. Some of these models can explain shear thinning partially but not completely, because essential effects are lost during the approximations made in the continuum approach. For the phenomenon of elastic turbulence the comprehension is still rather preliminary.

In both cases, it is desirable to develop improved mesoscopic models with several particles in shear flow, which could contribute to the understanding of the effects. However, the realization of the complex interactions among the particles is an intricate issue. Especially the nonlinear, long-range hydrodynamic interactions have to be considered as well as wall-effects.

One way to address the problem is to perform simulations. For instance, in molecular dynamics simulations the suspended objects are usually described by bead-spring chains, and their equation of motion is solved numerically. Depending on the considered situation one can choose between many schemes like Brownian dynamics [13, 14], multiparticle-collision dynamics [15], and lattice Boltzmann methods [16]. The effect of shear thinning has been observed numerically in many studies [17, 18], while the mechanisms of elastic turbulence were mainly explored by the analysis of single dumbbells or polymers in random flows [19, 20].

In order to understand more about the connection between the rheology of polymer solutions and the dynamics of the individual colloidal particles, we perform a numerical study on a deterministic model system. We consider a suspension of Hookean dumbbells in an incompressible Newtonian fluid. The geometry is a rectangular flow channel, where we impose a linear shear flow. The numerical scheme that we chose is called Fluid Particle Dynamics (FPD) and was developed by Tanaka and Araki [21]. It is based on the continuum description of the suspension by the unsteady Stokes equations.

The advantage of FPD is an efficient implementation of the moving boundary conditions on the particle surfaces. Compared to other schemes like Brownian dynamics and multiparticle-collision dynamics, the beads have a finite size and start to rotate in shear flows. Moreover, the complete hydrodynamic interactions between the particles are included in the velocity and pressure field of the solvent. Even at high volume fractions or large particle numbers no approximations must be made. Wall-effects are contained by the boundary conditions for the velocity and pressure field. Since the velocity field in the whole solvent is computed, one can calculate the stress tensor, σ, which allows rheological investigations. The possible applications of FPD are wide-ranging. It has been successfully applied to explore the dynamics of colloids in complex fluids [22], the polymer coil-globule transition [23], the effect of confinement on the rheology of a suspension of spheres [24], and the effective viscosity of microswimmer suspensions [25].

The structure of the paper is as follows: In Sect. II the numerical scheme of fluid particle dynamics is presented as well as the dumbbell model. The connection between a single tumbling dumbbell and the rheological response of the fluid is analyzed in detail in Sect. III. We explain that the effective viscosity in this case is composed of three different contributions: the volume fraction, elastic correlation effects, and the hydrodynamic interaction. In Sect. IV we investigate the effective viscosity of dumb-

bell suspensions as a function of the volume fraction. We observe a significant enhancement of the viscosity compared to the case of independent spheres. This increase is a function of the dumbbell size and the volume fraction. The distribution functions for the dumbbell dynamics illustrate the complex dynamics of the individual objects in the suspension.

II. FPD AND DUMBBELL MODEL

Fluid Particle Dynamics (FPD) is a powerful method for simulations of colloidal suspensions at small values of the Reynolds number. Within this scheme, which was developed by Tanaka and Araki [21], the unsteady Stokes equations for an incompressible Newtonian fluid are solved in three dimensions. The special feature of FPD is that colloidal particles are described by regions of high viscosity, which lead to a spatially dependent viscosity field, $\eta(\mathbf{r})$, as given by

$$\eta(\mathbf{r}) = \eta_s + (\eta_p - \eta_s) \sum_{i=1}^{N} \varphi_i(\mathbf{r}) \,. \tag{1}$$

η_s is the bulk viscosity and $\eta_p = 100\eta_s$ is the viscosity in the range of a bead at $\mathbf{r}_i$, which is described by the density field,

$$\varphi_i(\mathbf{r}) = \frac{1}{2}\left[1 + \tanh\left(\frac{\nu - |\mathbf{r} - \mathbf{r}_i|}{\xi}\right)\right] . \tag{2}$$

The parameter ν describes the diameter of the η_p plateau and ξ the width of the depletion layer. In our model we fix the values $\nu = 2$ and $\xi = 1/2$, which results in an effective radius $a = 3$ for each particle. Every bead consists of more than 100 cells of the numerical grid. The solution of the unsteady Stokes equations leads to the velocity and pressure field of the fluid. The averaged velocity field in the range of the enhanced viscosity is used to update the particle positions. For further details and tests of the method we refer to [18, 21].

The dynamics of a single as well as up to $N = 180$ dumbbells is investigated in a rectangular flow channel of the size $H_x \times H_y \times H_z$ with periodic boundary conditions in the z direction, which is the direction of the flow. At the walls in x and y direction no-slip boundary conditions are imposed. By moving the upper plate at $x = H_x$ with a velocity $v_0\hat{\mathbf{z}}$ and the lower plate at $x = 0$ with $-v_0\hat{\mathbf{z}}$ we create a stationary linear shear flow with a shear rate

$$\dot{\gamma} = \frac{2v_0}{H_x} \,, \tag{3}$$

as sketched in Fig. 1.

The effective viscosity of a suspension at constant shear stress is determined by the xz component of the stress tensor, σ, averaged over the whole surface of the moving plates,

$$\eta_{eff}(t) = \frac{\bar{\sigma}_{xz}(x = H_x) - \bar{\sigma}_{xz}(x = 0)}{2\dot{\gamma}} \,. \tag{4}$$

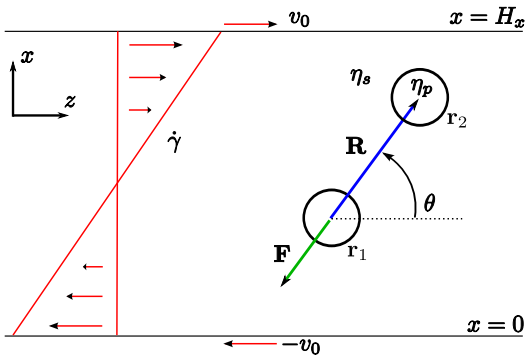

FIG. 1: This sketch illustrates the geometry of the investigated system. A dumbbell consists of two beads at the positions $\mathbf{r}_1$ and $\mathbf{r}_2$ which are connected by a linear spring along the connection vector $\mathbf{R}$.

According to the tumbling motion of a dumbbell, $\eta_{eff}(t)$ is a function of time as described in Sect. III. For its time average, we will use the notation $\bar{\eta}_{eff} = \langle \eta_{eff}(t) \rangle$.

The effective viscosity for a suspension of passive spheres can be given in terms of a virial expansion for the volume fraction Φ,

$$\bar{\eta}_{eff}(\Phi) = \eta_s \left(1 + w_1\Phi + w_2\Phi^2 + \mathcal{O}(\Phi^3)\right) . \tag{5}$$

For the dilute regime, where hydrodynamic interactions are negligible, Einstein calculated $w_1 = 2.5$ [26, 27]. Batchelor and Green determined the value of the second order coefficient $w_2 = 5.2$ [28], which has later been evaluated for the high frequency regime as well by Felderhof and Cichocki to $w_2 = 5.0$ [29]. By the use of FPD it was shown that both coefficients, w_1 and w_2, change if the suspension of spheres is strongly confined [25]. The shape of the suspended objects has an influences on the viscosity too [30].

Throughout this work we will analyze the dimensionless relative viscosity change defined by

$$\Delta\eta(t) = \frac{\eta_{eff}(t) - \eta_s}{\eta_s} \,. \tag{6}$$

All simulations were performed at Reynolds numbers $\mathrm{Re} \sim a^2\dot{\gamma}/\eta_s \leq 0.64$. If not stated otherwise we set $H_x = H_y = 60$ and $H_z = 100$.

The dumbbells consist of two beads of radius a at the positions $\mathbf{r}_1$ and $\mathbf{r}_2$. They are connected by a spring which has an equilibrium length R_0 and a spring constant k. In general the spring force $\mathbf{F}$ is directed along the connection vector $\mathbf{R} = (R_x, R_y, R_z)$ between the two beads and a function of the spring elongation $R - R_0$,

$$\mathbf{F}(\mathbf{R}) = -\nabla\Phi^H = f(R)\mathbf{R} \,. \tag{7}$$

The angle between $\mathbf{R}$ and the flow direction is denoted by θ. In our notation $\mathbf{F}(\mathbf{R})$ is the spring force on particle $\mathbf{r}_1$ as illustrated in Fig. 1.

In this work we consider Hookean springs, where the harmonic potential

$$\Phi^H = \frac{k}{2}\left(R - R_0\right)^2 , \tag{8}$$

leads to a linear restoring force in Eq. (7). Other spring potentials could be used in order to take additional effects into account, e.g. FENE springs show a finite extensibility at high shear stresses but for weak deformations the deviations from Eq. (8) are small [7].

For further discussions it is useful to introduce the dimensionless Weissenberg number, Wi, which is defined as the product of the shear rate $\dot{\gamma}$ and the relaxation time τ of the dumbbell,

$$\mathrm{Wi} = \tau\dot{\gamma} . \tag{9}$$

In order to determine τ for the present model we compare the relaxation dynamics from the simulation with the prediction of the Fraenkel model [6], which neglects hydrodynamic interactions and the finite size of the two beads. After an initial deformation a Fraenkel dumbbell relaxes to its equilibrium shape in an exponential manner according to

$$\varepsilon(t) = \frac{R(t) - R_0}{R_0} = \frac{R(t=0) - R_0}{R_0} e^{-\frac{t}{\tau}} , \tag{10}$$

where ε is the relative spring deformation. τ is given by

$$\tau = \zeta/k , \tag{11}$$

with the Stokes friction coefficient $\zeta = 6\pi\eta_s a$ of a point-like particle with an effective radius a [31]. In confined geometries, it is known that ζ depends on the particle-wall distance [30], which has been investigated in detail with FPD in Ref. [18]. In our present study H_x is fixed to $20a$ and confinement effects are negligible. Our numerical results for the dumbbell relaxation are in good agreement with Eq. (10). Therefore we keep the formula (11) for the relaxation time. Small deviations from Eq. (10) are caused by hydrodynamic interactions between beads and with walls. With respect to Eq. (9), high Weissenberg numbers are equivalent to dumbbells with soft springs.

Note that in FPD simulations two approaching beads usually avoid each other, if the volume fraction or the driving forces are not too large. However, in order to exclude bead penetrations at any case, we use a short-range repulsive potential (Lennard-Jones-(12,6) potential) between all particles with a cut-off length $R_L = 2a$.

III. SINGLE DUMBBELL DYNAMICS

In a first step we explore the relation between the dynamics of a single dumbbell and the resulting relative viscosity $\Delta\eta(t)$.

For moderate values of the Weissenberg number Wi one observes a tumbling motion of the dumbbell, similar to that of ellipsoidal particles [32] or similar to vesicles with a high viscosity contrast [33, 34]. Above a critical value of Wi, which is not reached in our simulations, a vacillating-breathing mode is found too, as discussed recently [18]. In the tumbling regime the angle θ evolves as a function of time and passes periodically all values in the interval $[0, \pi]$. During this dynamics the spring is also deformed in a periodic manner, as shown in Fig. 2 for two different values of the Weissenberg number. In this figure the relative spring deformation ε is given as a function of the orientation angle θ, and it can be seen that the dumbbell is stretched in the range of smaller values of θ and compressed at larger values of θ. This successive elongation and compression is caused by one contribution of the shear flow. A linear shear flow is a superposition of a rotational and an elongational flow, where the second part stretches the dumbbell when $\theta \approx \pi/4$, and it compresses the dumbbell around $\theta = 3\pi/4$.

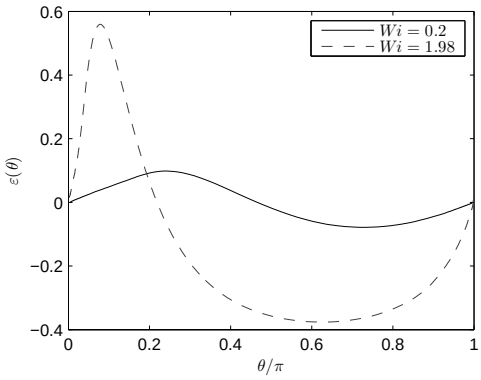

FIG. 2: Tumbling dynamics of a single dumbbell in shear flow during one half-turn. The relative spring deformation as a function of the orientation angle is shown for two different values of the Weissenberg numbers.

For small values of the Weissenberg number the spring is only slightly deformed and the resulting trajectory in the ε-θ phase space is nearly point-symmetric with respect to $\theta = \pi/2$. The deformation for Wi = 0.2 is below 10%. Increasing the Weissenberg number leads to asymmetric behavior of $\varepsilon(t)$ for the tumbling dynamics as illustrated for Wi = 1.98 in Fig. 2 too. This behavior influences the relative viscosity $\Delta\eta(t)$ as discussed in the following.

In the kinetic theory the dumbbell model is used to motivate constitutive equations for the stress tensor of complex fluids, cf. convected Jeffreys model in [5]. This connection provides a link between the effective viscosity of a suspension and the dynamics of the suspended objects. The total stress tensor for such a fluid includes according to the Kramers-Kirkwood equation a contribution

$$\bar{\lambda} = \langle\lambda(\mathrm{t})\rangle = \langle\mathbf{R} \otimes \mathbf{F}\rangle, \tag{12}$$

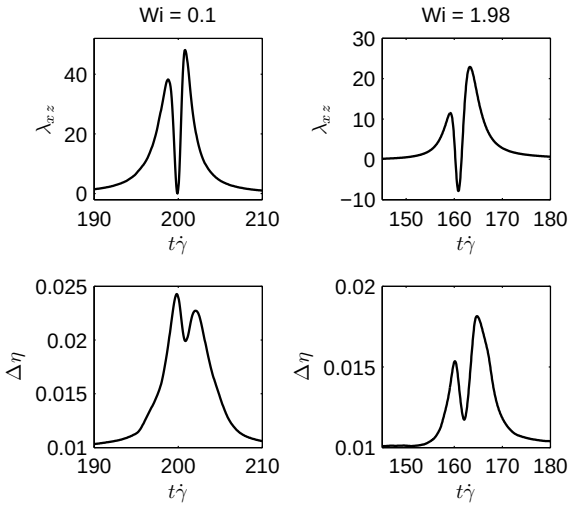

FIG. 3: Relative viscosity and $\lambda_{xz}(t)$ during one half turn of a single dumbbell at two different values of the Weissenberg number Wi.

where $\mathbf{R}$ is the connection vector between the two beads of a dumbbell and $\mathbf{F}$ is the spring force [5]. Using numerical methods like Brownian dynamics and multiparticle-collision dynamics on can only determine $\lambda(t)$, but $\Delta\eta(t)$ has to be calculated indirectly [35]. In our FPD simulations with a steady shear flow in the xz shear plane, we determine the direct effects on the viscosity $\Delta\eta(t)$ via Eq. (4) and $\lambda_{xz}(t)$ via the spring forces and particle positions according to

$$\lambda_{xz}(t) = f(R)R_xR_z = f(R)\frac{R^2}{2}\sin(2\theta)\,. \qquad (13)$$

$\Delta\eta(t)$ and $\lambda_{xz}(t)$ are both plotted in Fig. 3 as a function of the dimensionless time $t\dot{\gamma}$ during one half turn of the dumbbell, where θ changes from π to 0. As can be clearly seen, the temporal behavior of $\Delta\eta(t)$ and $\lambda_{xz}(t)$ differ and depend on the Weissenberg number.

The relative viscosity change $\Delta\eta(t)$ depends on three different contributions. $\Delta\eta(t)$ increases according Eq. (5) with the volume fraction Φ occupied by the beads. In the present example of a single dumbbell one has $\Phi = 0.004$ which leads to an offset of $\Delta\eta(t)$ of about 0.01 as shown in Fig. 3. This corresponds to the viscosity enhancement caused by two independent beads, and it is constant in time.

Due to the hydrodynamic interaction between the two beads the drag force on the dumbbell is a function of its relative orientation in the flow, which causes the second contribution to $\Delta\eta(t)$. If $\mathbf{R}$ is parallel to the flow the resulting drag force is much smaller than for the perpendicular configuration. In the range $\theta \approx \pi/2$ the two beads cannot follow their local flow velocity according to the connecting spring. The correlation due to the connection causes a drag force on each bead which leads to an increase of the shear viscosity.

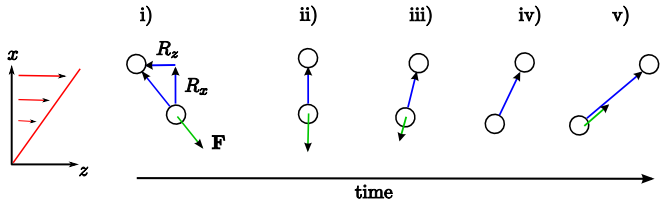

FIG. 4: Sketch of the tumbling motion at high Weissenberg numbers to illustrate the connection between dumbbell dynamics and $\lambda_{xz}(t)$.

Considering the third contribution we observe that $\Delta\eta(t)$ shows as a function of time two maxima separated by a local minimum, when θ is around $\pi/2$. This behavior may be illustrated by the temporal evolution of $\lambda_{xz}(t)$, which covers the tumbling dynamics via the dumbbell orientation $\mathbf{R}$ and the spring force $\mathbf{F}$, cf. Eq. (7),. Similar to the relative viscosity, also $\lambda_{xz}(t)$ shows two maxima separated by a minimum during one half turn, which can be explained by means of Fig. 4 in the following way.

According to Eq. (13), $\lambda_{xz}(t)$ is the product of three contributions: $\sin(2\theta)$ and the prefactors $f(R)$ and $R(t)$, which depend on the spring deformation $\varepsilon(t)$. In the interval $[0, \pi]$ $\sin(2\theta)$ is anti-symmetric with respect to $\pi/2$. Since the spring is stretched for small values of the angle θ and compressed at larger values, as indicated in Fig. 3, the spring force $f(R)$ being proportional to $\varepsilon(t)$ changes its sign with a similar anti-symmetric manner with respect to $\pi/2$ as $\sin(2\theta)$. For small values of Wi the spring is only slightly deformed during one half turn and in this case $\varepsilon(t)$ vanishes at $\theta = \pi/2$, cf. Fig. 2, as well as $f(R)$ and $\sin(2\theta)$. This results in a pronounced minimum of λ_{xz} at $\theta = \pi/2$ as indicated by the upper left graph in Fig. 3, where the different heights of the two maxima are caused by the different values of R^2. For configurations as sketched in Fig. 4 i), the spring is compressed and R is smaller than R_0, whereas in Fig. 4 v), the spring is stretched.

Eq. (13) includes essentially elastic effects of the dumbbell deformation and only partly the hydrodynamic interaction between the two beads. The latter effect is completely taken into account in the time-dependence of $\Delta\eta(t)$. Therefore, the differences in Fig. 3 between the temporal behavior of $\Delta\eta(t)$ and λ_{xz} are attributed to hydrodynamic interaction effects.

IV. SUSPENSION OF DUMBBELLS

The nonlinear hydrodynamic interaction between colloidal particles renders the dynamics of one dumbbell in a suspension to be far more complex than the tumbling motion of a single entity as described in Sect. III. Instead of characterizing the involved motion of a dumbbell in a suspension, we consider its statistical properties. In parallel, we calculate the time-averaged relative viscosity

change,

$$\Delta\bar{\eta} = \langle \Delta\eta(t) \rangle \,, \tag{14}$$

via Eq. (4), which gives further insight about the macroscopic rheological properties of the suspension. This quantity describes an overall response of the solution to the applied shear.

First, we investigate a suspension of $N = 80$ dumbbells. As initial condition they are all placed on a lattice with the same orientation angle θ each. Due to the shear flow and the hydrodynamic interactions, the suspension immediately starts to mix. The distribution functions for the bead positions as well as for the orientational angle θ, which were peaked at $t = 0$, broaden over time and reach finally a steady state. As an example, Fig. 5 shows the stationary distribution for the orientation angle, $\mathcal{P}(\theta)$, after the initial relaxation.

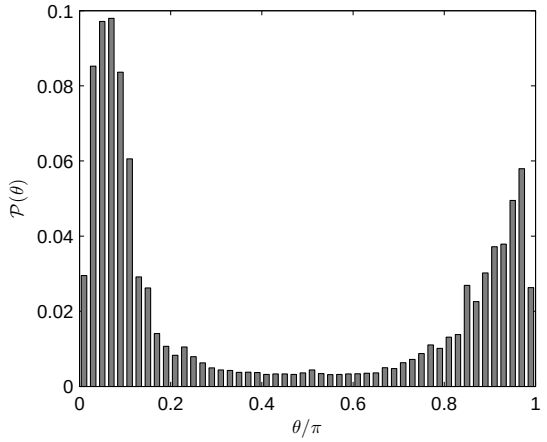

FIG. 5: Averaged distribution for the orientation angle, $\mathcal{P}(\theta)$, for a suspension of 80 dumbbells at Wi = 0.211. In the initial setup, all dumbbells had the same orientation.

It is remarkable, that $\mathcal{P}(\theta)$ is asymmetric with respect to $\pi/2$. This behavior is also indicated by the temporal evolution of $\theta(t)$ as shown in Fig. 6. The angle θ stays between the half-rotations a much longer time in the range around $\theta(t) \simeq 0$ than in the range $\theta(t) \simeq \pi$. The dumbbell rotation is caused by the rotational part of the shear flow, whereas the elongational contribution leads to a stretching and an alignment along a direction $\theta = \pi/4$, cf. Fig. 4. As described above for a isolated dumbbell, it is the elongational part, which breaks the symmetry of $\mathcal{P}(\theta)$. Dumbbell orientations with $\theta < \pi/2$, as sketched in Fig. 4 v), are preferred, while others with $\theta > \pi/2$ as in Fig. 4 i) are destabilized.

Fig. 7 shows the corresponding distribution of the relative spring deformations ε of the suspension of 80 dumbbells. In general, $\mathcal{P}(\varepsilon)$ is peaked around $\varepsilon = 0$ and broadens with increasing values of Wi, but it also shows a small asymmetry caused by the elongational part of the shear flow. The positional probability distributions across the channel are uniform other than the expected depletion layer near the boundaries [36].

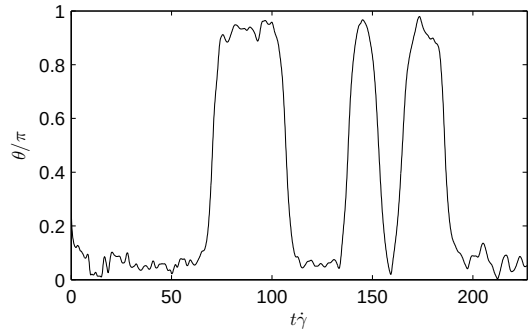

FIG. 6: Example of $\theta(t)$ for an individual dumbbell in a suspension. The dumbbell prefers to be aligned in flow direction, but due to the complex interactions in the system it tumbles from time to time. The preferred orientation angle θ is close to 0.

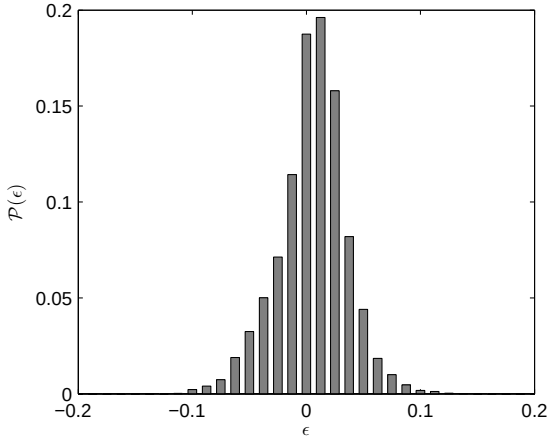

FIG. 7: Averaged distribution for the relative deformation, $\mathcal{P}(\varepsilon)$, for a suspension of 80 dumbbells at Wi = 0.211. In the initial setup, all springs were at equilibrium length R_0.

According to Eq. (5) the relative viscosity of a colloidal suspension of spheres is connected to the volume fraction. In the dilute regime, there is a linear relation between $\Delta\bar{\eta}$ and Φ in both cases, for beads and dumbbells. Above a critical value of about $\Phi_c = 0.02$ the hydrodynamic interaction between the spheres becomes important and deviations from the linear dependency on Φ come into play. The volume fraction determines the average distance l between the centers of two spheres according to

$$l = a \left(\frac{4\pi}{3\Phi} \right)^{1/3} \,. \tag{15}$$

Consequently, Φ_c corresponds to a characteristic length scale l_c, which reads in the present case $l_c \approx 6a = 18$.

If two spheres are connected by a spring with equilibrium length R_0, a second length scale is introduced in the system. Therefore, we expect deviations from the relation (5) with the coefficients from Einstein, Batchelor and Green. Indeed, for a suspension of dumbbells $\Delta\bar{\eta}$ depends on R_0 at constant values for the Weissenberg num-

ber Wi and the volume fraction Φ. For this, we consider suspensions where the number of beads changes from 10 to 320. These particle numbers corresponds to a volume fraction varying from $\Phi = 0.0066$ until $\Phi = 0.1056$. All simulations start with random initial distributions. The equilibrium spring length is in the range $8 \leq R_0 \leq 20$, and the Weissenberg number is fixed at $\mathrm{Wi} = 0.33$. After the initial relaxation process the averaged relative viscosity $\Delta\bar{\eta}$ is measured as well as other statistical properties.

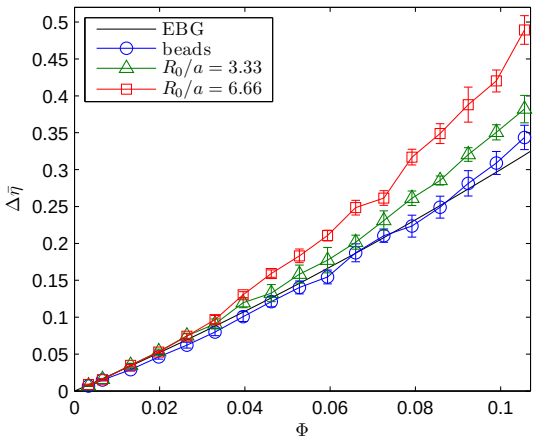

FIG. 8: The relative viscosity as a function of the volume fraction for different suspensions. The viscosity for unconnected beads differs from the prediction of Einstein, Batchelor and Green (EBG) if $\Phi > 0.08$. For dumbbell suspensions $\Delta\bar{\eta}$ increases with R_0.

In Fig. 8 we show numerical results for the dependency of $\Delta\bar{\eta}$ on the volume fraction Φ at the spring length $R_0 = 10 < l_c$ and $R_0 = 20 > l_c$. For a suspension of unconnected beads the findings are in good agreement with the prediction of Einstein, Batchelor and Green, Eq. (5), until Φ becomes larger than 0.08. The deviations at high volume fractions are expected, because at large values of Φ higher order terms in the virial expansion Eq. (5) have to be included. For dumbbell suspensions $\Delta\bar{\eta}$ is clearly enhanced and this increase is related to two effects. The first one has been already discussed in the previous section for a single dumbbell, where the spring connecting two beads leads to a correlation of the motion of two distant objects and therefore to an enhancement of the effective viscosity. The second effect appears in the parameter range $R_0 > l_c$. Here, we observe a strong overlap between moving dumbbells, which leads due to excluded volume effects and due to hydrodynamic interactions, to an additional correlation between many objects. This stronger correlation causes a further enhancement of the viscosity.

This qualitative expectation, that an increasing size of the dumbbells leads to an enhancement of the effective viscosity of the suspension, is confirmed by the data shown in Fig. 9, where $\Delta\bar{\eta}$ increases as a function of R_0 in a nonlinear manner for $\Phi = 0.1056$.

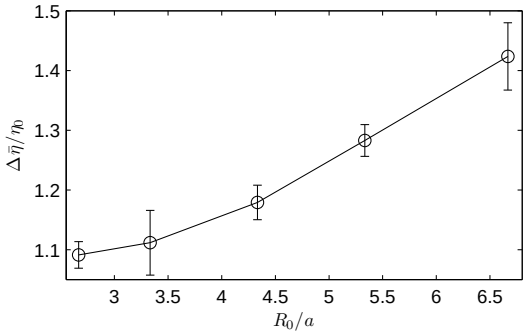

FIG. 9: The relative viscosity as a function of the spring length R_0/a for a dumbbell suspension with $\Phi = 0.1056$. η_0 is the viscosity of a suspension of spheres at the same volume fraction.

V. CONCLUSION

We have investigated the dynamics and statistics of dumbbells in a linear shear flow as well as the rheology of the whole suspension by using Fluid Particle Dynamics simulations. Our numerical results on the tumbling motion of a single dumbbell show, that the viscosity is influenced by three different contributions: the volume fraction, elastic correlation effects and the hydrodynamic interaction between the two beads of the dumbbell.

For a suspension of independent spheres, we determined numerically the viscosity as a function of the volume fraction. This reference curve shows expected deviations from the Einstein-Batchelor-Green prediction in the semi-dilute regime. If two beads are connected by a spring, the viscosity of the resulting dumbbell suspensions increases stronger as a function of the volume fraction, than in the reference case. This enhancement is attributed to the correlation between the motions of the two beads building up a dumbbell. If the size of the dumbbells, namely the length of the springs, becomes large enough, an additional correlation between the motion of the colloidal objects can be induced via hydrodynamic and excluded volume interactions, even at rather small volume fractions. This viscosity depends in a nonlinear way on the dumbbell size.

Furthermore, a detailed analysis of the individual trajectories in a suspension with many dumbbells could probably reveal characteristics of the so called elastic turbulence [3], which occurs a small values of the Reynolds number as used in this work. How this can cause an efficient fluid mixing in the suspension, as experimentally observed, is a further issue for forthcoming work.

Acknowledgments.- We would like to thank Chaouqi Misbah for useful discussions. This work has been supported by the German science foundation through the priority program on nano- and microfluidics SPP 1164, and by the Bayerisch-Französisches Hochschulzentrum.

[1] R. G. Larson, *The Structure and Rheology of Complex Fluids* (Oxford University Press, New York, Oxford, 1999).
[2] N. Y. Chan *et al.*, J. Phys. Chem. Lett. **1**, 1912 (2010).
[3] A. Groisman and V. Steinberg, Nature **405**, 53 (2000).
[4] A. Groisman and V. Steinberg, Nature **410**, 905 (2001).
[5] R. B. Bird, C. F. Curtiss, R. C. Armstrong, and O. Hassager, *Dynamics of Polymeric Liquids I, II* (Wiley & Sons, New York, 1987).
[6] G. K. Fraenkel, J. Chem. Phys. **20**, 642 (1952).
[7] H. R. Warner, Jr., Ind. Eng. Chem. Fundamen. **11**, 379 (1972).
[8] S. I. Abdelkhalik and R. B. Bird, Appl. Sci. Res. **30**, 269 (1975).
[9] E. J. Hinch and L. G. Leal, J. Fluid Mech. **71**, 481 (1975).
[10] J. F. Brady, A. S. Khair, and M. Swaroop, J. Fluid Mech. **554**, 109 (2006).
[11] P. Degond, A. Lozinski, and R. G. Owens, J. Non-Newtonian Fluid Mech. **165**, 509 (2010).
[12] R. G. Winkler, Phys. Rev. Lett. **97**, 128301 (2006).
[13] R. M. Jendrejack *et al.*, Phys. Rev. Lett. **91**, 038102 (2003).
[14] R. Prabhakar and J. R. Prakash, J. Non-Newtonian Fluid Mech. **116**, 163 (2004).
[15] A. Malevanets and R. Kapral, J. Chem. Phys. **112**, 7260 (2000).
[16] R. Kekre, J. E. Butler, and A. J. C. Ladd, Phys. Rev. E **82**, 011802 (2010).
[17] B. Z. Dlugogorski, M. Grmela, and P. J. Carreau, J. Non-Newtonian Fluid Mech. **48**, 303 (1993).
[18] P. Peyla, EPL **80**, 34001 (2007).
[19] A. Celani, S. Musacchio, and D. Vincenzi, J. Stat. Phys. **118**, 531 (2005).
[20] M. Chertkov, I. Kolokolov, V. Lebedev, and K. Turitsyn, J. Fluid Mech. **531**, 251 (2005).
[21] H. Tanaka and T. Araki, Phys. Rev. Lett. **85**, 1338 (2000).
[22] T. Araki and H. Tanaka, Prog. Theor. Phys. Supp. 37 (2008).
[23] K. Kamata, T. Araki, and H. Tanaka, Phys. Rev. Lett. **102**, 108303 (2009).
[24] Y. Davit and P. Peyla, EPL **83**, 64001 (2008).
[25] S. Rafai, L. Jibuti, and P. Peyla, Phys. Rev. Lett. **104**, 098102 (2010).
[26] A. Einstein, Ann. Phys. **19**, 289 (1906).
[27] A. Einstein, Ann. Phys. **34**, 591 (1911).
[28] G. K. Batchelor, J. T. Green, J. Fluid Mech. **56**, 401 (1972).
[29] B. Cichocki, B. U. Felderhof, J. Chem. Phys. **89**, 1049 (1988).
[30] J. Happel and H. Brenner, *Low Reynolds Number Hydrodynamics* (Prentice-Hall, Englewood Cliffs, 1981).
[31] M. Doi and S. F. Edwards, *The Theory of Polymer Dynamics* (Clarendon Press, Oxford, 1986).
[32] G. B. Jeffery, Proc. R. Soc. Lond. A **102**, 161 (1922).
[33] C. Misbah, Phys. Rev. Lett. **96**, 028104 (2006).
[34] V. Kantsler and V. Steinberg, Phys. Rev. Lett. **96**, 036001 (2006).
[35] T. C. B. Kwan and E. S. G. Shaqfeh, J. Non-Newtonian Fluid Mech. **82**, 139 (1999).
[36] L. Cannavacciuolo, R. G. Winkler, and G. Gompper, EPL **83**, 34007 (2008).

Bibliography

[1] J. Bammert, S. Schreiber, and W. Zimmermann. Dumbbell diffusion in a spatially periodic potential. *Phys. Rev. E*, 77:042102, 2008.

[2] J. Bammert and W. Zimmermann. Dumbbell transport and deflection in a spatially periodic potential. *Eur. Phys. J. E*, 28:331, 2009.

[3] L. Holzer, J. Bammert, R. Rzehak, and W. Zimmermann. Dynamics of a trapped Brownian particle in shear flows. *Phys. Rev. E*, 81:041124, 2010.

[4] J. Bammert and W. Zimmermann. The probability distribution of a trapped Brownian particle in plane shear flows. *Phys. Rev. E*, 82:052102, 2010.

[5] J. Bammert, L. Holzer, and W. Zimmermann. Dynamics of two trapped Brownian particles: Shear-induced cross-correlations. *Eur. Phys. J. E*, 33:313, 2010.

[6] A. Ziehl, J. Bammert, L. Holzer, C. Wagner, and W. Zimmermann. Direct Measurement of Shear-Induced Cross-Correlations of Brownian Motion. *Phys. Rev. Lett.*, 103:230602, 2009.

[7] J. Bammert, P. Peyla, and W. Zimmermann. Dynamics and rheology of dumbbell suspensions: a numerical study. *preprint*, 2010.

[8] M. K. Cheezum, W. F. Walker, and W. H. Guilford. Quantitative comparison of algorithms for tracking single fluorescent particles. *Biophys. J.*, 81:2378, 2001.

[9] A. Ashkin. Trapping of atoms by resonance radiation pressure. *Phys. Rev. Lett.*, 40:729, 1978.

[10] A. Ashkin, J. M. Dziedzic, J. E. Bjorkholm, and S. Chu. Observation of a single-beam gradient force optical trap for dielectric particles. *Opt. Lett.*, 11:288, 1986.

[11] T. T. Perkins, S. R. Quake, D. E. Smith, and S. Chu. Relaxation of a single DNA Molecule observed by Optical Microscopy. *Science*, 264:822, 1994.

[12] R. M. Simmons, J. T. Finer, S. Chu, and J. A. Spudich. Quantitative measurements of force and displacement using an optical trap. *Biophys. J.*, 70:1813, 1996.

[13] J. C. Crocker, M. T. Valentine, E. R. Weeks, T. Gisler, P. D. Kaplan, A. G. Yodh, and D. A. Weitz. Two-point microrheology of inhomogeneous soft materials. *Phys. Rev. Lett.*, 85:888, 2000.

[14] M. Atakhorrami, G. H. Koenderink, C. F. Schmidt, and F. C. MacKintosh. Short-time inertial response of viscoelastic fluids: Observation of vortex propagation. *Phys. Rev. Lett.*, 95:208302, 2005.

[15] S. Henderson, S. Mitchell, and P. Bartlett. Propagation of Hydrodynamic Interactions in Colloidal Suspensions. *Phys. Rev. Lett.*, 88:088302, 2002.

[16] M. Polin, D. G. Grier, and S. R. Quake. Anomalous vibrational dispersion in holographically trapped colloidal arrays. *Phys. Rev. Lett.*, 96:088101, 2006.

[17] A. J. Pascall and T. M. Squires. Induced Charge Electro-osmosis over Controllably Contaminated Electrodes. *Phys. Rev. Lett.*, 104:088301, 2010.

[18] P. Tabeling. *Introduction of Microfluidics*. Oxford Univ. Press, Oxford, 2006.

[19] J. Knight. Microfluidics: Honey, I shrunk the lab. *Nature*, 418:474, 2002.

[20] R. Skalak and P. I. Branemar. Deformation of red blood cells in capillaries. *Science*, 164:717, 1969.

[21] R. B. Bird, C. F. Curtiss, R. C. Armstrong, and O. Hassager. *Dynamics of Polymeric Liquids I, II*. Wiley & Sons, New York, 1987.

[22] S. Grossmann. The onset of shear flow turbulence. *Rev. Mod. Phys.*, 72:603, 2000.

[23] A. Groisman and V. Steinberg. Elastic turbulence in a polymer solution flow. *Nature*, 405:53, 2000.

[24] A. Groisman and V. Steinberg. Elastic turbulence in curvilinear flows of polymer solutions. *New J. Phys.*, 6:29, 2004.

[25] A. Groisman and V. Steinberg. Efficient mixing at low Reynolds numbers using polymer additives. *Nature*, 410:905, 2001.

[26] P. G. deGennes. Polymer physics - Molecular individualism. *Science*, 276:1999, 1997.

[27] T. T. Perkins, D. E. Smith, and S. Chu. Single polymer dynamics in an elongational flow. *Science*, 276:2016, 1997.

[28] A. Einstein. Über die von der molekularen Theorie der Wärme geforderte Bewegung von in ruhenden Flüssigkeiten suspendierten Teilchen. *Ann. Phys.*, 17:549, 1905.

[29] D. Bedeaux and P. Mazur. Brownian-motion and fluctuating hydrodynamics. *Physica (Amsterdam)*, 76:247, 1974.

[30] J. K. G. Dhont. *An Introduction to Dynamics of Colloids*. Elsevier, Amsterdam, 1996.

[31] K. Kamata, T. Araki, and H. Tanaka. Hydrodynamic Selection of the Kinetic Pathway of a Polymer Coil-Globule Transition. *Phys. Rev. Lett.*, 102:108303, 2009.

[32] L. Holzer and W. Zimmermann. Particles held by springs in a linear shear flow exhibit oscillatory motion. *Phys. Rev. E*, 73:060801(R), 2006.

[33] L. M. Hocking. The behaviour of clusters of spheres falling in a viscous fluid. Part 2. Slow motion theory. *J. Fluid Mech.*, 20:129, 1964.

[34] R. E. Caflisch, C. Lim, J. H. C. Luke, and A. S. Sangani. Periodic-solutions for 3 sedimenting spheres. *Phys. Fluids*, 31:3175, 1988.

[35] S. Schreiber, T. Fischer, and W. Zimmermann. Hydrodynamic attraction and repulsion between asymmetric rotors. *New J. Phys.*, 12:073017, 2010.

[36] C. W. Oseen. *Neuere Methoden und Ergebnisse in der Hydrodynamik*. Akad. Verlagsges. Leipzig, Leipzig, 1927.

[37] G. J. Hancock. The self-propulsion of microfluidic organisms through liquids. *Proc. R. Soc. Lond. A*, 217:96, 1953.

[38] E. Lauga and T. R. Powers. The hydrodynamics of swimming microorganisms. *Rep. Prog. Phys.*, 72:096601, 2009.

[39] M. Doi and S. F. Edwards. *The Theory of Polymer Dynamics*. Clarendon Press, Oxford, 1986.

[40] G. G. Stokes. On the Effect of the Internal Friction of Fluids on the Motion of Pendulums. *Trans. Cambridge Phil. Soc.*, IX:8, 1850.

[41] J. Rotne and S. Prager. Variational treatment of hydrodynamic interaction in polymers. *J. Chem. Phys.*, 50:4831, 1969.

[42] J. R. Blake. Image system for a Stokeslet in a no-slip boundary. *Proc. Cambridge Philos. Soc.*, 70:303, 1971.

[43] Y. W. Kim and R. R. Netz. Electro-osmosis at inhomogeneous charged surfaces: Hydrodynamic versus electric friction. *J. Chem. Phys.*, 124:114709, 2006.

[44] S. Schreiber and J. Bammert and P. Peyla and W. Zimmermann. Wall attraction and repulsion of hydrodynamically interacting particles. *in preparation*, 2010.

[45] M. Reichert and H. Stark. Hydrodynamik coupling of two rotating spheres trapped in harmonic potentials. *Phys. Rev. E*, 69:031407, 2004.

[46] J. Honerkamp. *Stochastic Dynamical Systems.* Wiley-VCH, New York, 1994.

[47] N. G. van Kampen. *Stochastic Processes in Physics and Chemistry.* Elsevier, Amsterdam, 2004.

[48] C. W. Gardiner. *Handbook of Stochastic Methods.* Springer, New York, 1983.

[49] H. C. Öttinger. *Stochastic Processes in Polymeric Fluids.* Springer, Heidelberg, 1996.

[50] M. Burgis, V. Schaller, M. Glässl, W. Köhler, A. Krekov, and W. Zimmermann. Anomalous diffusion in viscosity landscapes. *submitted*, :, 2010.

[51] R. Rzehak and W. Zimmermann. Dynamics of strongly deformed polymers in solution. *EPL*, 59:779, 2002.

[52] C. M. Schroeder, R. E. Teixeira, E. S. G. Shaqfeh, and S. Chu. Characteristic periodic motion of polymers in shear flow. *Phys. Rev. Lett.*, 95:018301, 2005.

[53] C. A. Lueth and E. S. G. Shaqfeh. Experimental and Numerical Studies of Tethered DNA Shear Dynamics in the Flow-Gradient Plane. *Macromolecules*, 42:9170, 2009.

[54] R. Rzehak, D. Kienle, T. Kawakatsu, and W. Zimmermann. Partial draining of a tethered polymer in flow. *EPL*, 46:821, 1999.

[55] R. Rzehak, W. Kromen, T. Kawakatsu, and W. Zimmermann. Deformation of a tethered polymer in uniform flow. *Eur. Phys. J. E*, 2:3, 2000.

[56] D. Kienle, R. Rzehak, and W. Zimmermann. Hydrodynamic interaction effects along and between tethered polymers in flow. *submitted*, :, 2010.

[57] J. A. Davis and et. al. Deterministic hydrodynamics: Taking blood apart. 103:14779, 2006.

[58] M. P. MacDonald, G. C. Spalding, and K. Dholakia. Microfluidic sorting in an optical lattice. *Nature*, 426:421, 2003.

[59] P. T. Korda, M. B. Taylor, and D. G. Grier. Kinetically locked-in colloidal transport in an array of optical tweezers. *Phys. Rev. Lett.*, 89:128301, 2002.

[60] K. Ladavac, K. Kasza, and D. G. Grier. Sorting mesoscopic objects with periodic potential landscapes: Optical fractionation. *Phys. Rev. E*, 70:010901 (R), 2004.

[61] R. L. Smith, G. C. Spalding, K. Dholakia, and M. P. MacDonald. Colloidal sorting in dynamical optical lattices. *J. Opt. A: Pure Appl. Opt.*, 9:S134, 2007.

[62] P. M. Johnson, C. M. van Kats, and A. van Blaaderen. Synthesis of colloidal silica dumbbells. *Langmuir*, 21:11510, 2005.

[63] T. C. B. McLeish and R. G. Larson. Molecular constitutive equations for a class of branched polymers: The pom-pom polymer. *J. Rheol.*, 42:81, 1998.

[64] G. Taylor. Disperion of soluble matter in solvent flowing slowly through a tube. *Proc. R. Soc. London A*, 219:186, 1953.

[65] J. M. Ottino and S. Wiggins. Introduction: mixing in microfluidics. *Phil. Trans. R. Soc. Lond. A*, 362:923, 2004.

[66] F. Brochard-Wyart. Polymer Chains under Strong Flows: Stems and Flowers. *EPL*, 30:387, 1995.

[67] D. E. Smith, H. P. Babcock, and S. Chu. Single-polymer dynamics in steady shear flow. *Science*, 283:1724, 1999.

[68] R. F. Rodriguez, E. Salinasrodriguez, and J. W. Dufty. Fokker-Planck and Langevin descriptions of fluctuations in uniform shear-flow. *J. Stat. Phys.*, 32:279, 1983.

[69] Y. Katayama and R. Terauti. Brownian motion of a single particle under shear flow. *Eur. J. Phys.*, 17:136, 1996.

[70] Y. Drossinos and M. W. Reeks. Brownian motion of finite-inertia particles in a simple shear flow. *Phys. Rev. E*, 71:031113, 2005.

[71] I. Santamaria-Holek, D. Reguera, and J. M. Rubi. Diffusion in stationary flow from mesoscopic nonequilibrium thermodynamics. *Phys. Rev. E*, 63:051106, 2001.

[72] I. Santamaria-Holek, J. M. Rubi, and A. Perez-Madrid. Mesoscopic thermodynamics of stationary non-equilibrium states. *New J. Phys.*, 7:35, 2005.

[73] M. San Miguel and J. M. Sancho. Brownian-motion in shear flow. *Physica A*, 99:357, 1979.

[74] R. T. Foister and T. G. M. van de Ven. Diffusion of Brownian particles in shear flows. *J. Fluid Mech.*, 96:105, 1980.

[75] J. E. Shea and I. Oppenheim. Fokker-Planck and non-linear hydrodynamic equations of an inelastic system of several Brownian particles in a non-equilibrium bath. *Physica A*, 250:265, 1998.

[76] G. Subramanian and J. F. Brady. Multiple scales analysis of the Fokker-Planck equation for simple shear flow. *Physica A*, 334(’):343, 2004.

[77] G. Szamel. Self-diffusion in sheared colloidal suspensions: Violation of fluctuation-dissipation relation. *Phys. Rev. Lett.*, 93:178301, 2004.

[78] M. Krueger and M. Fuchs. Nonequilibrium fluctuation-dissipation relations of interacting Brownian particles driven by shear. *Phys. Rev. E*, 81:011408, 2010.

[79] L. D. Landau and E. M. Lifschitz. *Lehrbuch der Theoretischen Physik: Hydrodynamik*. Akademie Verlag, Berlin, second edition, 1987.

[80] B. Eckhardt and R. Pandit. Noise correlations in shear flows. *Eur. Phys. J. B*, 33:373, 2003.

[81] G. Khujadze, M. Oberlack, and G. Chagelishvili. Direct numerical simulation of stochastically forced laminar plane Couette flow: Peculiarities of hydrodynamic fluctuations. *Phys. Rev. Lett.*, 97:034501, 2006.

[82] K. Miyazaki and D. Bedeaux. Brownian-motion in a fluid in simple shear-flow. *Physica A*, 217:53, 1995.

[83] L. Holzer. *Einfluss einer Scherströmung auf die thermischen Fluktuationen in einer Flüssigkeit*. PhD thesis, Universität Bayreuth, 2009.

[84] G. G. Fuller, J. M. Rallison, R. L. Schmidt, and L. G. Leal. The measurement of velocity-gradients in laminar-flow by homodyne light-scattering spectroscopy. *J. Fluid Mech.*, 100:555, 1980.

[85] J. Derksen and W. van de Water. Light-scattering off Brownian particles in shear flows. *Appl. Sci. Res.*, 47:221, 1990.

[86] M. Hoppenbrouwers and W. van de Water. Dynamic light scattering in shear flow. *Phys. Fluids*, 10:2128, 1998.

[87] Maplesoft, a division of Waterloo Maple I. Maple 11. 2007.

[88] B. Bamieh and M. Dahleh. Energy amplification in channel flows with stochastic excitation. *Phys. Fluids*, 13:3258, 2001.

[89] J. M. O. de Zarate and J. V. Sengers. Transverse-velocity fluctuations in a liquid under steady shear. *Phys. Rev. E*, 77:026306, 2008.

[90] J. C. Meiners and S. R. Quake. Direct measurement of hydrodynamic cross correlations between two particles in an external potential. *Phys. Rev. Lett.*, 82:2211, 1999.

[91] D. C. Swailes, Y. Ammar, M. W. Reeks, and Y. Drossinos. Stochastic transport of particles in straining flows. *Phys. Rev. E*, 79:036305, 2009.

[92] M. H. Vainstein and J. M. Rubi. Gaussian noise and time-reversal symmetry in nonequilibrium Langevin models. *Phys. Rev. E*, 75:031106, 2007.

[93] H. Noguchi and G. Gompper. Shape Transitions of Fluid Vesicles and Red Blood Cells in Capillary Flows. *Proc. Natl. Acad. Sci. U.S.A.*, 102:14159, 2005.

[94] G. Danker, P. M. Vlahovska, and C. Misbah. Vesicles in Poiseuille Flow. *Phys. Rev. Lett.*, 102:148102, 2009.

[95] B. Kaoui, G. Biros, and C. Misbah. Why Do Red Blood Cells Have Asymmetric Shapes Even in a Symmetric Flow? *Phys. Rev. Lett.*, 103:188101, 2009.

[96] P. S. Virk. Drag Reduction Fundamentals. *American Institute of Chemical Engineers*, 21:625, 1975.

[97] P. S. Virk. Conformational effects in drag reduction by polymers. *Nature*, 262:46, 1976.

[98] N. Y. Chan, M. Chen, X. T. Hao, T. A. Smith, and D. E. Dunstan. Polymer Compression in Shear Flow. *J. Phys. Chem. Lett.*, 1:1912, 2010.

[99] R. G. Larson. *The Structure and Rheology of Complex Fluids*. Oxford University Press, New York, Oxford, 1999.

[100] A. Malevanets and R. Kapral. Solute molecular dynamics in a mesoscale solvent. *J. Chem. Phys.*, 112:7260, 2000.

[101] R. Kekre, J. E. Butler, and A. J. C. Ladd. Comparison of lattice-Boltzmann and Brownian-dynamics simulations of polymer migration in confined flows. *Phys. Rev. E*, 82:011802, 2010.

[102] H. Tanaka and T. Araki. Simulation method of colloidal suspensions with hydrodynamic interactions: Fluid particle dynamics. *Phys. Rev. Lett.*, 85:1338, 2000.

[103] P. Peyla. Rheology and dynamics of a deformable object in a microfluidic configuration: A numerical study. *EPL*, 80:34001, 2007.

[104] P. Espanol. Stochastic differential equations for non-linear hydrodynamics. *Physica A*, 248:77, 1998.

[105] R. Prabhakar and J. R. Prakash. Multiplicative separation of the influences of excluded volume, hydrodynamic interactions and finite extensibility on the rheological properties of dilute polymer solutions. *J. Non-Newtonian Fluid Mech.*, 116:163, 2004.

[106] E. Allahyarov and G. Gompper. Mesoscopic solvent simulations: Multiparticle-collision dynamics of three-dimensional flows. *Phys. Rev. E*, 66:036702, 2002.

[107] T. Araki and H. Tanaka. Dynamics of Colloidal Particles in Soft Matters. *Prog. Theor. Phys. Supp.*, page 37, 2008.

[108] Y. Davit and P. Peyla. Intriguing viscosity effects in confined suspensions: A numerical study. *EPL*, 83:64001, 2008.

[109] S. Rafai, L. Jibuti, and P. Peyla. Effective viscosity of microswimmer suspensions. *Phys. Rev. Lett.*, 104:098102, 2010.

[110] A. Einstein. Eine neue Bestimmung der Moleküldimension. *Ann. Phys.*, 19:289, 1906.

[111] A. Einstein. Berichtigung zu meiner Arbeit: 'Eine neue Bestimmung der Moleküldimension'. *Ann. Phys.*, 34:591, 1911.

[112] G. K. Batchelor, J. T. Green. Determination of bulk stress in a suspension of spherical-particles to order c-2. *J. Fluid Mech.*, 56:401, 1972.

[113] J. Happel and H. Brenner. *Low Reynolds Number Hydrodynamics.* Prentice-Hall, Englewood Cliffs, 1981.